ENERGY HARVESTING FROM SHIP VIBRATION

by

YAO YAO

B.E.Sc., Tianjin University, 2002

A THESIS SUBMITTED IN PARTIAL FULFILLMENT OF

THE REQUIREMENTS FOR THE DEGREE OF

MASTER OF APPLIED SCIENCE

in

THE FACULTY OF GRADUATE STUDIES

(Electrical and Computer Engineering)

THE UNIVERSITY OF BRITISH COLUMBIA

November 2005

Abstract

Advances in low power electronic devices design open up the possibility of self powering a small wireless device from harvested ambient power. In a ship environment, low level vibration is considered as an appropriate power source to extract energy. After a survey of three mechanisms to convert mechanical motion to electricity, electromagnetic conversion was chosen as a mechanism of energy harvesting in this thesis.

One of the major drawbacks of today's energy harvesters is that they are designed to provide power of only a few milliwatts and no power conversion control is integrated. Since the power requirement in this thesis is 0.3W, maximum power conversion becomes a critical objective in the harvester design. To achieve this objective, at first, a mathematical model of the electromagnetic converter (linear generator) with a resistive load was developed and the relations of system parameters to power output were deduced. Based on these relations, the design principles of the harvested are summarized into two steps: i) tune the natural frequency of the linear generator to match the main frequency of the vibration spectrum. ii) tune some electrical parameters to maintain the induced voltage at a optimal value which makes the electrical damping factor close to the mechanical damping factor.

A power management circuit was designed to condition the power flow to a supercapacitor. The relations deducted with a resistive load still holds in the capacitive load circuitry and thus spring constant and duty cycle of a DC-DC converter become two adjustable variables to control the power. An algorithm "MCCT" makes sure the energy harvester performs maximum power conversion under any conditions based on adjustment of the two variables.

Finally, the performance of the energy harvester is assessed under various disturbance scenarios by simulation.

Table of Contents

List of Tables

List of Figures

List of Symbols

f	Frequency of ship vibration (Hz)
z	Relative displacement of the mass (m)
F_e	Total electromagnetic force on a coil (N/m)
k	Spring constant (N/m)
c_m	Mechanical damping coefficient
c_e	Electrical damping coefficient
m	Mass (kg)
ω	Angular frequency of ship vibration (rad/s)
ω_n	Natural angular frequency
Φ	Magnetic flux (Wb)
B	Average magnetic flux density (T)
s	Area (m^2)
x	Position of edge between N and S pole (m)
w	Width of a coil (m)
l	Length of a magnet (m)
r	Coil resistance (Ω)
N	Number of turns of a coil
n	Active number of coils in spring
I_0	Magnitude of induced current
Y_1, Y_2, Y_3	Displacement magnitudes of the fundamental frequency, 2nd harmonic and 3rd harmonic
α_1, α_2	Phase angle of 2nd harmonic and 3rd harmonic
R_l	Load resistance (Ω)
R	Total resistance (Ω)
C	Capacitance (F)
D	Duty cycle of DC-DC converter
T_s	Period of switching signal (s)
rp	Harmonics magnitude ratio

f_v	Frequency of induced voltage (Hz)
ζ_m	Mechanical damping factor
ζ_e	Electrical damping factor
P_{av}	Average total power dissipated (W)
P_{in}	Average converted electrical power (Input power) (W)
P_{out}	Average output electrical power on resistive load (W)
P_{in_max}	Maximum input power (W)
P_{out_max}	Maximum output power (W)
V_{in}	Induced voltage of linear generator (V)
k_{opt}	Optimal value of spring constant (N/m)
D_{opt}	Optimal value of duty cycle
ζ_{eopt}	Optimal value of ζ_e
i_{charge}	Present steady-state average charging current (A)
i_{max}	Achieved largest average charging current so far (A)
i_{av}	Averaged charging current (A)
v_{cap}	Supercapacitor's voltage (V)
v_{cap}	Supercapacitor's voltage (V)

Acknowledgements

I would like to thank my supervisor, Dr. William G. Dunford. His kind guidance, thorough comments and constant support have made it possible for me to make my dissertation complete. I would also like to thank my co-supervisor, Dr. Guy Dumont, who has been extremely helpful in not only suggesting worthwhile content, but also offering advice on authoring and styling techniques.

Thanks are extended to my colleagues in the Power Electronics Research Lab, who made the period of my research more pleasant and fruitful. Special thanks to Weidong Xiao, David Majaess, Kenneth Wicks and Magnus Lind for many helpful discussions we shared and enjoyed.

Finally, I would like to show my great appreciation to my wonderful parents for encouraging and supporting me all the way down to this end.

Chapter 1 Introduction

The main reasons which spurred the interest in power harvesting and literature review are presented in the first section of this introductory chapter. The second section presents the main goal of the thesis and briefly describes the structure of the energy harvester. Finally, general outline of this thesis is presented in the third section.

1.1 Power Harvesting Review

In recent years there have been major advancements in the development of low powered devices such as digital signal processors (DSP) and wireless sensor networks that use power on the order of 10's to 100's of microwatts. The traditional way of supplying power to these low powered devices is through batteries. However, replacing batteries, even long-lived ones, in remote locations is labor-intensive and cost-prohibitive [1]. As a result, researchers are looking at the potential of energy harvesting converting ambient energy into electrical energy these devices can use [1].

Ambient energy is energy that is in the environment of the system and is not stored explicitly [2]. When compared with the energy stored in common storage elements such as batteries and the like, the environment represents a relatively inexhaustible source.

The most common used ambient energy sources are:

- Solar power (used by photovoltaic)
- Thermal gradient (Thermal gradients are directly converted to electrical energy through thermoelectric effect)
- Mechanical energy from movement and vibration

This research is funded by the United Technologies Research Centre. Its main issue is to design an energy harvesting device to be operational with a power load of 0.3 W on ships.

In ship environment, exposure to the sun is limited by the weather and the temperature differentials are typically low. Only the vibration energy is abundant enough to be a moderate source. Energy extraction from vibrations is based on the movement of a "spring-mounted" mass relative to its support frame [3]. Mechanical acceleration is produced by vibrations and in turn causes the mass to oscillate. During the movement, opposing frictional and damping forces act against the mass and thereby reduce the oscillations. The damping forces absorb the kinetic energy of the mass and convert it into electrical energy by three mechanisms: electro-magnetic, electrostatic and piezoelectric.

Electrostatic energy harvesting relies on the changing capacitance of vibration dependant variable capacitor [3]. If the charge on the capacitor is constrained, the voltage will increase as the capacitance decreases while if the voltage across the capacitor is constrained, charge will move from the capacitor as the capacitance decreases [4]. In both cases, mechanical energy is transformed into electrical energy. However, a charge source, which could be a pre-charged capacitor or rechargeable battery, is required to initiate the conversion process. This makes it unpractical to apply in ships since the reservoir will discharge much during ships dry dock time or repair time.

Piezoelectric energy harvesting converts mechanical energy to electrical by straining a piezoelectric material [5]. When a piezoelectric material is placed under a mechanical stress, a charge separation appears across the material and produces voltage [4]. This open circuit voltage is proportional to the stress applied. A cantilever beam configuration with a mass placed on the free end has been chosen as the oscillating system, since it provides a relatively high average strain for a given input force and results in the lowest stiffness for a given size [6]. One application of the piezoelectric mechanism is the Ferro Solutions Energy Harvester (FSEH). This device uses new magnetic materials to glean "milliwatts of power from input vibrations of a few tens of milli-g's with the size of a pack of gum" [7]. The FSEH is more valuable than its competitors of similar size in that it churns out 10 to 100 times power with the same input energy. However, the FSEH is still not an optimal generator since it can not always generate maximum power as the vibration frequency

changes. In order to induce maximum electric energy, the piezoelectric generator should vibrate at its resonant frequency. In [8], the resonant frequency is proposed to be related to elastic constant for the piezoelectric material, shape of the mass and beam and the mechanical mass. These parameters, however, can not be changed after the oscillating system is built. Thus, the piezoelectric generator can only induce maximum electric energy when the driving frequency is equal to its natural frequency.

Considering the drawbacks of electrostatic and piezoelectric schemes, electro-magnetic mechanism is used in this project. It uses the relative motion between a coil and a magnetic field to induce a voltage in the coil. Unlike electrostatic conversion, no separate voltage source is needed to get the process started. Also, the system can be designed without mechanical contact between any parts, thus improving reliability and reducing mechanical damping [9]. In theory, this type of converter could be designed to have very little mechanical damping.

Williams and Yates [10] have designed and built a micro-electromagnetic converter. They developed a generic second order linear model for power conversion which turns out to be fit for electromagnetic conversion very well. Also, they showed close agreement between the model and experimental results. However, they drove the converter to generate 1 mW with vibration of 50 μm magnitude at 330 Hz which are far more energetic and of higher frequency than those measured in the ship environment. Thus, this device is not well suited to very low vibration frequencies in a ship.

The primary characteristic of today's energy harvesters is that they are designed to power wireless sensor or transmitters which only require the order of a few milliwatts power. At this power level, any adjustment in parameters is too power-consummative to execute. Nevertheless, when the power demand level increase to watts at vibration frequency below 20 Hz, these energy harvesters should be redesigned not only for larger size but also to maximize power output.

1.2 Thesis Objective

The objective of this thesis is to design an energy harvester to extract maximum possible electrical energy from the movement of ship. This energy harvester must fulfill the two following tasks:

- Continuously generates maximum electrical output power at various low vibration frequencies under any conditions
- Contains power-management circuit allowing charge buildup in a supercapacitor to support a load.

With these tasks in mind, the energy harvester is composed of two parts: a linear generator using an electromagnetic scheme to convert vibration energy to electrical energy; a power management circuit to maintain the largest dc current to charge a supercapacitor. Figure 1.1 shows the architecture of the energy harvester. In the linear generator, four connected magnets move relatively to two coils under the effect of two springs. The coils cut a varying amount of magnetic flux, inducing a voltage according to Faraday's law. In order to get a DC current to charge the supercapacitor, the induced AC voltage feeds to an AC/DC rectifier and capacitor filter to make the output voltage essentially constant. Then a switch mode DC/DC converter is placed between the filter and the supercapacitor to achieve maximum power transfer. An algorithm called Maximum Charging Current Tracking (MCCT) is used in a controller to find and maintain the maximum power flow to the supercapacitor. By adjusting spring constant in the linear generator and duty cycle of the DC/DC converter, the algorithm works successfully at circuit startup as well as environmental conditions deviation. In this thesis, we demonstrate the effectiveness of the energy harvester under various environmental conditions by simulation.

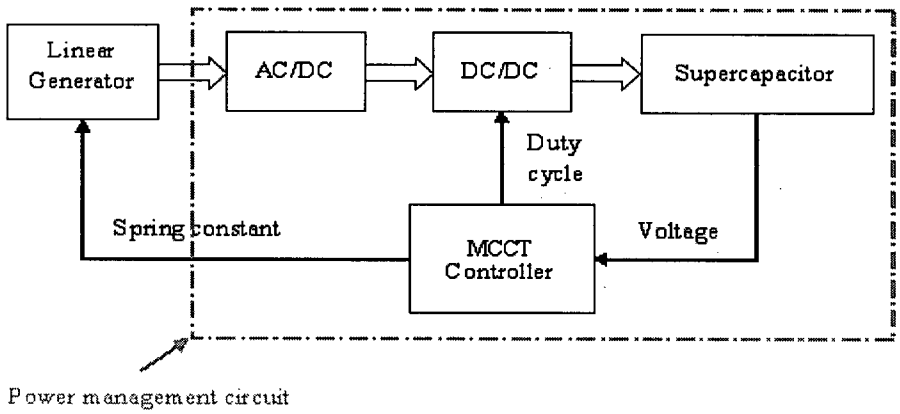

Figure 1. 1 Architecture of the energy harvester

1.3 Thesis Outline

The remainder of this thesis is organized as follows:

Chapter 2 describes the construction and the operational principle of the linear generator. The linear generator is connected to a load resistance and a math model of the linear generator is formed in Simulink.

Chapter 3 illustrates all system parameters that affect the power output including spring constant, load resistance and induced voltage, and their relations with the power. The design principles of energy harvester are proposed based on these relations. The effect of harmonics is also discussed and a method to escape from a local maximum caused by the harmonics is proposed.

In Chapter 4, a power management circuit is designed to charge a supercapacitor as well as conditioning the power flow to it. Then the energy harvester is modeled with Simulink and Psim by substituting the power management circuit to the resistive load in the model of linear generator. An algorithm called MCCT to achieve maximum power flow to the supercapacitor is proposed and evaluated by simulation.

Conclusions and recommendations will be given in Chapter 6. Appendix A demonstrates the derivation of equation 3.11 and 3.16. Appendix B gives three tables in chapter 2 and chapter 3. Appendix B represents three flow charts for adjusting spring constant, duty cycle with step size 0.04 and 0.01 respectively.

Chapter 2 Linear Generator with Resistive Load

A comparison of electrostatic, electromagnetic, and piezoelectric converters was presented in chapter 1 and electromagnetic converter is chosen to apply in this research. Chapter 2 will consider the design and modeling of this type of converter. In the first section, the brief description of ship vibration characteristics is proposed. Then, the mechanical structure and operation principle of the linear generator (electromagnetic converter) is described. Finally, the mathematical model and transfer function of linear generator with resistive load are discussed.

2.1 Ship Vibration

Ship vibration can conveniently be classified as either low frequency motion induced by sea conditions surrounding the vessel such as the subject of motion in waves (springing and whipping), ship motions (roll, heave and pitch) and vibrations of higher frequency originating from the engines, propeller shafts, and major pieces of onboard machinery.

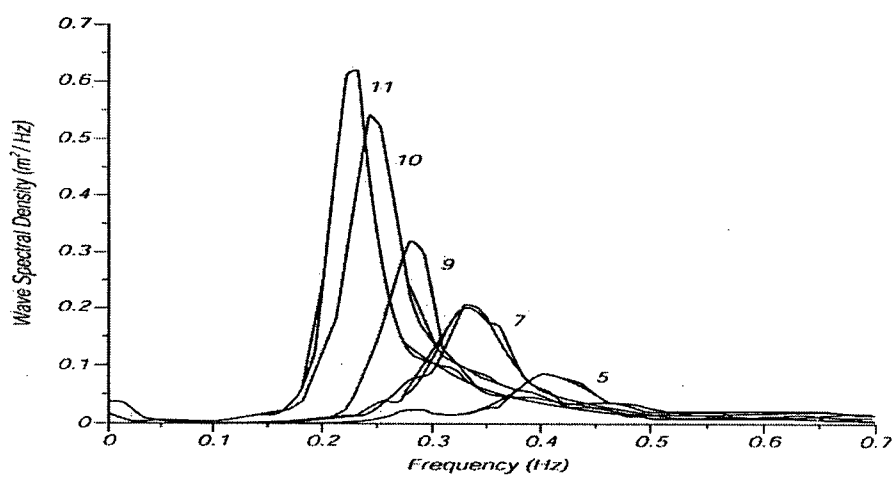

Figure 2. 1 Wave spectra of a developing sea for different fetches

Figure 2.1 shows that ocean wave frequency range is from 0.1 to 0.7 Hz [11]. The frequency range of ship vibrations caused by interference to the flow of water and from

imbalance and misalignment of the propeller shaft system is 1-11 Hz [12]. Diesel engine/generator is another main source of machinery vibration besides propeller. Vibration frequency of a diesel engine depends on its running speed: for medium speed level (300-1200 rpm), the vibration frequency is from 5 to 20 Hz [13]. Since medium-speed engines are a major force in cargo and passenger ship propulsion, in this thesis, the vibration frequency of ship is supposed to range from 2-20 Hz and the displacement magnitude is 5 mm.

2.2 Mechanical System Description

First we modeled the vibrations on a ship by a DC motor and an eccentric weight. The motor was mounted upright with a cylindrical eccentric weight attached to the shaft. When a DC voltage was supplied to the motor, the shaft rotated the eccentric weight. This should cause the motor to shake. The vibrations of the motor were transferred to test board which has four frictionless bearings underneath each corner of the board. Then the board began to oscillate horizontally with the bearings rotating. The frequency of vibration is dependent on the DC voltage supply and the geometric center of the cylindrical weight relative to the shaft. The higher is the DC voltage, the higher the frequency of the board vibration. The mechanism that converts mechanical vibrations to electricity, also called a linear generator, was placed on the center of the board. The mechanism itself approximately occupies 0.16 m by 0.11 m by 0.05 m in volume. It basically consisted of two iron cores, one top and bottom, with copper wires looped around the slots that were cut inside the iron core. The two iron cores, which provided path and guided the magnetic flux through it with a minimum flux leakage, were bolted onto the frame at each side. The use of two cores is to counteract cogging forces and make the slides easy to move. Four small magnets are glued between telescopic sides of two drawer slides and placed between the two iron cores. The air gaps between the magnets and iron cores were only a few millimeters. The fixed sides of slides are attached to the frame. Two springs are bolted onto the frame and the slides by

screws. A mechanical diagram of the linear generator is shown in Figure 2.2.

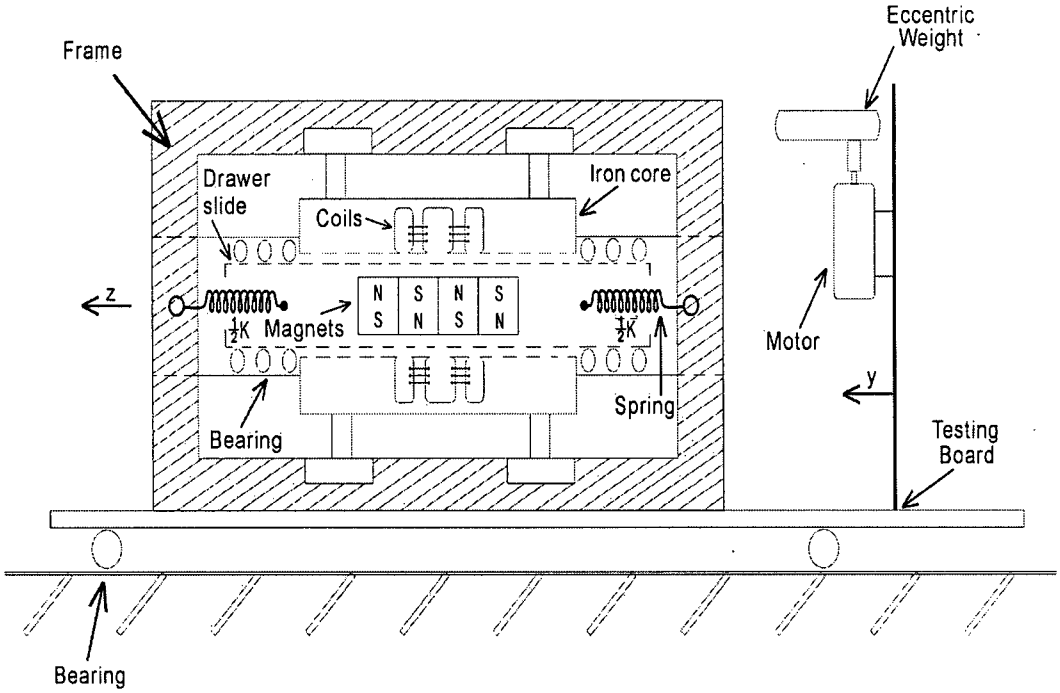

Figure 2. 2 Mechanical diagram of the linear generator

2.3 Vibration-to-Electricity Conversion Model

In the linear generator, coils work as a stator and the slides with magnets works as a rotor. The operating principle is as follows: as the testing board is vibrating, a mechanical input force feeds into a spring mass system. The mass (the slides with magnets) moves relative to the testing board and energy is stored in the mechanical system. The output of mechanical system is the relative displacement of the mass. This relative movement causes the magnetic flux to cut the coil and in turn induces a voltage proportional to the derivative of the mass position. The currents induced in the coils generate an electromechanical force f_e which feeds back and damps the mass motion. Thus, the complicated prototype in Figure 2.2 can be simplified to a schematic diagram in Figure 2.3 proposed by Williams and Yates [10]. The parameter identification and system analysis are presented in section 2.3.1 and 2.3.2

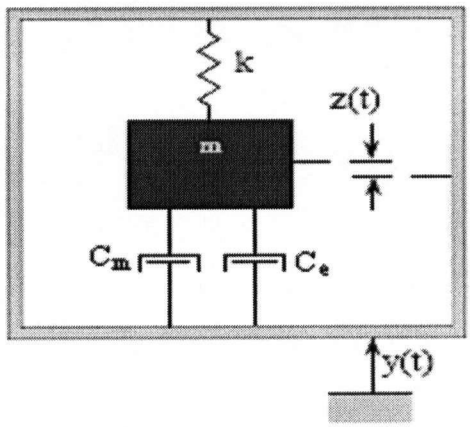

Figure 2. 3 Schematic diagram of the linear generator

2.3.1 Spring Mass and Mechanical Damper System

Since the vibration of the testing board is used to emulate ship vibration, it can be assumed that the mass of the vibration source is much greater than the mass in the generator, and that the vibration source is an infinite source of power [10]. Similarly, the movement of the source is unaffected by the energy extracted by the harvester. In order to simplify consideration of source vibration, it is proposed that the ship vibration is a simple harmonic excitation given by:

$$Y(s) = Y_1 \sin \omega t \tag{2.1}$$

Where

Y_0 = displacement amplitude of main frequency of ship vibration (m)

$\omega = 2\pi f$, angular frequency of ship vibration (rad/s)

f = frequency of ship vibration (Hz)

The differential equation that describes the movement of the mass with respect to the test board can be derived from dynamic forces on the mass:

$$-c_m \dot{z}(t) - kz(t) = m(\ddot{y}(t) + \ddot{z}(t))$$

or

$$m\ddot{z}(t) + c_m \dot{z}(t) + kz(t) = -m\ddot{y}(t) \tag{2.2}$$

where

z = relative displacement of the mass (m)

k = spring constant (N/m)

c_m = mechanical damping coefficient due to friction and cogging force

m = mass (kg)

Equation (2.2) can be also written in frequency domain:

$$Z(s)(ms^2 + c_m s + k) = -ms^2 Y(s) \tag{2.3}$$

The transfer function from $Y(s)$ to $Z(s)$ is obtained

$$\frac{Z(s)}{Y(s)} = \frac{-ms^2}{(ms^2 + c_m s + k)} \tag{2.4}$$

Substituting in expressions for mechanical damping factor $\zeta_m = c_m / 2m\omega_n$, and the natural angular frequency $\omega_n = \sqrt{k/m}$, equation (2.4) can be written as

$$\frac{Z(s)}{Y(s)} = \frac{-s^2}{s^2 + 2\zeta_m \omega_n s + \omega_n^2} \tag{2.5}$$

2.3.2 Electrical Damper

As the slides move back and forth, the magnetic field changes position and consequently, the flux linkage of the copper coils varies as shown in the following flux linkage equation:

$$\begin{aligned} \Phi &= \int B ds \\ &= Bl[x - (w - x)] \\ &= Bl(2x - w) \end{aligned} \tag{2.6}$$

where:

Φ = magnetic flux (Wb)

B = average magnetic flux density (T)

s = area (m^2)

x = position of edge between N and S pole (m)

w = width of a coil (m), which equals to width of a magnet

l = length of a magnet (m)

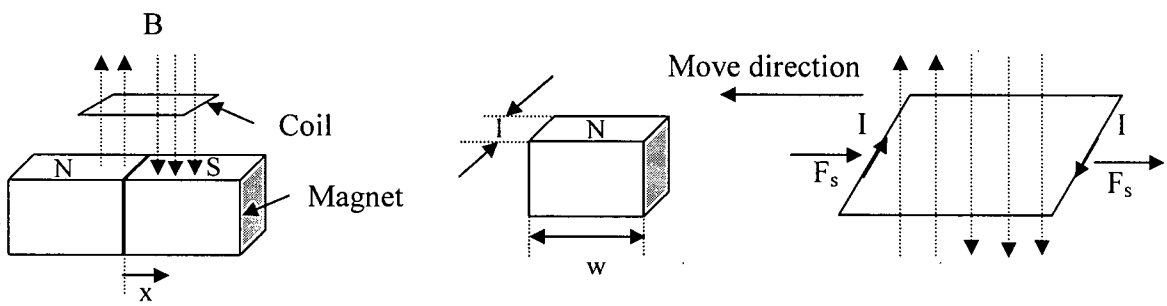

Figure 2.4 Moving process of magnets

This in turn induces a voltage on the coil in accordance with Faraday's law as follows:

$$v_{in} = N\frac{d\Phi}{dt}$$

$$= 2NBl\,z \qquad (2.7)$$

where:

N = number of turns of a coil

If a simple resistive load is attached to the linear generator, the electrical system is a first-order L-R circuit, with the coils inductance L in series with load resistance R_l and coils resistance r which is shown in Figure 2.5.

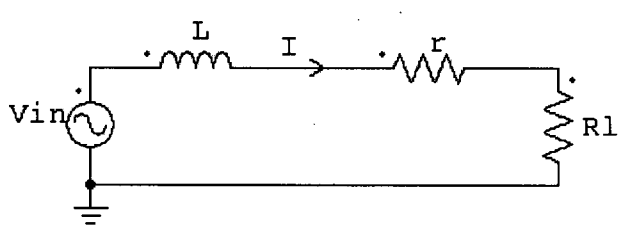

Figure 2.5 Schematic of simplified electrical system

The induced current in the coils is

$$I(s) = \frac{V_{in}(s)}{R_l + r + Ls}$$

$$= \frac{2NBlZ(s)s}{R_l + r + Ls} \tag{2.8}$$

The total electromechanical force on the coil is:

$$F_e(s) = 2F_s(s)$$

$$= 2NBlI(s)$$

$$= \frac{4N^2B^2l^2Z(s)s}{R_l + r + Ls} \tag{2.9}$$

where F_s is an electromechanical force generated by the induced current on one side of the coil. This force opposes the relative motion between the magnets and coils. Since the vibration frequency range is from 2 to 20 Hz, we assume the inductive impedance is much lower than the resistive impedances and can be neglected. Equation (2.9) can be written as

$$F_e = \frac{4N^2B^2l^2Z(s)s}{R} \tag{2.10}$$

where

$$R = R_l + r\ (\Omega)$$

Hence, the electrical damping coefficient is $c_e = \frac{4N^2B^2l^2}{R}$ and electrical damping factor is

$$\zeta_e = \frac{2N^2B^2l^2}{m\omega_n R} \tag{2.11}$$

2.4 Transfer Function and Simulation Model

The total transfer function from $I(s)$ to $Y(s)$ is:

$$\frac{I(s)}{Y(s)} = \frac{\dfrac{2BNls}{(ms^2 + c_m s + k)(Ls + R)}}{1 + \dfrac{2BNls}{(ms^2 + c_m s + k)(Ls + R)} * BNl} * m\omega^2$$

$$\approx \frac{2m\omega^2 BNls}{mRs^2 + (c_m R + 2B^2N^2l^2)s + kR} \tag{2.12}$$

Figure 2.6 shows the simulation model of the energy harvester with resistive load.

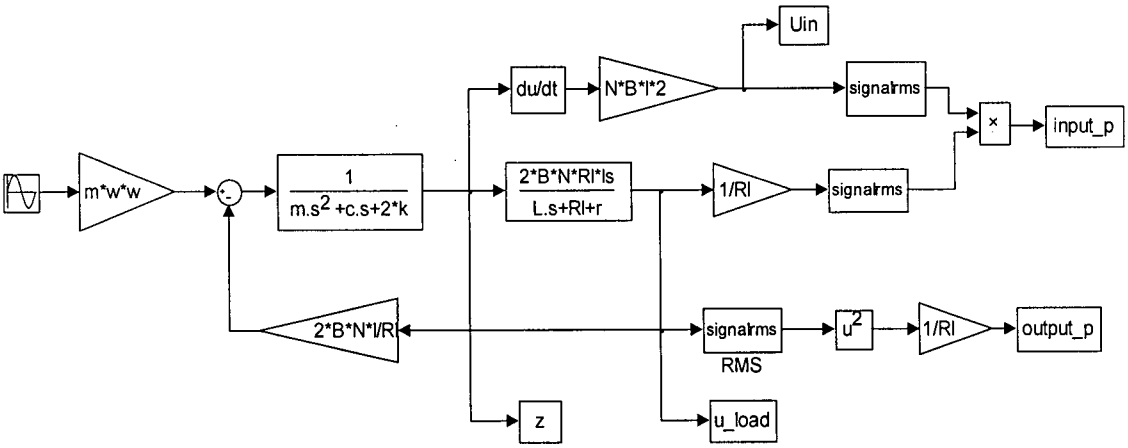

Figure 2.6 Simulation model of the linear generator with resistive load

The parameters applied in this model are shown in Table 1 in Apendix B. Among these parameters, the values of B, l and ζ_m are gained from the model built in Dec 2004 while the values of N, L and r are gained by assumption. ζ_m is measured by applying an impulse to the linear generator, and then measuring open circuit output voltage. The magnitude of oscillations in the output voltage is measured at two separate points, n periods apart. The damping ratio can then be calculated as a function of the log decrement of the two magnitudes and the number of periods as shown in equation 2.13 [14].

$$\zeta_m = \frac{1}{2\pi n}\ln(\frac{x_1}{x_2}) \tag{2.13}$$

An example of the resulting damped oscillations (tested with the Dec 2004 Model) is shown in Figure 2.7.

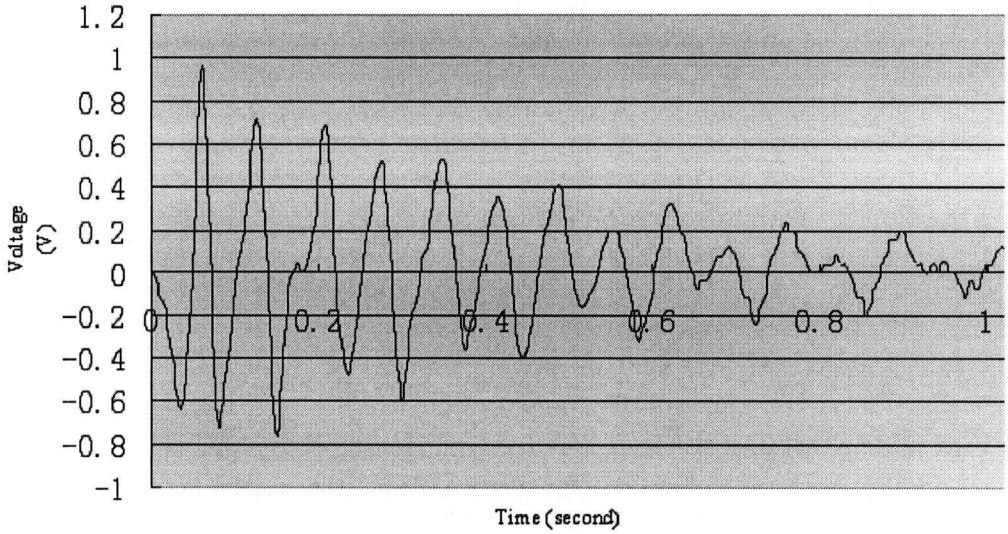

Figure 2.7 Damped oscillations from a force impulse to the energy harvester

Chapter 3 Maximum Power Analysis

A model to predict the output current of the linear generators was developed and discussed in the previous chapter. This chapter will utilize the model to explore the design of the harvester for power maximization. The relation between the spring constant, load resistance and output power is discussed as well as the relation between the induced voltage and power. Simulations are provided to validate these relations. The effect of harmonics is also discussed and the initiation process of the spring constant is presented based on this effect.

3.1 Maximum Converted Electrical Power (P_{in})

Two ways to represent the converted electrical power are discussed in the following sections. The analytical expressions derived by the first one fit for all types of load while the expressions derived by the second are suited for resistive load only.

3.1.1 Discussion of P_{in} Based on Damping Factor

One way is to calculate the power consumed by the electrical damping force in the second order system:

$$m\ddot{z}(t)+(c_m+c_e)\dot{z}(t)+kz(t)=-m\ddot{y}(t) \tag{3.1}$$

As has been reported in [15], the steady state solution z for equation (3.1) is

$$z(t)=Z_1\beta\sin(\omega t-\varphi) \tag{3.2}$$

where

$$Z_1=\frac{m\omega^2 Y_1}{k},\quad \beta=\frac{1}{\sqrt{(1-\omega_c^2)^2+(2\omega_c\zeta)^2}},\quad \varphi=\tan^{-1}\left(\frac{2\omega_c\zeta}{1-\omega_c^2}\right)$$

$$\zeta = \zeta_m + \zeta_e = \frac{c_e + c_m}{2m\omega_n}$$

The total energy dissipated per cycle is:

$$W = \int_0^{2\pi/w} (c_m + c_e)\, \dot{z}\, \dot{z}\, dt$$

$$= \frac{\pi(c_m + c_e)\omega Y_0^2 \omega_c^4}{(1-\omega_c^2)^2 + (2\zeta\omega_c)^2}$$

Where

$$\omega_c = \frac{\omega}{\omega_n}$$

The average power dissipated is:

$$P_{av} = \frac{W}{2\pi/\omega} = \frac{m\zeta Y_0^2 \omega^3 \omega_c^3}{(1-\omega_c^2)^2 + (2\zeta\omega_c)^2}$$

Part of the above power transfers to the electrical system (input power):

$$P_{in} = \frac{m\zeta_e Y_0^2 \omega^3 \omega_c^3}{(1-\omega_c^2)^2 + (2\zeta\omega_c)^2} \tag{3.3}$$

In figure 3.1, P_{av} is plotted against frequency for various damping factors ζ when natural frequency $f_n = \frac{\omega_n}{2\pi}$ equals 10 Hz. For a low damping factor, there is a peak in P_{av} around the natural frequency. Hence, when the vibration frequencies are concentrated around the natural frequency, a low damping factor can largely increase power generated at that point. When the main vibration frequency varies over time and the natural frequency of the system is fixed, the peak caused by the low damping factor is very narrow and a large portion of vibration energy at other frequencies will be rejected. In this case, a higher damping factor should be used to get broadband power.

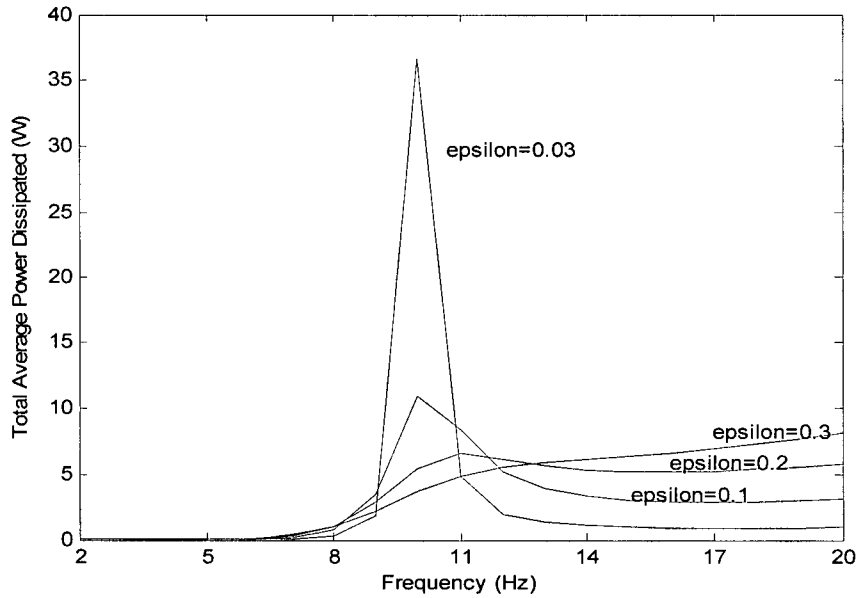

Figure 3.1 Frequency spectrum of total average power dissipated at various damping factors when natural frequency is 10 Hz

The optimal k for maximum input power is at stationary point $\frac{dP_{in}}{dk}=0$ when ζ is constant:

$$k_{opt}=\frac{m\omega^2}{2\zeta^2-1+\sqrt{(2\zeta^2-1)^2+3}} \tag{3.4}$$

The optimal value of ζ_e for maximum input power is at the stationary point $\frac{dP_{in}}{d\zeta_e}=0$ when k is constant

$$\zeta_{eopt}=\sqrt{\frac{(1-\omega_c^2)^2}{4\omega_c^2}+\zeta_m^2} \tag{3.5}$$

If the spectrum of the target vibrations is known beforehand, the device can be designed to resonate at the main vibration frequency. As seen in equation (2.11), ζ_e is a function of R and so can be set by properly choosing the load resistance. Thus, the converted electrical power is maximized when we design mechanical components to make ζ_m as low as

possible and adjust R_l to let $\zeta_e = \zeta_m$. In this case, the input power is half of the total dissipated power. However, as shown in Figure 3.1, there is a large penalty even if a small difference between the natural frequency and the vibration frequency appears. While a more lightly damped system (like $\zeta = 0.03$) has the potential for higher power output, the power output also drops off more quickly as the driving vibrations move away from the natural frequency. This highlights the critical importance of designing a device to match the main vibration frequency. In some environments such as ship, the main vibration frequency changes with conditions, it would be necessary to actively tune the natural frequency of the harvesting device.

One way to change the natural frequency is to change the spring constant. For a helical spring with the load acting along the axis of spring, the spring constant is given by [16]:

$$k = \frac{Gd^4}{8D^3 n} \tag{3.6}$$

where

d = wire diameter, D = mean coil diameter

n = active number of coils, G = shearing modulus of elasticity

With other parameters unchanged, the spring constant is inverse proportional to n. This means we can change k by varying active number of coils. This idea is applied in progressive springs which are widely used in cars nowadays. In a progressive spring, each coil is spaced differently and they have a variable spring constant [17]. When free, it is easy to compress the spring for first centimeters. As more forces were applied, coils on the progressive spring come closer. After a certain point, coils at the top 1/4 of the spring begin to touch each other and finally become inactive or dead, and that makes the spring stiffer [18]. Applying more forces to the progressive spring can make the number of active coils in the spring decreases, and then the spring constant increases. The flexibility in the progressive spring makes it much easier to tune the natural frequency of electromagnetic

converter than the electrostatic and piezoelectric converters. Thus, the electromagnetic converter outperforms other type of converters in term of maximum power conversion.

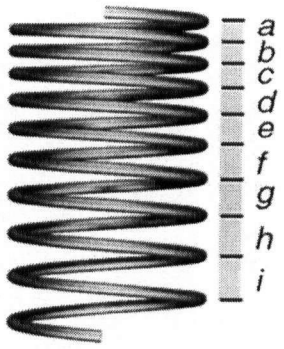

Figure 3.2 Structure of progressive spring [17]

Based on the equation 3.3, the design principles for energy harvester are summarized below:

- Power is linearly proportional to mass. Therefore, the energy harvester should have the largest mass that is possible while staying within the space constraints.
- The mechanical damping factor should be made as small as possible.
- The electrical damping factor is designable, and when it is equal to the mechanical damping factor, the input electrical power is optimized.
- For a given displacement magnitude, the input electrical power is proportional to triple the main vibration frequency. Thus, the energy harvester should be placed at a high frequency spot.
- Finally, the natural frequency of the harvester should closely match the main vibration frequency.

3.1.2 Discussion of P_{in} Based on k and R

The other way to calculate P_{in} is to add the power consumed on the coil resistance and load resistance together. Neglecting the inductive impedance, Figure 2.4 is redrawn below with new notations:

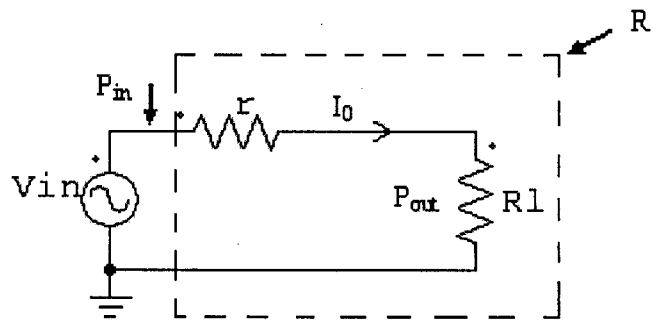

Figure 3.3 Scheme of the simplified electrical system without coil inductance

The average input power is:

$$P_{in} = \frac{I_0^2 R}{2} \tag{3.7}$$

where

I_0 is the magnitude of $I(s)$

I_0 is found by taking absolute value of equation (2.12)

$$I_0 = \frac{2mBNlY_0\omega^3}{\sqrt{R^2(k-m\omega^2)^2 + (c_m R + 4B^2N^2l^2)^2\omega^2}} \tag{3.8}$$

Substitute equation (3.8) into equation (3.7), we get

$$P_{in} = \frac{2m^2B^2N^2l^2Y_0^2\omega^6 R}{R^2(k-m\omega^2)^2 + (c_m R + 4B^2N^2l^2)^2\omega^2} \tag{3.9}$$

which has the same form as equation (3.3) with expression $\frac{2N^2B^2l^2}{m\omega_n\zeta_e}$ replacing R.

Equation (3.9) is a function contains two variables: k and R. The optimal value of R for maximum P_{in} is achieved by substituting equation (2.11) into equation (3.5):

$$R_{opt} = \frac{4B^2N^2l^2\omega}{\sqrt{c_m^2\omega^2 + (k - m\omega^2)^2}} \tag{3.10}$$

The optimal value of k is achieved by differentiating equation (3.9) such that

$$\frac{\partial P_{in}}{\partial k} = 0 \tag{3.11}$$

which can be simplified to a cubic equation (the derivation process is shown in Appendix A.1):

$$k^3 + k^2 m\omega^2(3\zeta_m^2 - 2) + km^2\omega^4(1 - 2\zeta_m^2) - m^3\omega^6\zeta_m^2 = 0 \tag{3.12}$$

while $\quad k < m\omega^2(1 - 2\zeta_m^2)$

Equation (3.12) cannot be easily solved by means of algebra. In Matlab, a function called "fsolve" finds a zero of a nonlinear equation. Choosing m, ζ_m, r, B, N, l values from Table 1 in Appendix B, we get optimal values of k, R_l and ζ_e for various vibration frequencies which are shown in Table 3.1. The table show that for a given value of ζ_m, power is maximized when ζ_e is close to ζ_m (0.11).

f (Hz)	k_{opt} (N/m)	R_{l_opt} (Ω)	ζ_{eopt}	$P_{in\_\max}$ (W)	f (Hz)	k_{opt} (N/m)	R_{l_opt} (Ω)	$P_{in\_\max}$ (W)	ζ_{eopt}
3	100	49.6	0.16	0.0617	12	1900	14.6	4.353	0.114
4	200	45.1	0.124	0.159	13	2200	13.2	5.544	0.116
5	300	33.4	0.134	0.304	14	2600	12.3	6.94	0.113
6	500	31.4	0.11	0.542	15	3000	11.3	8.536	0.113
7	700	26.2	0.11	0.846	16	3400	10.5	10.359	0.113
8	900	22.9	0.11	1.276	17	3800	9.7	12.417	0.114
9	1100	20.3	0.111	1.84	18	4300	9.1	14.749	0.113
10	1300	17.7	0.116	2.523	19	4800	8.5	17.347	0.113
11	1600	16.1	0.114	3.366	20	5300	8	20.231	0.113

Table 3.1 Optimal k, R_l and ζ_e for various input frequencies

Note: (1) k_{opt} is equal to half of the solution in equation (3.12) since there are two springs in the linear generator.

(2) The value of k_{opt} is rounded to hundred. When $f = 2\,\text{Hz}$, $k_{opt} = 50\,\text{N/m}$ which is smaller than step size of adjustment (100 N/m) and is omitted in this thesis.

The generated power in above table is calculated under the same displacement magnitude $Y_1 = 5$ mm. In fact, displacement magnitude is generally decreasing with frequency. Also acceleration magnitude is more commonly used in frequency spectra than displacement magnitude. Assuming the natural frequency of the linear generator matches the main vibration frequency and the mechanical and electrical damping factors are equal, the minimum acceleration magnitudes at each frequency to generate 0.3 W can be calculated by equation (3.3). We can see from Table 3.2, as f increase, a larger

acceleration magnitude is needed to generate the same amount of power. Moreover, the mechanical damping is an important limiting factor in producing maximum power and it should be made as small as possible through better spring linearity and vacuum operation [19].

f	$\zeta_m = 0.11$	$\zeta_m = 0.015$	f	$\zeta_m = 0.11$	$\zeta_m = 0.015$
3	3.75	1.38	12	7.49	2.77
4	4.33	1.6	13	7.8	2.88
5	4.84	1.79	14	8.09	2.99
6	5.3	1.96	15	8.38	3.09
7	5.72	2.11	16	8.65	3.2
8	6.11	2.26	17	8.92	3.29
9	6.49	2.4	18	9.18	3.39
10	6.84	2.53	19	9.43	3.48
11	7.17	2.65	20	9.67	3.57

Table 3.2 Minimum acceleration magnitudes at each frequency to generate 0.3 W

3.2 Relation Between V_{in} and P_{in}

As seen from Figure 3.3, the magnitude of induced voltage is:

$$V_{in} = I_0 R \tag{3.13}$$

Substituting equation (3.8) into equation (3.13), we get

$$V_{in} = \frac{2mBNlY_0\omega^3}{\sqrt{(k - m\omega^2)^2 + (c_m + 4B^2N^2l^2/R)^2\omega^2}}$$

The expression for R can then be represented by V_{in}

$$R = \frac{2B^2N^2l^2\omega}{\sqrt{4Y_0^2m^2\omega^6B^2N^2l^2/V_{in}^2 - (k-m\omega^2)^2} - c_m\omega} \tag{3.14}$$

where

$$V_{in} < \frac{2Y_1m\omega^3BNl}{|m\omega^2 - k|}$$

Thus, P_{in} can be represented by V_{in}

$$P_{in} = \frac{V_{in}^2}{2R} = \frac{V_0\sqrt{4Y_0^2m^2\omega^6B^2N^2l^2 - V_0^2(k-m\omega^2)^2} - V_0^2c_m\omega}{8B^2N^2l^2\omega} \tag{3.15}$$

The relation of P_{in} and V_{in} based on equation 3.15 at $f = 10\,\text{Hz}$, $k = 1300\,\text{N/m}$ is demonstrated in figure 3.4.

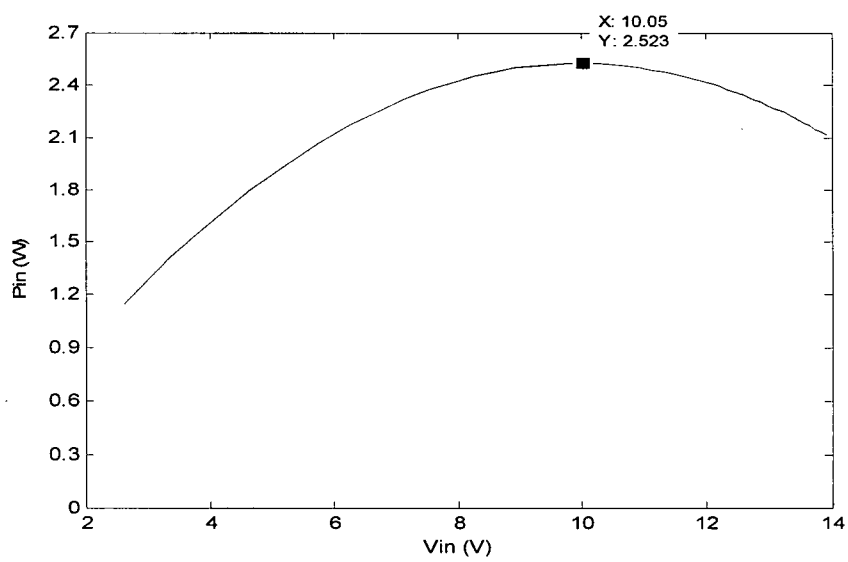

Figure 3.4 P_{in} vs V_{in} when $f = 10\,\text{Hz}$, $k = 1300\,\text{N/m}$, R = 3:1:46 Ω

This P_{in} - V_{in} curve has a well defined maximum power point. We can get the corresponding value of V_{in} by differentiating equation 3.15 such that

$$\frac{\partial P_{in}}{\partial V_{in}} = 0 \tag{3.16}$$

which results in:

$$V_{in\_opt} = \frac{\sqrt{2}E}{G}\sqrt{1-\frac{c_m\omega}{\sqrt{G^2+c_m^2\omega^2}}}$$

$$= \frac{\sqrt{2}mY_0\omega^3 BNl}{|m\omega^2-k|}\sqrt{1-\frac{c_m\omega}{\sqrt{(k-m\omega^2)^2+c_m^2\omega^2}}} \tag{3.17}$$

where

$$V_{in\_opt} < \frac{2E}{G} = \frac{2Y_1 m\omega^3 BNl}{|m\omega^2-k|} \quad , \quad E = Y_1 m\omega^3 BNl, \quad G = |k-m\omega^2|$$

The maximum input power is

$$P_{in\_\max} == \frac{Y_0^{\,2}m^2\omega^5}{4G^2}\left(\sqrt{G^2+c_m^2\omega^2}-c_m\omega\right) \tag{3.18}$$

Using optimal values of k in Table 3.1 and parameters in Table 1 in Appendix B, we can get the maximum input power and corresponding optimal V_{in} at various input frequencies which are shown in Table 2 in Appendix B.

The relation between P_{in} and V_{in} proves the maximum input power can be achieved by maintaining the induced voltage at its optimal value. This idea is applied in capacitive load circuitry by tuning duty cycle of a DC-DC converter.

3.3 Discussion in Maximum Output Power

As seen from Figure 3.3, the average output power in the resistive load is:

$$P_{out} = P_{in} - \frac{P_{in}r}{R} = P_{in}(1-\frac{r}{R}) \tag{3.19}$$

Substitute equation (3.14) and (3.15) into (3.19), we get

$$P_{out} = \frac{V_{in}^2(\sqrt{4E^2/V_{in}^2-G^2}-c\omega)}{8B^2N^2l^2\omega}(1-\frac{\sqrt{4E^2/V_{in}^2-G^2}-c\omega}{4B^2N^2l^2\omega}*r) \tag{3.20}$$

The relationship of P_{out} and V_{in} based on equation (3.20) with constant k is demonstrated in Figure 3.5

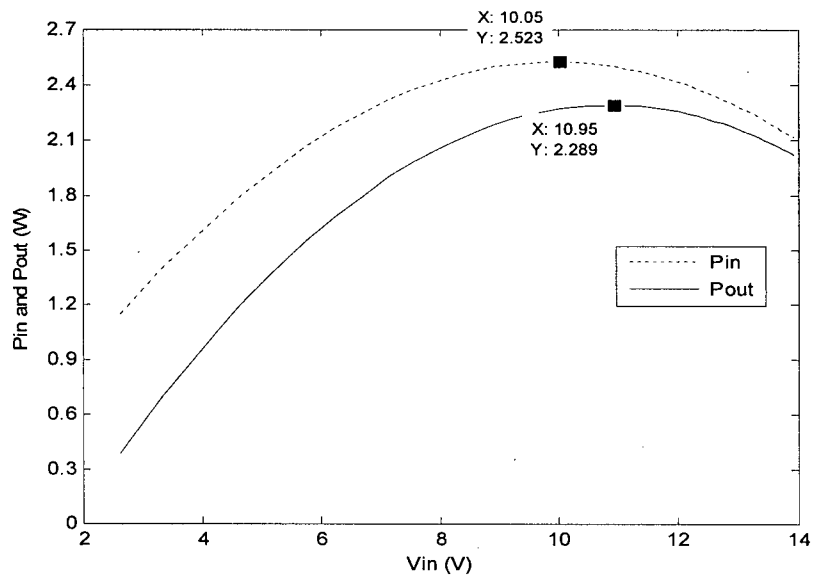

Figure 3.5 P_{out}, P_{in} vs V_{in} when $f = 10\,\text{Hz}$, $k = 1300\,\text{N/m}$, $R_l \in [1, 44]\ \Omega$

In Figure 3.5, the value of V_{in} corresponding to maximum P_{out} is larger than which corresponds to maximum P_{in}. The reason is that although P_{in} begins to decrease after it reaches maximum, the multiplication factor $1-\frac{r}{R}$ keeps increasing as R_l increases. Hence, P_{out} will keep increasing until V_{in} reaches a certain value which makes the effect of increase in multiplication factor equals the effect of reduction in P_{in}. This value is achieved at the stationary point $\frac{\partial P_{out}}{\partial V_{in}} = 0$.

We can see from equation 2.11: $\zeta_e = \frac{2N^2B^2l^2}{m\omega_n R}$, increasing R_l will decrease ζ_e. Thus, the value of ζ_e corresponding to maximum P_{out} will be smaller than counterpart of maximum P_{in}. Furthermore, it is shown in equation 3.4 that a smaller value of ζ_e will require a larger value of k_{opt}. Thus, after the system reaches the maximum input power point, both k and R_l need increasing to reach the maximum output power point.

As it is difficult to deduct the formula form of optimal v_{in} for maximum P_{out} from equation 3.20, the quickest way to get maximum P_{out} is to first find optimal k and R_l in table 3.1 for certain vibration frequency. Then increase k until it reaches a local maximum. Last, keep this optimal k constant and begin to increase R_l until P_{out} reaches another maximum. This maximum power turns out to be the global maximum we are looking for.

3.4 Simulation Test

Using parameters in Table 1 in Appendix B, we can initialize the model shown in Figure 2.6. Figure 3.6 shows the surface plot for P_{in} and P_{out} when $f = 13$Hz. In figure 3.6 (b), there is a small area ($k \in [2200, 2300]$ N/m, $R_l \in [16, 18]\,\Omega$) in P_{out} surface where P_{out} changes from increasing to decreasing. This proves if we can adjust k and R_l to stay in this area, we can get maximum output power. Figure 3.6 (b) also shows that stationary point of R_l varies according to different value of k (k=2000 N/m, R_{sta} =15 Ω; k=2100 N/m, R_{sta} =16 Ω; k=2200-2400 N/m, R_{sta} =17 Ω; k=2500 N/m, R_{sta} =16 Ω; k=2600N/m, R_{sta} =15 Ω) while the stationary point of k is almost constant (k=2200 or 2300 N/m). Hence, it is better to fix R_l first and get the stationary point of k. Compared figure 3.6 (b) with (a), we can see both values of k and R_l corresponding to the maximum P_{out} ($k_{out\_opt} = 2300$ N/m, $R_{lout\_opt} = 17\,\Omega$) is larger than that corresponding to the maximum P_{in} ($k_{in\_opt} = 2200$ N/m, $R_{lin\_opt} = 13\,\Omega$).

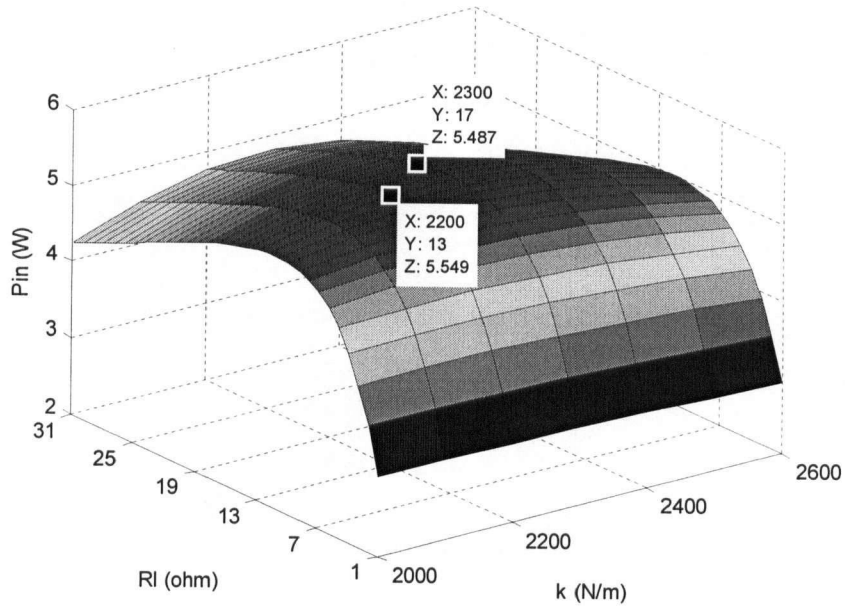

Figure 3.6 (a) Simulation result of P_{in} at 13 Hz

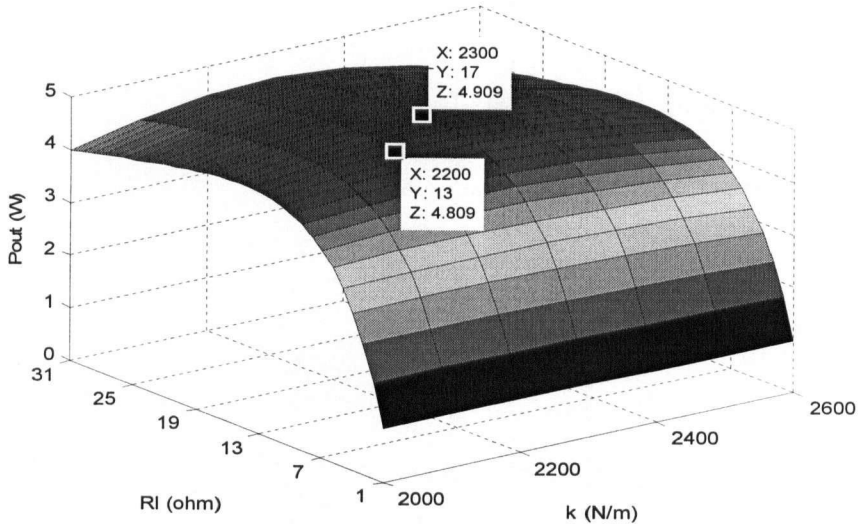

Figure 3.6 (b) Simulation result of P_{out} at 13 Hz

Figure 3.7 shows the simulation results of P_{out}, P_{in} and V_{in} when f is 10Hz and k is 1300 N/m. The comparison between Figure 3.7 and 3.5 shows that the shapes of the simulated P_{out}-V_{in} and P_{in}-V_{in} curves are the same as those calculated curves. The maximum input power and the maximum output power in the simulated curve are

0.04 % higher than those in the calculated curves. These slight magnitude differences are due to neglecting the inductor impedance.

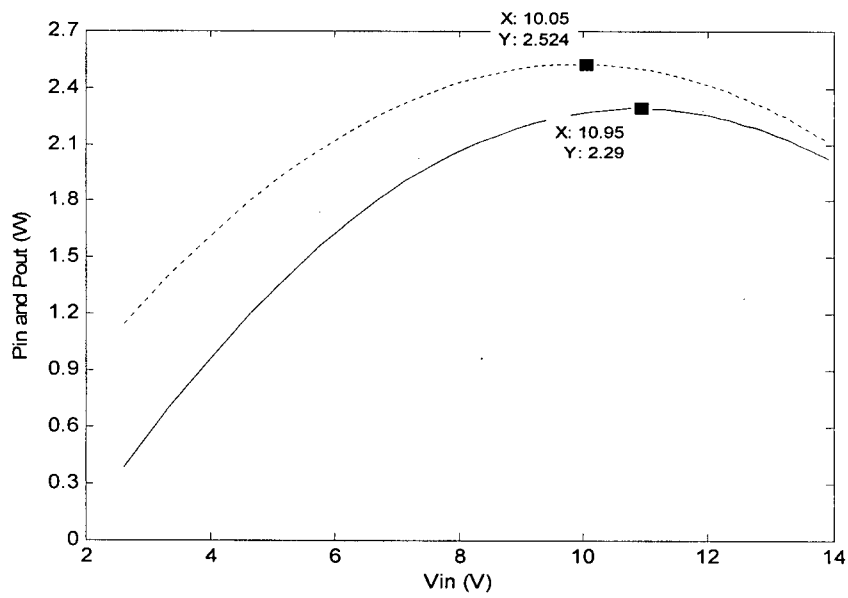

Figure 3.7 Simulation result of P_{out}, P_{in} vs V_{in} when $f_1 = 5\,\text{Hz}$, $k = 1300\,\text{N/m}$

3.5 Effect of Harmonics

Harmonics are sinusoidal waveforms with frequencies that are integral multiples of the fundamental frequency. For example, a waveform that has twice the frequency of the fundamental frequency is called the second harmonic. All repetitive waveforms are formed by the addition of harmonics. In the low-frequency range, the main sources of ship vibration are the working machinery. These machines' types (diesel engines, gearboxes and generators, and the propeller/propulsion system) and their speed levels (low, medium and high) will affect their vibration frequencies and generate harmonics. Hence, the fundamental vibration frequency and harmonics change with time and conditions.

Suppose higher orders of harmonics will quickly dies away and only 2nd or 3rd harmonic is relative stable, we can form the vibration signal as

$$y(t) = Y_1 \sin \omega t + Y_2 \sin(2\omega t + \alpha_1) + Y_3 \sin(3\omega t + \alpha_2) \qquad (3.21)$$

where Y_1, Y_2, Y_3 are displacement magnitudes of the fundamental frequency, 2nd harmonic and 3rd harmonic respectively. α_1 and α_2 are phase angle of 2nd harmonic and 3rd harmonic respectively. Figure 3.8 shows the power spectrum for signal

$$y(t) = 0.005[\sin(2\pi * 5 * t) + 0.5 * \sin(2\pi * 10 * t + 6/\pi) + 0.3 * \sin(2\pi * 15 * t + 3/\pi)]$$

As the power spectrum describes how power of a signal is distributed with frequencies, the three peaks in Figure 3.8 represents that the fundamental frequency and harmonics carry most amount of the signal power.

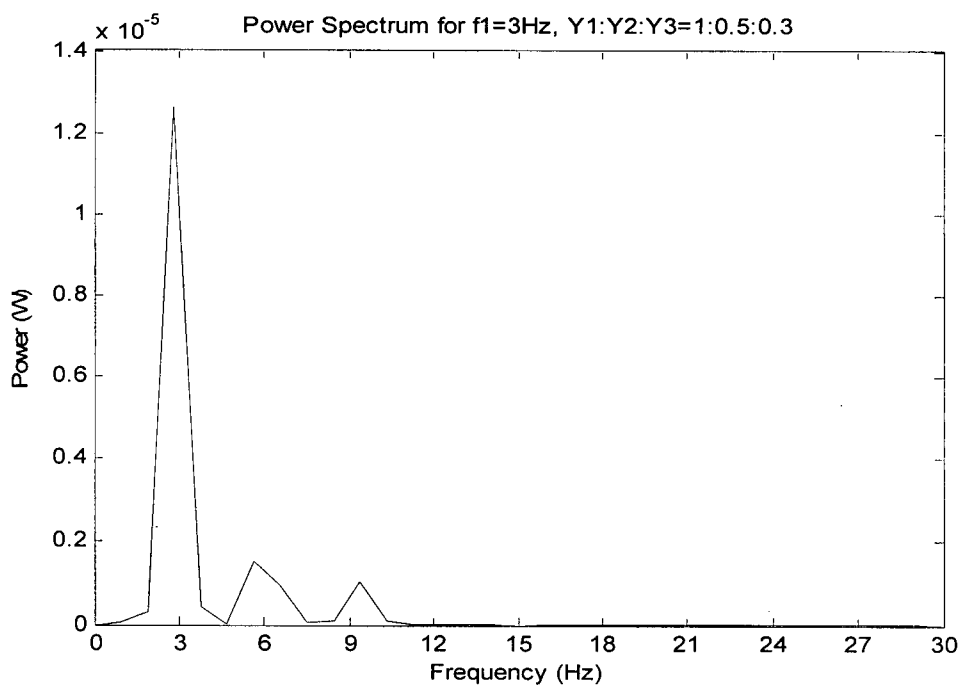

Figure 3.8 Fundamental, 2nd and 3rd harmonics power spectrum density when $f_1 = 3\,\text{Hz}$,

$$Y_1 = 5\text{ mm},\ Y_1 : Y_2 : Y_3 = 1 : 0.5 : 0.3$$

3.5.1 Effect of Harmonics on Output Voltage

Since the transfer function from V_{out} to Y_1 is linear, the system response of V_{out} to the vibration signal in equation 3.21 is the sum of the fundamental frequency, 2nd harmonic and 3rd harmonic responses. As the fundamental frequency response may be smaller than the

harmonics responses, we rename the fundamental, 2nd and 3rd harmonic as: f_1, f_2 and f_3. The model in Figure 3.9 is used to test f_2 and f_3 effects in the output voltage. In section 3.5.1 and 3.5.2, f_2 and f_3 are supposed to be in phase with f_1.

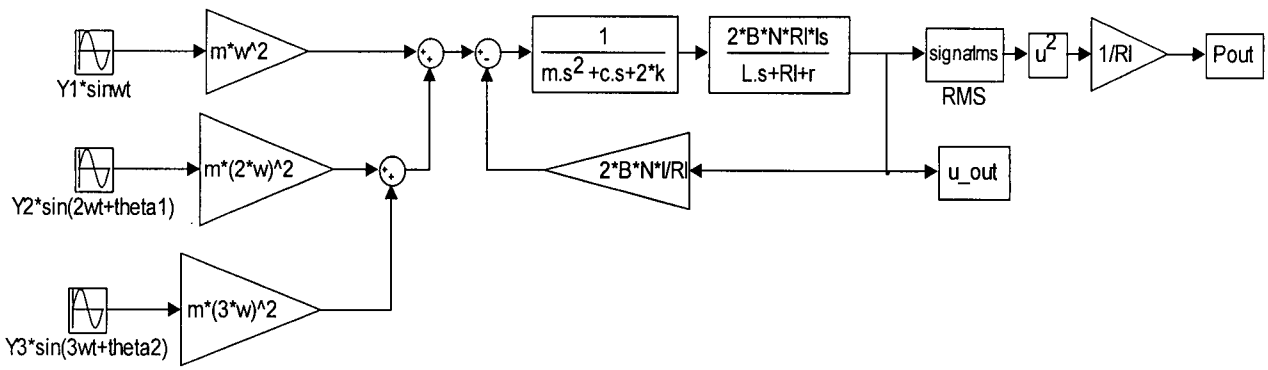

Figure 3.9 Simulation model for harmonics effect

We can see from Figure 3.10, V_{out} waveform not only depends on the magnitude ratio (rp) of f_1, f_2 and f_3, but also depends on the spring constant. When k is resonant at f_1, the shape of V_{out} is close to a sine wave with frequency f_1. When k is resonant at f_2 or f_3 and magnitude of f_2 or f_3 is above certain values such as $Y_2 > 0.09Y_1$ or $Y_3 > 0.02Y_1$, the sine wave form is distorted and the number of zero crossing points in a fixed period will be doubled or tripled. This is because the linear generator (second order system) resonant at f_2 or f_3 can get dramatically large relative movement of the magnets at this frequency which in turns increases the induced voltage and distorts the normal sine wave.

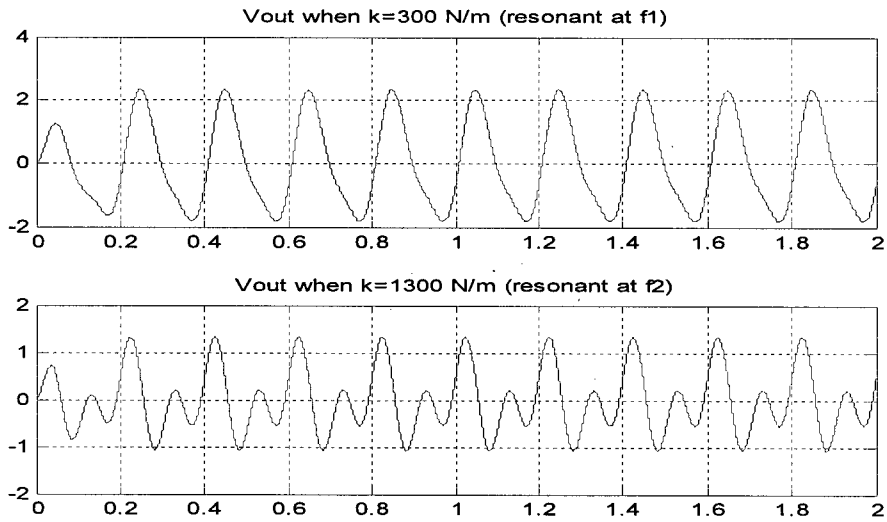

Figure7 3.10 a) V_{out} at $k = 300$ and 1300 N/m when $f_1 = 5$ Hz, $Y_2 = 0.12Y_1$

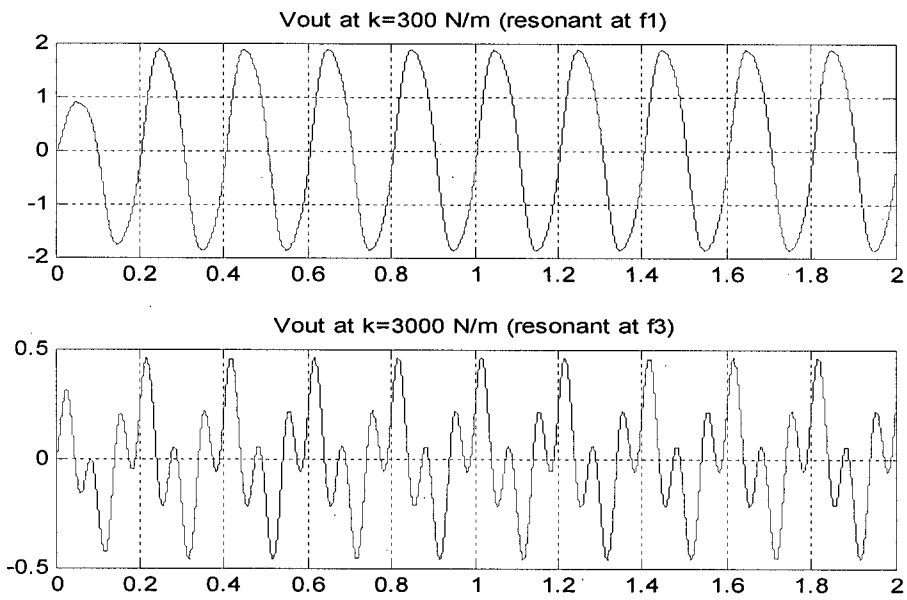

Figure 3.10 b) V_{out} at $k = 300$ and 3000 N/m when $f_1 = 5$ Hz, $Y_3 = 0.02Y_1$

3.5.2 Effect of Harmonics on Output Power

In second order LTI system $m\ddot{z}(t)+(c_e+c_m)\dot{z}(t)+kz(t)=-m\ddot{y}(t)$, the system response of $z(t)$ for vibration signal in equation 3.21 is the sum of f_1, f_2 and f_3 response: $z(t)=z_1(t)+z_2(t)+z_3(t)$. If we just consider f_1 and f_2, the relative displacement of the mass can be calculated as in section 3.1.1:

$$z(t)=z_1(t)+z_2(t)=Z_1\beta_1\sin(\omega t-\varphi_1)+Z_2\beta_2\sin(2\omega t-\varphi_2)$$

where

$$Z_1=\frac{m\omega^2 Y_1}{k}, \qquad \beta_1=\frac{1}{\sqrt{(1-\omega_c^2)^2+(2\omega_c\zeta)^2}}$$

$$Z_2=\frac{4m\omega^2 Y_2}{k}, \qquad \beta_2=\frac{1}{\sqrt{(1-4\omega_c^2)^2+(4\omega_c\zeta)^2}}$$

$$\varphi_1=\tan^{-1}\left(\frac{2\omega_c\zeta}{1-\omega_c^2}\right) \qquad \varphi_2=\tan^{-1}\left(\frac{4\omega_c\zeta}{1-4\omega_c^2}\right)$$

The energy stored in the electrical system per cycle is

$$W=\int_0^{2\pi/\omega} c_e\,\dot{z}\,\dot{z}\,dt$$

$$=\pi c\omega(Z_1^2\beta_1^2+4Z_2^2\beta_2^2)$$

The average power convert to the electrical system is

$$P_{in}=\frac{W}{2\pi/\omega}$$

$$=m\omega^3\omega_c^3\zeta_e\left[\frac{Y_1^2}{(1-\omega_c{}^2)^2+(2\zeta\omega_c)^2}+\frac{64Y_2{}^2}{(1-4\omega_c{}^2)^2+(4\zeta\omega_c)^2}\right] \qquad (3.22)$$

Figure 3.11 presents the theoretical input power calculated by equation 3.22 when f_1 is 5 Hz and Y_2 equals $0.1Y_1$, $0.35Y_2$, $0.5Y_2$ and $0.7Y_2$ respectively. When $Y_2=0.1Y_1$, P_{in} curve only has one peak of 0.308 W at $k=300$ N/m which makes the system resonant at 5

Hz. When Y_2 increases to $0.35Y_1$, two peaks appear in the curve. A global peak of 0.362 W is achieved at $k = 300$ N/m, while a local peak of 0.325 W is achieved at $k = 1300$ N/m which makes the system resonant at 10 Hz. When Y_2 increases to $0.5Y_1$, the positions of global peak and local peak alternate. The global peak of 0.64 W is achieved at $k = 1300$ N/m whereas the local peak of 0.468 W is achieved at $k = 300$ N/m. When Y_2 reaches $0.7Y_1$, again only one peak exists: $P_{in\_\max} = 1.251$ W at $k = 1300$ N/m.

The reason why a local maximum appears only at the resonant values is that resonance can considerably strengthens the power increase at that frequency caused by rp increase. A local maximum can transform to a global maximum if rp is big enough, say 0.5. Since the optimal value of k corresponding to $P_{out\_\max}$ is only slightly larger than which corresponds to $P_{in\_\max}$, it is also near the resonant value at f_1 or f_2 depending on rp (see Figure 3.12).

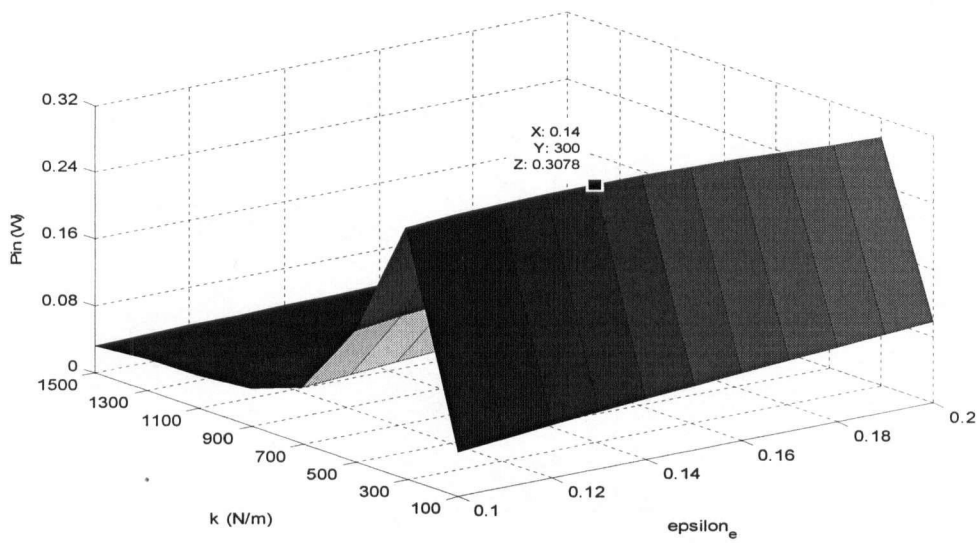

Figure 3.11 a) Calculated P_{in} at $Y_2 = 0.1Y_1$, $f_1 = 5$ Hz

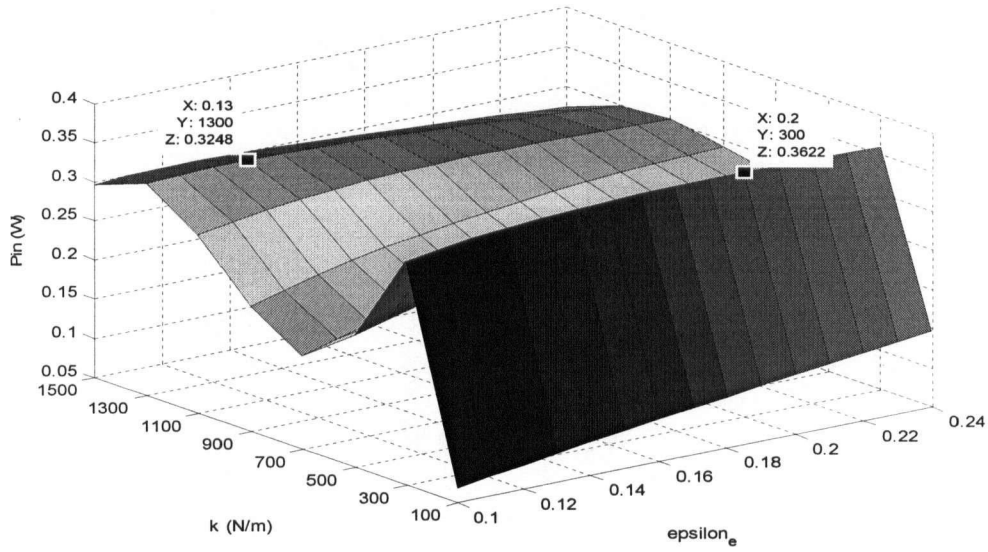

Figure 3.11 b) Calculated P_{in} at $Y_2 = 0.35Y_1$, $f_1 = 5\,\text{Hz}$

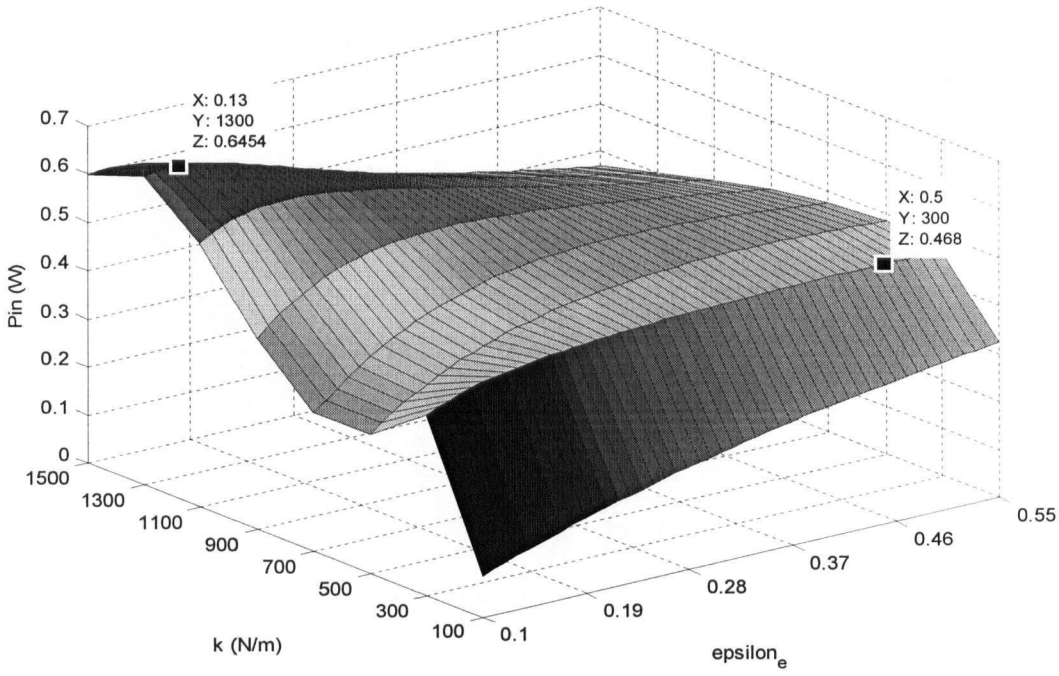

Figure 3.11 c) Calculated P_{in} at $Y_2 = 0.5Y_1$, $f_1 = 5\,\text{Hz}$

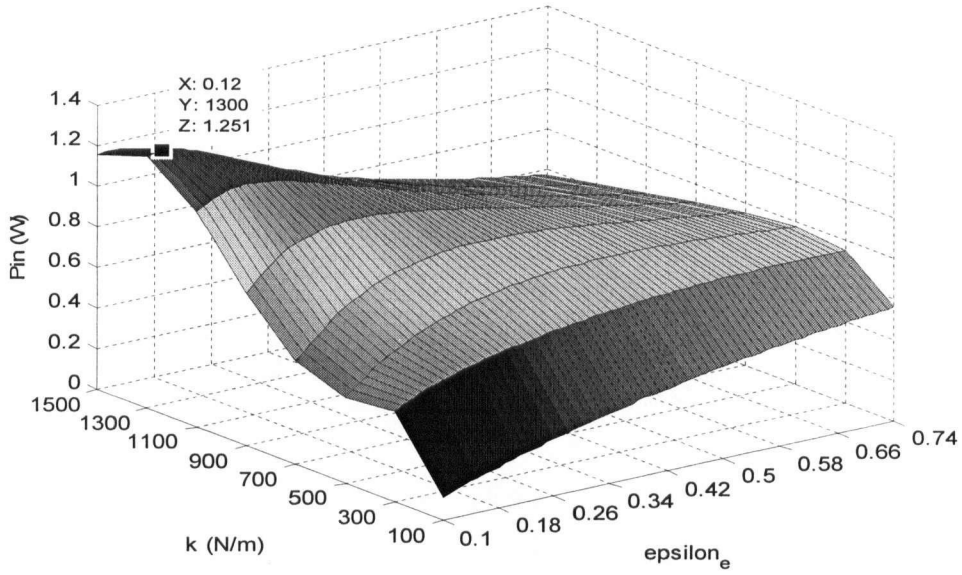

Figure 3.11 d) Calculated P_{in} at $Y_2 = 0.7Y_1$, $f_1 = 5\,\text{Hz}$

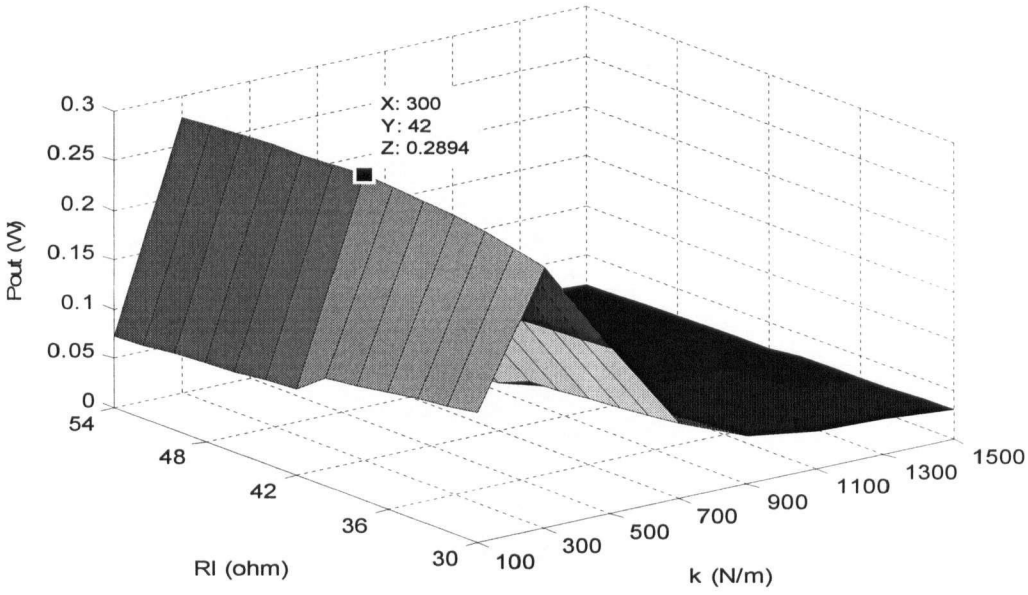

Figure 3.12 a) Simulated P_{out} at $Y_2 = 0.1Y_1$, $f_1 = 5\,\text{Hz}$

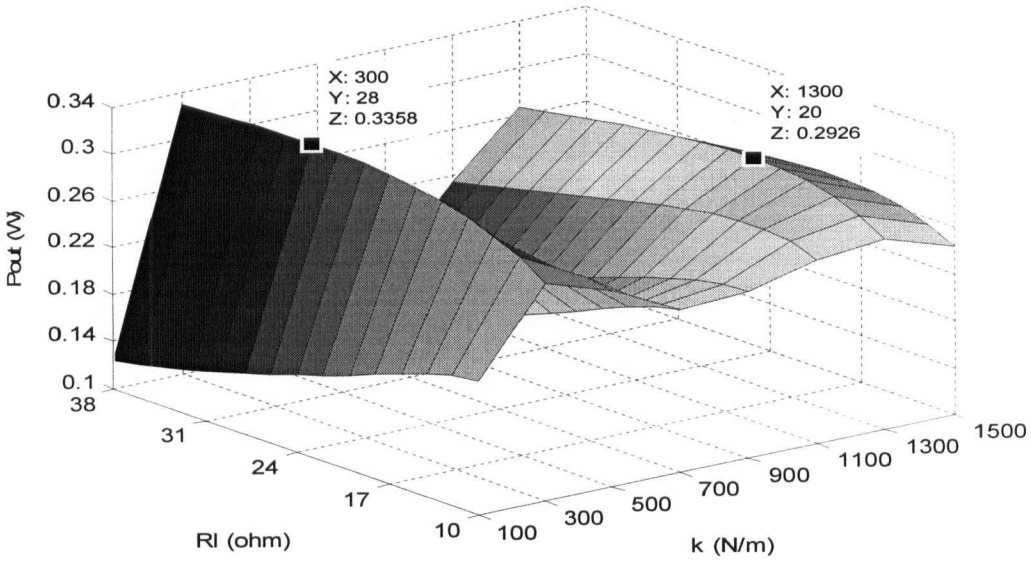

Figure 3.12 b) Simulated P_{out} at $Y_2 = 0.35Y_1$, $f_1 = 5\,\text{Hz}$

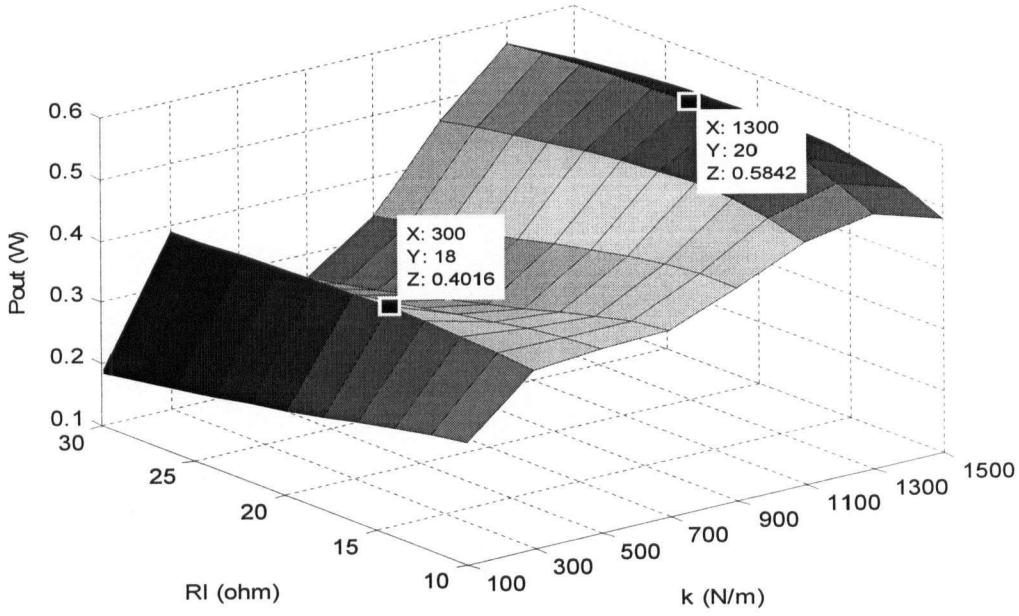

Figure 3.12 c) Simulated P_{out} at $Y_2 = 0.5Y_1$, $f_1 = 5\,\text{Hz}$

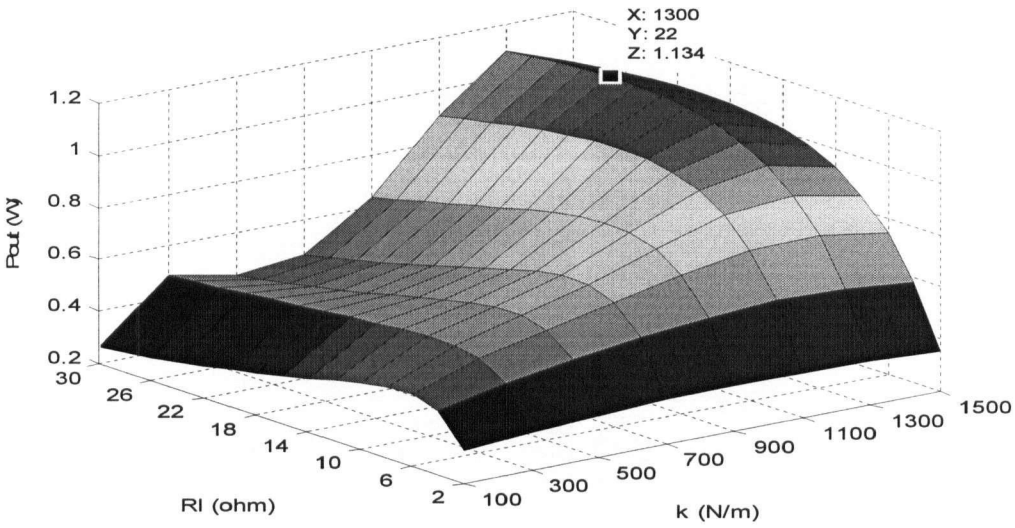

Figure 3.12 d) Simulated P_{out} at $Y_2 = 0.7Y_1$, $f_1 = 5\,\text{Hz}$

After f_3 is added in the vibration signals, the optimal value of k for $P_{out\_\max}$ should be chosen among the resonant values at f_1, f_2 and f_3. Figure 3.13 show that the increase of rp causes the optimal value of k to rise from 300 N/m to 1300 N/m and stops at 2900 N/m. This proves the optimal value of k does have three choices according to different rp.

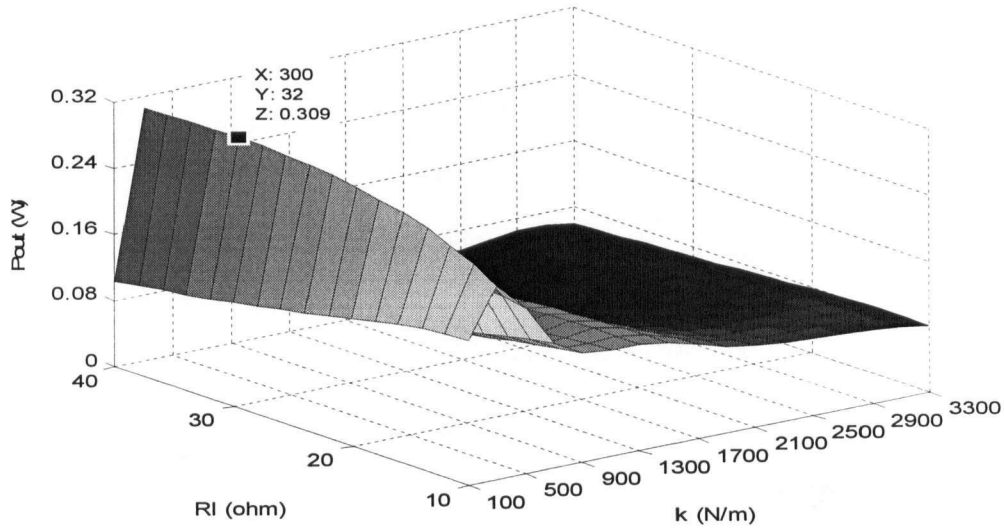

Figure 3.13 a) Simulated P_{out} at $Y_1 : Y_2 : Y_3 = 1 : 0.2 : 0.1$, $f_1 = 5\,\text{Hz}$

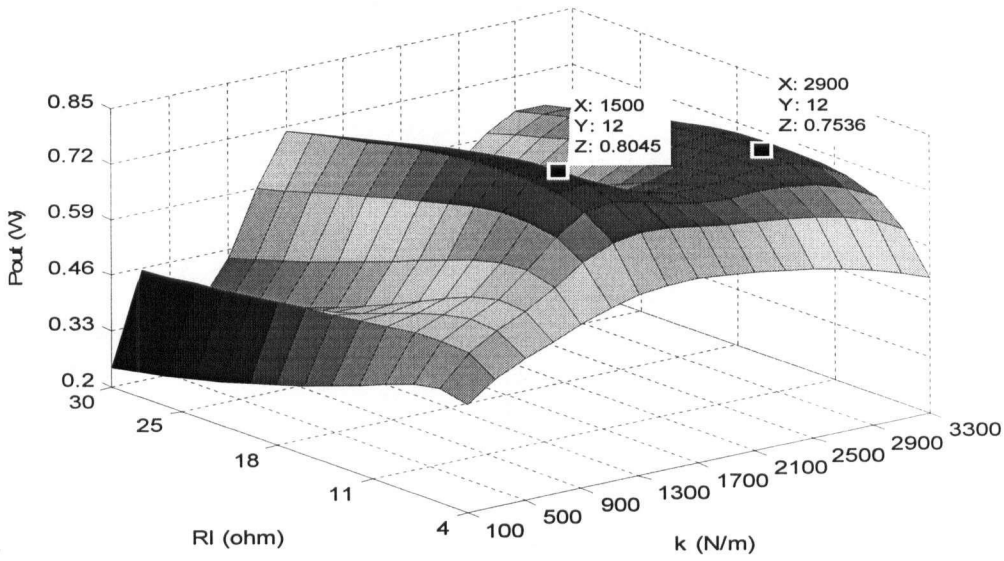

Figure 3.13 b) Simulated P_{out} at $Y_1 : Y_2 : Y_3 = 1 : 0.5 : 0.3$, $f_1 = 5\,\text{Hz}$

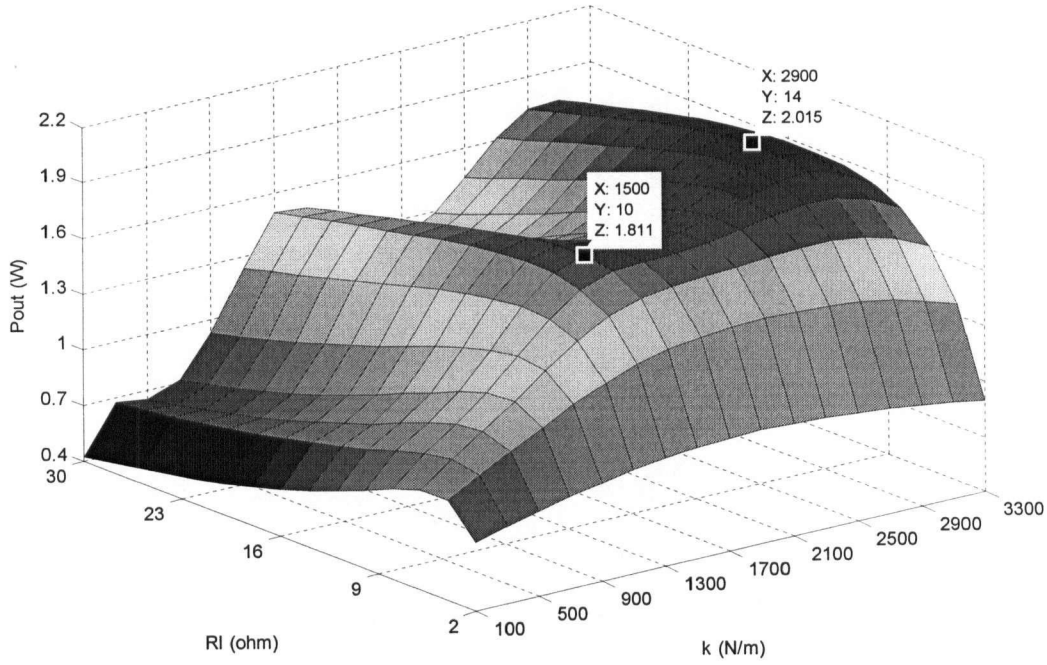

Figure 3.13 c) Simulated P_{out} at $Y_1 : Y_2 : Y_3 = 1 : 0.7 : 0.5$, $f_1 = 5\,\text{Hz}$

3.5.3 Effect of Phase Angle

Phase angles in the harmonics cause distortion in waveform of the induced voltage. The measured frequency of V_{out} by means of zero-crossing can be different according to phase angle even though other parameters are all the same. Figure 3.15 shows the waveform of V_{out} when f_1= 5 Hz with different phase angles of f_2. When phase angle is 0, $\pi/2$ and π, the measured frequency of V_{out} (f_v) is 10 Hz. When phase angle is $\pi/3$ and $2\pi/3$, f_v is 5 Hz. The output power at different phase angles are all equal to 0.0353 W.

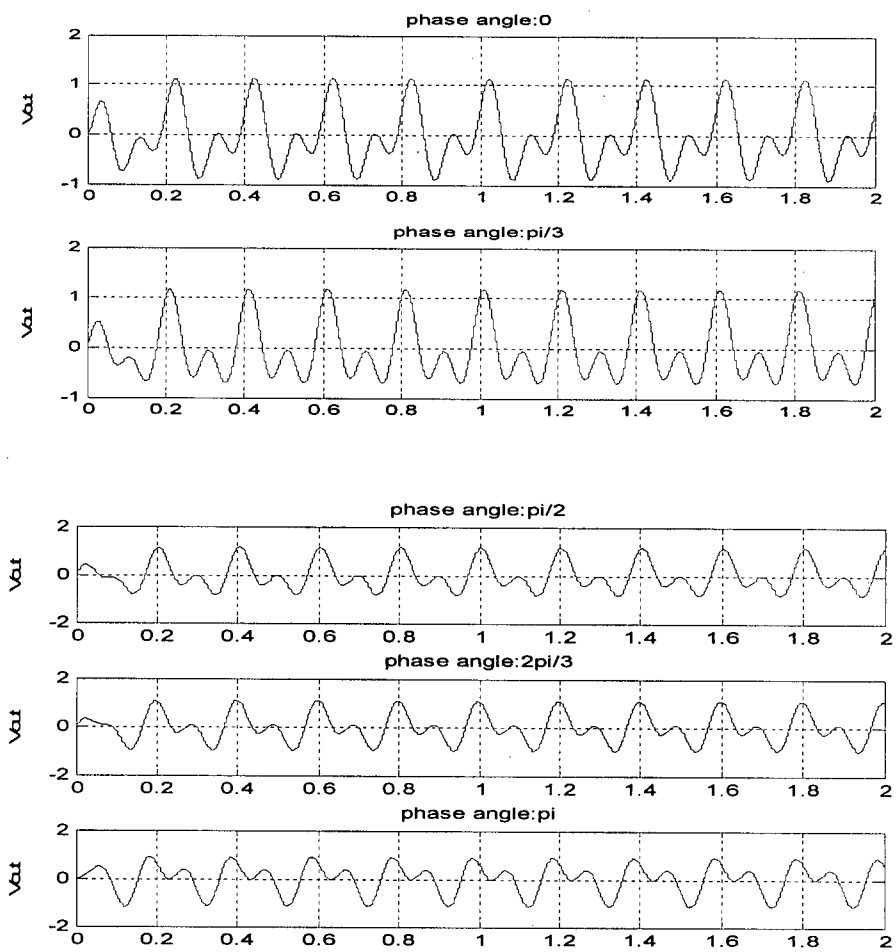

Figure 3.14 Waveform of V_{out} at different phase angle of f_2 when $f_1 = 5$ Hz,

$$Y_2 = 0.09Y_1,\ k = 1300\ \text{N/m},\ R_l = 10\,\Omega$$

3.5.4 Initialization of k Based on Harmonics

In this project, we use a zero crossing detector attached to the coils to measure the frequency of V_{out} (f_v). If the vibration signal is a pure sine wave, this frequency will be the same as f_1. However, for the existence of harmonics, f_v is affected by rp, k and phase angle and so can be the harmonic frequency (f_2 or f_3). Thus, f_1 can equals f_v, $f_v/2$ or $f_v/3$, f_2 can equals $2f_v$, f_v and $2f_v/3$ while f_3 can equals $3f_v$, $3f_v/2$ and f_v. Since P_{out} can be maximized when k is among the resonant values at f_1, f_2 or f_3, we need to test these values and pick an optimal one as a start point in hill climbing method (will be discussed in section 5.3).

The initiation process is shown as following:

1) Measure frequency of V_{out} at $k = 1300$ N/m and change the value of k to resonant at f_v.

2) Measure the frequency of V_{out} again. If the new frequency does not equal the previous frequency, change the value of k so that the system's natural frequency is identical to the new frequency. The value of k will keep changing until the measured frequency f_v equals the natural frequency.

3) Adjust k to make the natural frequency equal $f_v/3$, $f_v/2$, $2f_v$ and $3f_v$ respectively and measure the frequency of V_{out}. If any measured frequency equals the natural frequency, this frequency is contained in the vibration spectrum as a harmonic or subharmonic. Also, compare the resulting output power at each frequency. If any of the four frequencies is close to the already measured frequencies in step 2, skip the adjustment according to this frequency.

4) Finally, the initial value of k is set to the value corresponding to the largest power.

3.6 Summary

In this chapter, parameters optimization has been proposed in term of maximum power. The input electrical power (P_{in}) can be roughly estimated by equation 3.3 given only the magnitude and frequency of the driving vibrations. The principle of designing harvester has been presented based on this equation. After the energy harvester is fabricated, for a resistive load, the only tunable parameters are k and R_l. k should be tuned to resonate at the vibration frequency since P_{in} falls off dramatically if the natural frequency of the linear generator does not match that of the driving vibrations. R_l should be tuned to make the electrical damping factor equal the mechanical damping factor. In reality, the load will not be as simple as a resistor. However, it will remove kinetic energy from the vibrating system, and so act as an electrical damper [9]. Even with a more complicated load circuitry, some circuit parameters can be adjusted such that the power transfer to the load is maximized.

The correlation between the induced voltage (V_{in}) and P_{in} is presented based on the optimal expressions of k and R_l. It has been validated that P_{in}-V_{in} curve is convex and the optimal value of V_{in} is not affected by the load resistance. Thus, this relation will also hold in other circuitries so that some circuit parameters can be changed to affect the induced voltage and achieve maximum power. Although the optimal expressions of k, R_l and V_{in} are deducted on behalf of P_{in}, the relations still fit for the power output. Also, the differences between the two sets of optimal values are small. We can further increase the values of k, R_l and V_{in} to achieve maximum power output after the maximum P_{in} is achieved. Finally, the effects of harmonics are discussed. The harmonics can deform the voltage waveform and introduce local maxima in the power surface. An initiation process of k should be used to pick out the frequency which carries the largest power among the spectrum and set k to resonant at this frequency.

Chapter 4 Power Management Circuit

The above analysis and optimization is based on a simple resistive load. However, a capacitive load is more like a realistic electrical load than a resistive load. Due to the relation of P_{in}-V_{in}, the induced voltage should be rectified and conditioned by power electronics to an optimal value to maximally charge a supercapacitor. A full bridge rectifier with capacitor filter is used to convert AC current to DC. A PWM controlled DC-DC converter is placed between the rectifier output and the supercapacitor to facilitate the attainment of the optimal voltage by controlling its duty cycle. In each section, an inherent element in the power management circuit is discussed separately.

4.1 Full Bridge Rectifier

A full wave bridge rectifier is a circuit, which converts an AC voltage into a pulsating DC voltage using both half cycles of the applied AC voltage. It uses four diodes of which two conduct during one half cycle while the other two conduct during the other half cycle of the AC voltage while the load pass current remains in the same direction in each half cycle [20]. After rectification, the load has a large pulsating voltage (ripple) compared with the average component. A capacitor filter in parallel with the load is needed to smooth out the pulsation.

The schematic of the full wave bridge rectifier with a capacitor filter is shown in Figure 4.1 and the filtering voltage is shown in Figure 4.2.

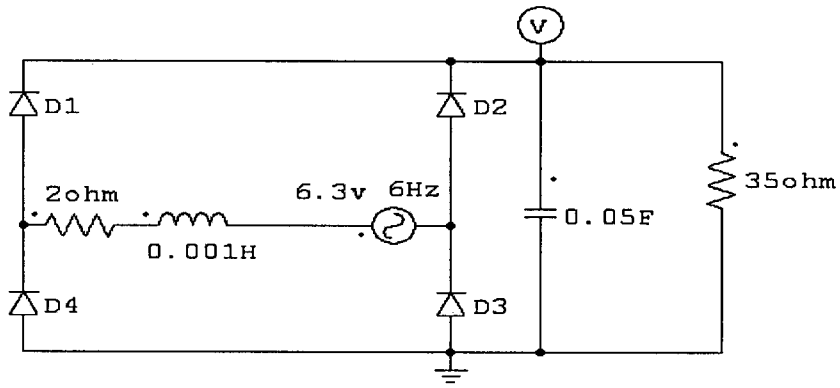

Figure 4.1 A full bridge rectifier with a capacitor filter

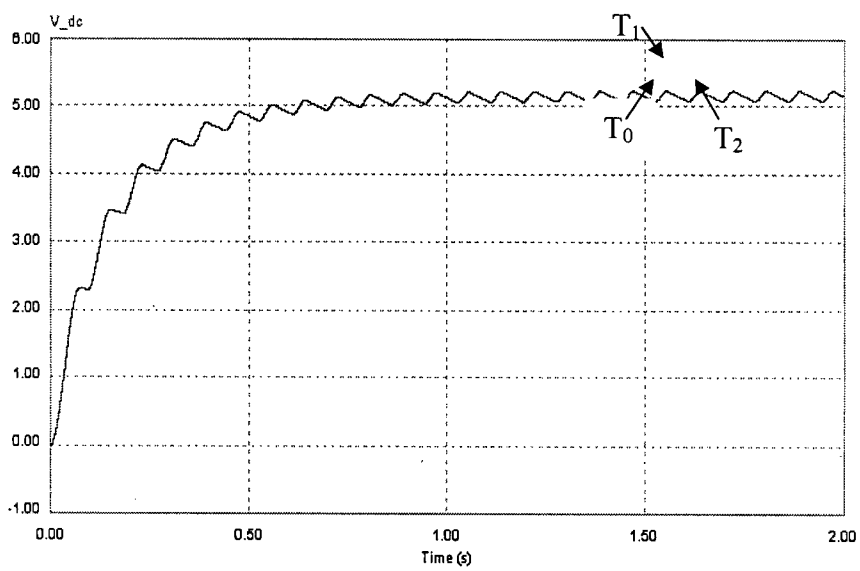

Figure 4.2 Filtering voltage of full bridge rectifier

In the time period from T_0 to T_1, diodes D1, D3 (or D2, D4, depending on the phase of input voltage) are forward biased since the source voltage is higher than capacitor voltage. The capacitor charges and the load voltage increases. From T_1 to T_2, the diodes D1, D3 are reverse biased since the source voltage begins to decrease after it achieved peak value and the capacitor voltage is higher than the source voltage. The capacitor discharges and the load voltage reduce. The load voltage during this discharging period is [21]:

$$V_{out}(t) = V_{\max} e^{-\frac{(t-T_1)}{R_l C}} \tag{4.1}$$

where

R_l = load resistance (Ω)

C = capacitance (F)

$V_{\max}$ = source voltage amplitude (V)

The peak to peak voltage ripple is

$$\begin{aligned} V_{pp} &= V_{out}(T_1) - V_{out}(T_2) \\ &= V_{\max}(1 - e^{-\frac{(T_2-T_1)}{R_l C}}) \\ &\approx V_{\max} \frac{(T_2 - T_1)}{R_l C} \qquad (R_l C \gg T_2 - T_1) \end{aligned} \tag{4.2}$$

Since $T_2 - T_1 \sim T/2$, where T is the period of source voltage, the above equation can be written as [20]

$$V_{pp} = \frac{V_{\max}}{2 f R_l C} \tag{4.3}$$

Suppose the frequency of source voltage is 6 Hz and the ripple is 5 % of the peak voltage, we can assume other parameters in equation 4.3 by using values from Table 3 in Appendix B: $V_{\max}$ = 6.3 V, R_l = 35 Ω. The calculated capacitance is 0.05 F.

4.2 DC-DC Converter

4.2.1 Overview

A DC-DC converter is a switch mode regulator that accepts a DC input voltage and produces a DC output voltage of the same or opposite polarity. Typically the output voltage is at a different level than the input. The main principle of the switch mode regulator is a high frequency switch turning on and off to get a lower (buck converter) or higher average

out voltage (boost converter). The output voltage variations caused by the switching are filtered out by an LC filter. The switch mode regulator is better than a linear regulator in that it doesn't dissipate any power internally (except for some small resistive losses).

The DC-DC converter has three topologies: buck, boost and buck-boost (or Cuk). A buck converter lowers the input voltage and a boost converter increases the input voltage while both of them keep the same polarity. A buck-boost or Cuk converter can either increase or decrease the magnitude of the input voltage and inverts the polarity [22]. As we can see from Table 3 in Appendix B, the optimal values of k corresponding to the maximum output power are all higher than 3 V except at 3 Hz. Suppose the initial supercapacitor's voltage is 3 V, a buck converter can be used at most cases in simulation to maintain the induced voltage around the optimal value. However, if the supercapacitor's voltage is higher than the optimal value, a buck-boost converter would be used. Furthermore, the DC-DC converter in this thesis, in spite of its type, is designed to work in continuous mode by correctly choosing the value of inductor.

4.2.2 Buck Converter

Figure 4.3 shows schematic of a buck converter after a full bridge rectifier. When the switch (Mosfet) is on, the voltage after the switch is equal to the input voltage. So the inductor voltage is $V_L = V_{in} - V_{out}$. During this period, the current through the inductor increases as well as the energy stored in the inductor. When the switch is off, the inductor acts as a source and maintains current flow with the flywheel diode on. During this period, $V_L = -V_{out}$ and the energy stored in the inductor decreases as its current falls. According to *Inductor Volt-second balance* principle stated in [23], the integration over one completes switching period of inductor voltage is zero which means

$$\int_0^{T_s} V_L(t)dt = (V_{in} - V_{out})DT_s + (-V_{out})(1-D)T_s = 0$$

where

D = Duty cycle of switching signal

T_s = Period of switching signal

Solution for V_{out} yields

$$V_{out} = DV_{in} \tag{4.4}$$

The inductor in the buck converter can reduce the ripple in current. During the first interval, the slope of the inductor current waveform is

$$\frac{di_L(t)}{dt} = \frac{V_{in} - V_{out}}{L}$$

Hence, the peak to peak ripple is

$$i_{L-pp} = \frac{V_{in} - V_{out}}{L} DT_s$$

To get a desired current ripple the inductance should be chosen larger than

$$L = \frac{V_{in} - V_{out}}{i_{L-pp}} DT_s \tag{4.5}$$

The load of the buck converter is a large supercapacitor with capacitance over 10 F. For a short charging period, the voltage change in the supercapacitor can be neglected. Therefore, the supercapacitor can be approximated to a fixed voltage source. Suppose the initial voltage of supercapacitor is 3 V and the peak to peak ripple current is no more than 0.03 amp (about 20% of the average inductor current), we can take the output voltage of full bridge rectifier in Figure 4.2 as the input of the buck converter and calculate the inductance by equation (4.5)

$$L \geq \frac{5.15-3}{0.03} * \frac{3}{5.15} * 10^{-3} = 0.04H$$

This inductance is sufficiently large to ensure operation in continuous conduction mode.

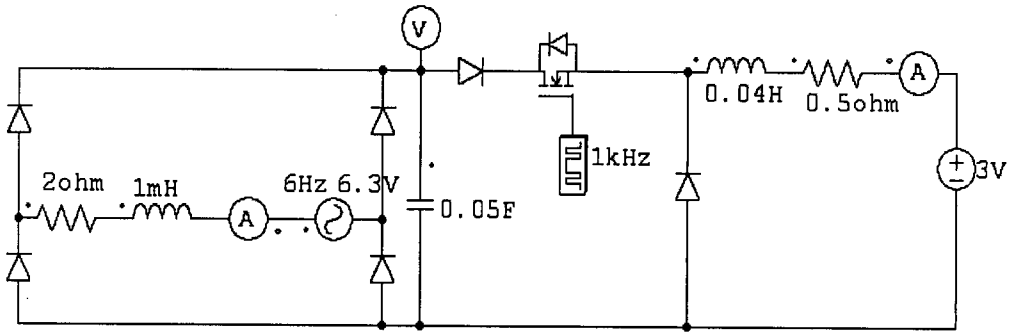

Figure 4.3 Topology of the power management circuit with a buck converter

4.2.3 Buck-Boost Converter

Figure 4.4 shows schematic of a buck-boost converter after a full bridge rectifier. When the switch is on, the input voltage is forced across the inductor $V_L = V_{in}$, causing an increasing current to flow through it and energy to store in the inductor. The diode is reverse biased so no energy is transferred to the supercapacitor. When the switch turns off, the inductor will reverse its polarity in order to maintain the peak current. This action turns on the diode, $V_L = V_{out}$, allowing the current in the inductor to charge the supercapacitor. Since the integration over one completes switching period of inductor voltage is zero: $V_{in}D + V_{out}(1-D) = 0$, which gives the voltage ratio:

$$\frac{V_{out}}{V_{in}} = \frac{D}{1-D} \tag{4.6}$$

During the first interval, the slope of the inductor current waveform is

$$\frac{di_L(t)}{dt} = \frac{V_{in}}{L}$$

To get a desired current ripple so the converter works in the continuous mode, the inductance should be chosen larger than

$$L = \frac{V_{in}}{i_{L-pp}} DT_s \tag{4.7}$$

Suppose the initial voltage of supercapacitor is 3V and the peak to peak ripple current is no more than 0.03 amp, the inductance is calculated by equation (4.7)

$$L \geq \frac{5.15}{0.03} * \frac{3}{8.15} * 10^{-3} = 0.06H$$

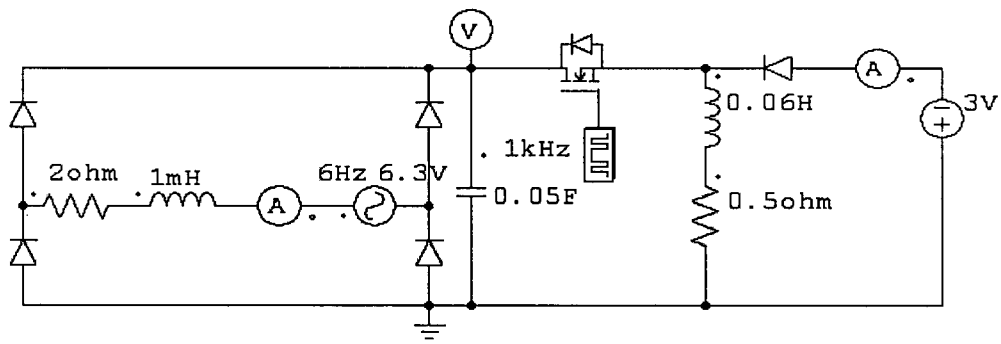

Figure 4.4 Topology of the power management circuit with a buck-boost converter

4.3. Supercapacitor

Supercapacitor, also known as ultracapacitor, resembles a regular capacitor with the exception that it offers very high capacitance in a small package [24]. Unlike normal capacitor which has capacitance of microfarads, supercapacitor has capacitance in order of Farads.

Supercapacitors are recognized as an excellent compromise between normal capacitor and batteries. Generally, supercapacitors have up to 80 times energy density than normal capacitors and up to 10 times power density than batteries [25]. Supercapacitors can charge and discharge in seconds with enormous current until a set voltage limit is reached and stop accepting charge. Whereas batteries take time to charge and discharge since the process involves chemical reactions with non-instantaneous rates. Besides, supercapacitor avoids many of battery's disadvantages [24]: it can be charged and discharged almost an unlimited number of times; it has a very long lifetime (in normal use, a supercapacitor deteriorates to about 80 percent after 10 years); it has lower impedance which enhances load handling when parallel with a battery; it produces very little hazardous substances that can damage

the environment; it does not release any thermal heat during discharge.

In this project, the supercapacitor is chosen as the means of energy storage rather than a rechargeable battery for two primary reasons. First, a capacitor can be charged up by any method. It can be slowly charged up by pulses of current from the energy harvester while rechargeable batteries generally prefer to be charged up quickly with relatively large currents [9]. In particular, lithium-ion batteries perform better when charged at constant current. This type of charge-up profile is simply not possible using a vibration generator unless sophisticated battery charging circuitry is used. However, the use of such circuits would greatly increase the power dissipation of the system, and therefore is not practical. The second reason is that rechargeable batteries have a relatively short life time. The life of a rechargeable battery operating under normal conditions is generally between 500 to 800 charge-discharge cycles, which means after 1 to 2 years of operation the batteries would need to be replaced [26].

Capacitors, on the other hand, have a virtually infinite lifetime as stated previously. However, the supercapacitor has some limitations in applications which need to be taken into consideration:

- Unable to use the full energy spectrum--- the voltage of the supercapacitor is linear and drops from full voltage to zero volts [24]. Because of this linear discharge, the supercapacitor can only deliver the amount of charge that guarantees the supercapacitor voltage above the voltage requirement of the application.
- Cells have low voltages - series connections are needed to obtain higher voltages. Voltage balancing is required if more than three capacitors are connected in series to protect single cell from overcharge.
- High self-discharge - the self-discharge of the supercapacitor is substantially higher than that of electrochemical battery. It is stated by Isidor Buchmann [24] that "In 30 to 40 days, the capacity decreases from full charge to 50 percent. In comparison, a nickel-based battery discharges about 10 percent during that time."

Chapter 5 Maximum Charging Current Tracking

A power management circuit to store and condition the output electrical power is designed in the previous chapter. In this chapter, a new simulation model is built using Matlab and Psim in which the load resistor in the model of linear generator is replaced by the power management circuit. An algorithm named MCCT is proposed to achieve maximum power flow to the supercapacitor under any conditions. The performance of the energy harvester is validated by simulations.

5.1 Overview

After the rectifier, the fundamental current is in phase with the rectified voltage which means approximating the voltage-current relation of the converter as a resistor is reasonable. As a consequence, the overall system in Figure 4.3 is equivalent to the simplified electrical system in Figure 2.5. Since the simulation results from Table 3 in Appendix B prove existence of maximum output power in the resistive load, adjusting duty cycle of the DC-DC converter lets the induced voltage shift on the $P_{out} - V_{in}$ curve and finally stops around the maximum power point.

As the supercapacitor's voltage changes very slowly, maximizing the power flow to the supercapacitor is equivalent to maximizing the current into the supercapacitor. Thus, we can consider the charging current as a target variable. An example of the relation between the charging current (i_{charge}) and the duty cycle is shown in Figure 5.1. The analysis in chapter 3 regarding $P_{out} - V_{in}$ relation can also be applied to $i_{charge} - D$ relation.

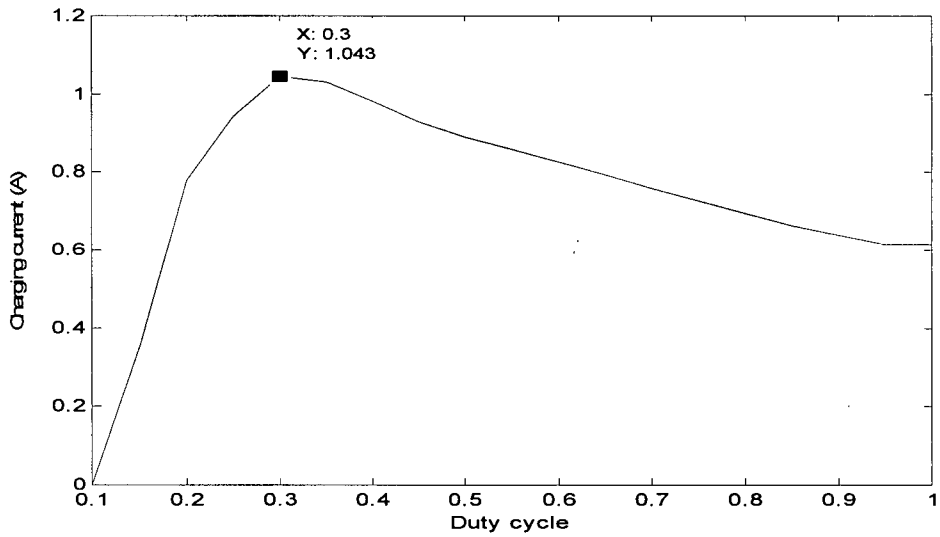

Figure 5.1 i_{charge} vs D (step size 0.05) when f =12 Hz, k = 2000 N/m

5.2 Simulation Tool

The vibration energy harvester contains two parts: i) a linear generator which can be modeled as a second order transfer function and feedback gain; ii) a power management circuit which consists of a rectifier, capacitor filter, dc-dc converter and supercapacitor. Since both the rectifier and converter work in switch mode, the electrical system has a nonlinear dynamic behavior which is hard to be described by transfer function. Thus, the electrical system will be simulated by circuit schematic. There are several simulation tools for modeling an electrical circuit: Psim, Pspice and Simpower. In order to easily represent transfer functions, build electrical circuit and speed simulation, Psim and Simulink will be used to simulate the overall system.

PSIM is a simulation package specifically designed for power electronics and motor control. With fast simulation, friendly user interface and waveform processing, PSIM provides a powerful simulation environment for power converter analysis [27]. Simulink is a software package for modeling, simulating, and analyzing dynamic systems. It has instant access to all the analysis tools in MATLAB, so users can take the results, analyze and

visualize them [28]. In this project, Simulink is used to simulate the mathematical model of linear generator and Psim is used to implement and simulate the electrical system in original circuit form. A module called SimCoupler in PSIM is used to interface with Matlab/Simulink for co-simulation so that part of a system can be implemented and simulated in PSIM, and the rest of the system in Simulink [29].

Certain restrictions are imposed on the selection of the solver type and the time step in Simulink when performing the PSIM-Matlab/Simulink co-simulation. In order to speed up simulation, the time step should be chosen as large as possible in Psim as well as in Simulink. Since switching frequency of DC-DC converter should be at least 1 kHz and the resolution of duty cycle is set to percentage, 50μs was chosen as step size for Psim. The step size of Simulink is set to 1ms so that Simulink can read the charge current from Psim every switching period.

The electrical circuit in Psim and mechanical model in Simulink are shown in Figure 5.2 and Figure 5.3 respectively. There are two In-Link Nodes and three Out-Link Nodes in Psim electrical circuit. An In-Link Node receives a value from Simulink, and behaves as a voltage source. An Out-Link Node passes a value to Simulink [29]. Each node's function is presented in Table 5.1. Since the In Link Node "Uin" only has one end, a voltage controlled voltage source with unity gain is used to connect it to the two-ends rectifier. A fixed frequency (1 kHz) PWM square wave signal is generated by comparing a sawtooth wave with a steady reference voltage. This reference voltage is duty cycle of the square wave which can vary between 0 and 1 according to the received value of In Link Node "Duty".

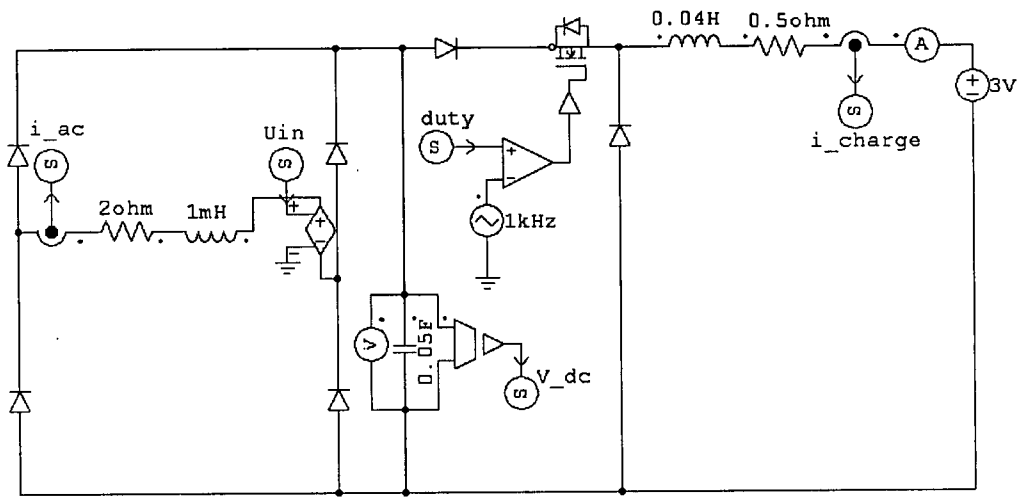

Figure 5.2 Simulation Schematic of Power Management Circuit

Note: In order to save simulation time and eliminate the effect of variation in the supercapacitor's voltage (v_{cap}), a constant dc voltage source is used to replace the supercapacitor.

In Link Node	Description
Uin	Input voltage of electrical system
Duty	Duty cycle of buck converter
Out Link Node	**Description**
i_ac	Input current of electrical system
i_charge	Charging current of supercapacitor
V_dc	Smoothed DC voltage, Input voltage of the buck converter

Table 5.1 Node function description

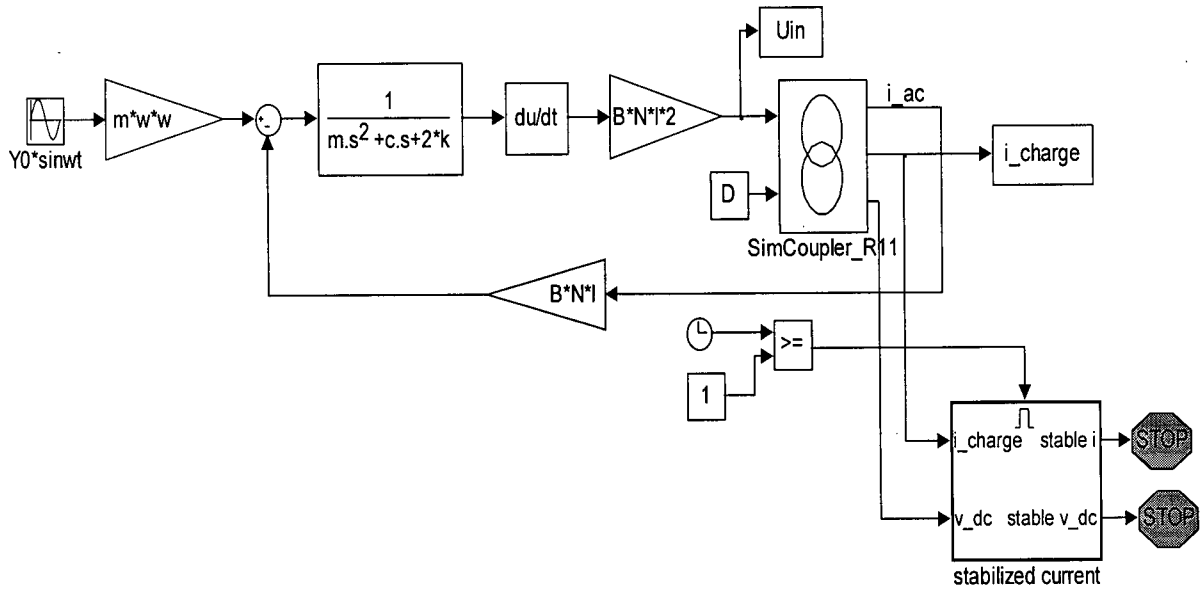

Figure 5.3 Simulink model of the energy harvester

5.3 Maximum Charging Current Tracking (MCCT) Algorithm

Under most conditions, the charging current will not be at the maximum point. Moreover, the maximum point varies constantly with environmental conditions: ship vibration frequency, displacement magnitude and mechanical damping factor. A maximum charging current tracking (MCCT) algorithm is used in a microcontroller to maximize power flow into the supercapacitor under all conditions. A flow chart in Figure 5.7 shows the working process of the energy harvesting under MCCT control.

5.3.1 Initiation Process of k

When the energy harvester first starts to work, the initial values of k and D are set to 1300 N/m and 1(100 percents). Then, the frequency of the induced voltage (f_v) is measured in a block called "measure frequency" in model "mfv1" using zero up-crossing detection. If vibrations are concentrated at a single frequency and are sinusoidal in nature,

the initiation of k is done simply by finding the spring constant value in Table 3.1 corresponding to this frequency.

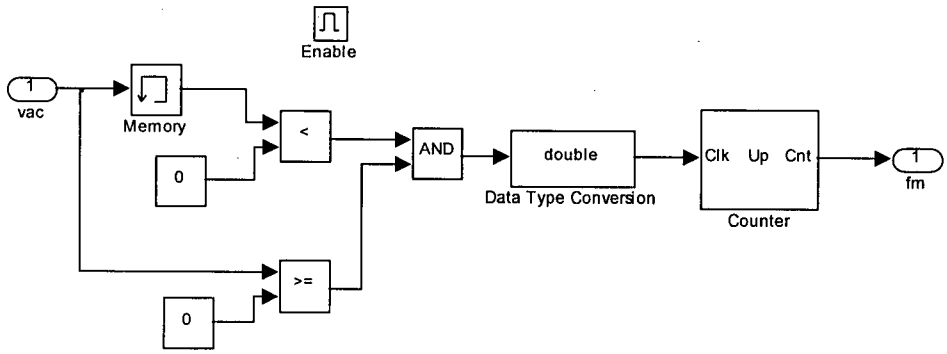

Figure 5.4 Block diagram of subsystem "measure frequency"

If the vibration signals contain harmonics as stated in section 3.5, f_v can be the fundamental frequency or harmonics. In order to escape from local maxima in Figure 3.12 or Figure 3.13, the testing process in section 3.5.4 is used to determine the optimal area of k and rewritten as below:

1) Measure frequency of the induced voltage (f_v) at $k = 1300\,\text{N/m}$, $D = 1$ and change the value of k to resonant at f_v.

2) Measure frequency of the induced voltage again. If the new frequency is not equal to the previous frequency, change the value of k so that the system's natural frequency is identical to the new frequency. The value of k will keep changing until the measured frequency f_v equals the natural frequency.

3) Adjust k to make the natural frequency equals $f_v/3$, $f_v/2$, $2f_v$ and $3f_v$ respectively and measure frequency of the induced voltage. If any measured frequency equals the natural frequency, this frequency is contained in the vibration spectrum as a harmonic or subharmonic. Also, compare the resulting charging current at each frequency. If any of the four frequencies is close to the already measured frequencies in step 2, skip the adjustment according to this frequency.

4) Finally, the initial value of k is set to the value corresponding to the largest charging current.

5.3.2 Stabilized Current Measurement

The charging current will change if any variation happens in the environmental conditions or the supercapacitor's voltage. Due to large capacitors and inductor in the electrical circuit, the total system response to parameters changes is slow and contains oscillation. It usually takes several seconds in simulation and even longer time in real system before the charging current stabilizes. Thus, a criterion is needed to decide whether the current is stable or not: when the charging current is higher than 2 mA and does not change more than 2 mA within 1 s, it is considered stable and the average charging current within the last 0.5 s is recorded as i_{charge}. Furthermore, it is possible to have no charging current at all if the stabilized input voltage of the converter (v_{dc}) is not higher than v_{cap}/D. In this case, another criterion is needed to stop measuring the current: when v_{dc} does not change more than 0.01 V within 1 s and the charging current is lower than 2 mA as well as v_{dc} is lower than v_{cap}/D, i_{charge} is recorded as zero. Then, two ways can be used to increase the current: if the measured f_v is different from the natural frequency, k needs to be adjusted to resonant at f_v; otherwise D needs to be increased by $D = D + 0.04$ until the current is above 2 mA. Figure 5.5 presents the implementation of these criteria in a subsystem named "stabilized current". In the subsystem, 1s delay is used in Transport Delay Block to delay the charging current by one second.

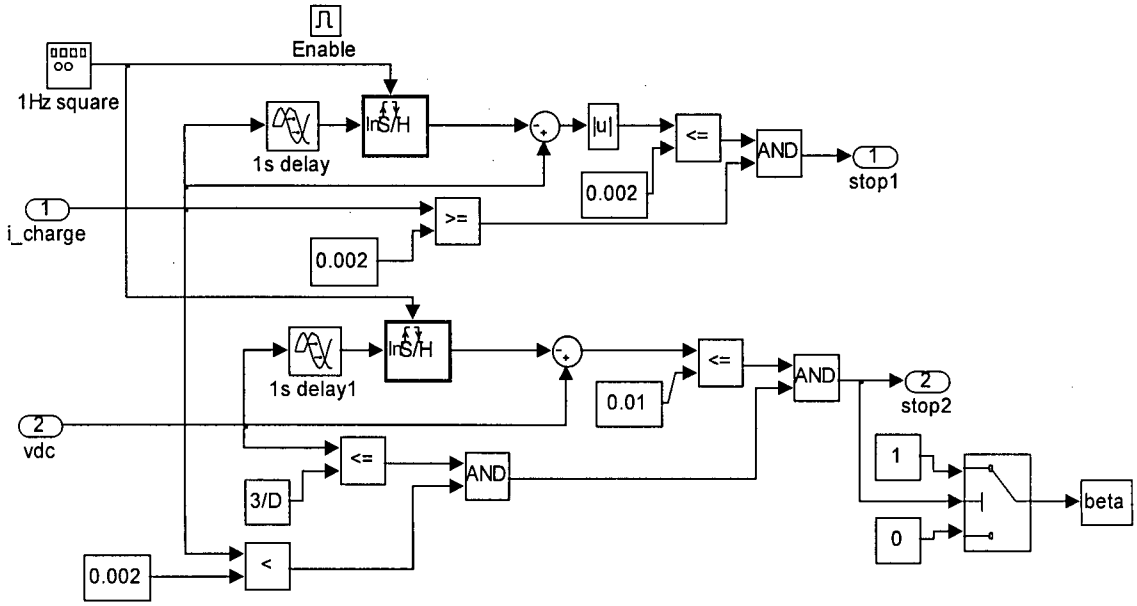

Figure 5.5 Block diagram of subsystem "stabilized current"

5.3.3 Adjusting k and D Using Hill Climbing Method

Considering the difficulty in grasping accurate overall system characteristics due to expensive measuring instrument and non-linearity of the system, a control method to achieve maximum charging current with unknown system characteristics is required.

The hill climbing method is a graph search method which iteratively adjusts control variables toward the direction of increasing target variable by comparing present target variable value with the one in previous iteration [30]. With this method, it is not necessary to know internal constants in detail or measure the environmental conditions. Duty cycle and spring constant are two control variables and charging current is the target variable of the hill climbing method in MCCT. Suppose i_{charge} is the present steady-state average charging current and i_{max} is the achieved largest average charging current so far, the basic idea of hill climbing method in MCCT is:

$$\begin{cases} \text{Follow the previous adjustment direction, for } i_{charge} > i_{\max} \\ \text{Resize adjustment step size } (\theta = \pm 0.04) \text{ or follow the direction, for } i_{charge} = i_{\max} \\ \text{Change the adjustment direction or resize adjustment step size, for } i_{charge} < i_{\max} \end{cases}$$

Normally, hill climbing searches for an optimum combination of a set of variables by varying each variable at a time as long as the result increases and stops when the result begins to decrease [31]. In the MCCT algorithm, k is adjusted first and its optimal value is found on its own without regard for D. Then keeping this optimal k constant we begin to adjust D until the optimal value of D is found. The generated charging current at these optimal values is the MCC under present environmental conditions.

The adjusting process of k is kind of simple compared to adjusting D since the step size is fixed to 100N/m (see Figure 1 in Appendix C). In the first iteration, $k = k + 100$, the values of w_n and c are revised based on this value of k. The changes in k, w_n and c cause variations in the charging current. After it is stable, i_{charge} is compared with $i_{\max}$. If i_{charge} is larger than $i_{\max}$, $i_{\max}$ is changed to this value and the direction "+" remains. Otherwise, $k = k - 100$ and the direction is complemented to "-". In both cases, the adjustment process will carry on until it reaches a maximum value. k corresponding to this maximum is the optimal value of the spring constant.

"θ" is a program variable used to adjust D. Its magnitude acts as step size and its sign acts as direction which must be followed on the hill-shaped $i_{charge} - D$ curve in order to increase the charging current. The magnitude of θ is hard to choose. If it is small, the system can't respond quickly to sudden changes in the environmental conditions due to long adjusting time; if it is large, there will be power loss under stable conditions. An

adjustable magnitude is preferred: large at the beginning ($\theta = \pm 0.04 / 0.02$), then change to small value ($\theta = \pm 0.01$) when D is close to the optimal value.

In the first iteration of adjusting D, we set $\theta = 0.04$, $D = D + \theta$. The sign of θ is determined by the difference between i_{charge} and $i_{\max}$. The iterations will go on until no larger i_{charge} can be found with the present value of θ. Then the magnitude of θ is changed to 0.01 and its sign remains unchanged. The hill climbing restarts until another maximum point is reached. This maximum is the actual maximum under the current environmental conditions. Then, this turn of MCCT operation is stopped and the values of k and D are maintained before the next execution. Figure 2 and Figure 3 in Appendix C show the adjusting process of D with $\theta = \pm 0.04$ and $\theta = \pm 0.01$ respectively.

A main drawback of hill-climbing method is that it fails to find the optimum when the function space contains "local maxima". If the hill-climbing method finds a local maximum, it will get stuck there. It can be noticed from Figure 3.6 and Figure 5.6 that for a single harmonic vibration signal, the surface plots of output power in resistive load and charging current for the supercapacitor are smooth and convex. Although the values of charging current are very close to the MCC in a small area around the MCC (see Figure 5.6), there is no observable local maximum in the surface. If the vibration signals contain harmonics and their magnitudes are large enough, local maxima would appear in the surface when k is resonant at the harmonics (see Figure 3.12). One way to overcome this problem is to start the hill climbing in the convex region around the global maximum by means of comparing the charging currents when k is resonant at the fundamental frequency and harmonics. This comparison process is called initiation process of k and has been discussed in detail in section 5.3.1.

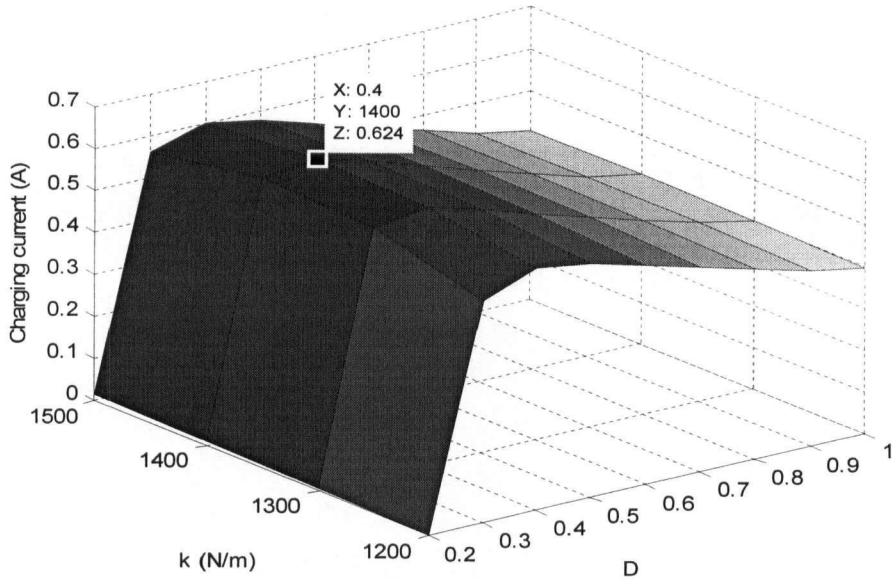

Figure 5.6 a) Global searching for MCC at 10 Hz, $D = 0.2:0.1:1$

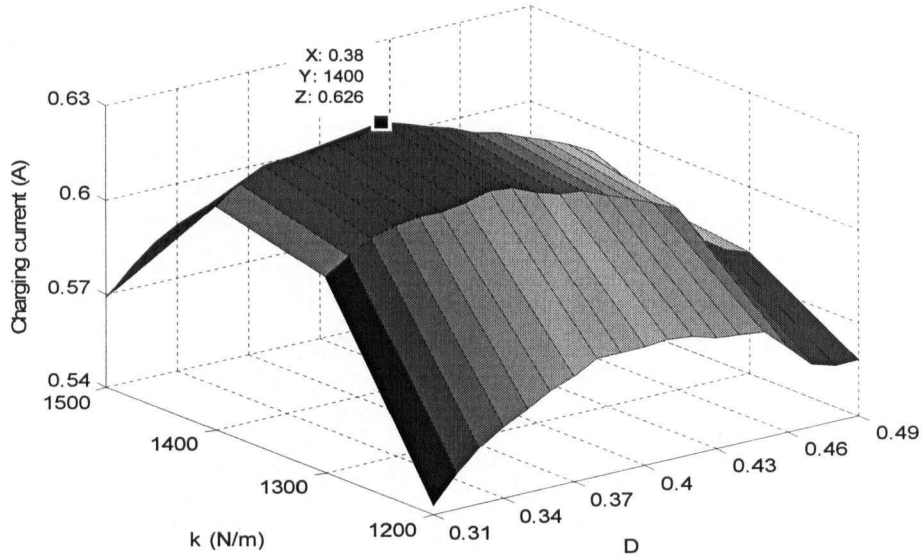

Figure 5.6 b) Global searching for MCC at 10 Hz, $D = 0.31:0.01:0.49$

Another possibility to generate local maxima is misreading the charging current. The closer D is to the optimal value, the slighter the difference of charging currents in a small move. Hence, it is critical to precisely measure the stabilized current. The criteria of stabilized current measurement have been discussed in the previous section.

The last way to guarantee that the charging current will not get stuck in the local maximum is the "every one minute scan" scheme which will be discussed in the next section. When the changes appear in the environmental conditions or v_{cap}, the $i_{charge} - D$ curve will shift and a new MCC forms. Moreover, these changes move the previous local maximum and let the adjustment of D redirect to the up-hill path.

5.3.4 Every One Minute Scan

Five parameters: f_v, Y_1, ζ_m, v_{cap} and harmonics magnitude ratio (rp)can easily change during the charging period of the supercapacitor. f_v, Y_1 and rp are affected by encountering wave frequency and length, ship machinery speed and smoothness of the blades and shafts [32]. ζ_m is influenced by f_v and Y_1 while v_{cap} is time-varying during the charging period. Limited by the expense, no accelerator or spectrum analyzer is integrated in the energy harvester. Also as discussed previously, measurement of ζ_m is not realistic since an impulse force is required to apply to the harvester before measuring the exponential decay in the magnitude. Thus practically, the change in Y_1, rp and ζ_m is immeasurable and the MCCT controller can only read the resulting variations in the charging current without telling the reasons.

Considering the adjust time spent by the MCCT, the interval between two turns of MCCT operation is set to 1 minute in simulation to let the energy harvester catch the changes in average charging current (i_{av}), f_v and v_{cap}. Scanning for v_{cap} mainly prevents v_{cap} exceeding its rated voltage. Assuming 5 V is the rated voltage which could be changed in the system design depending on the load circuitry, the charging process should be stopped at $v_{cap} = 4.9\,\text{V}$. Another limitation in v_{cap} is that it can not be lower than 2.5 V which is the microcontroller's minimum operating voltage. When v_{cap} is below

this voltage, the microcontroller will shut down since it is powered by the supercappacitor. In this case, the DC-DC converter also stops working as its switching signal is generated by the microcontroller. Then, the supercapacitor switches to another branch to connect to the rectifier and is charged directly until v_{cap} reaches 2.5 V.

As stated in section 3.2, the optimal value of induced voltage is mainly affected by f, Y_1, ζ_m and k. Thus, if these parameters do not change, the optimal value should be very close to the simulated optimal voltage V_{in_opt2} for resistive load in Table 3 in Appendix B, no matter what value of v_{cap} is. In order to stay at this optimal value, D should be increased as v_{cap} increases. Hence, D needs to be tuned every minute with step size 0.01 in the operation range $v_{cap} \in [2.5, 4.9]$ even no frequency or obvious current change appears.

If any variation in f_v is observed, the MCCT should begin from the initiation process of k. If any sudden change is found in i_{av}, both k and D should be adjusted since the controller can not tell the reason. The criterion of sudden change in i_{av} is $|\Delta i_{av}| \geq 0.02A$ in simulation.

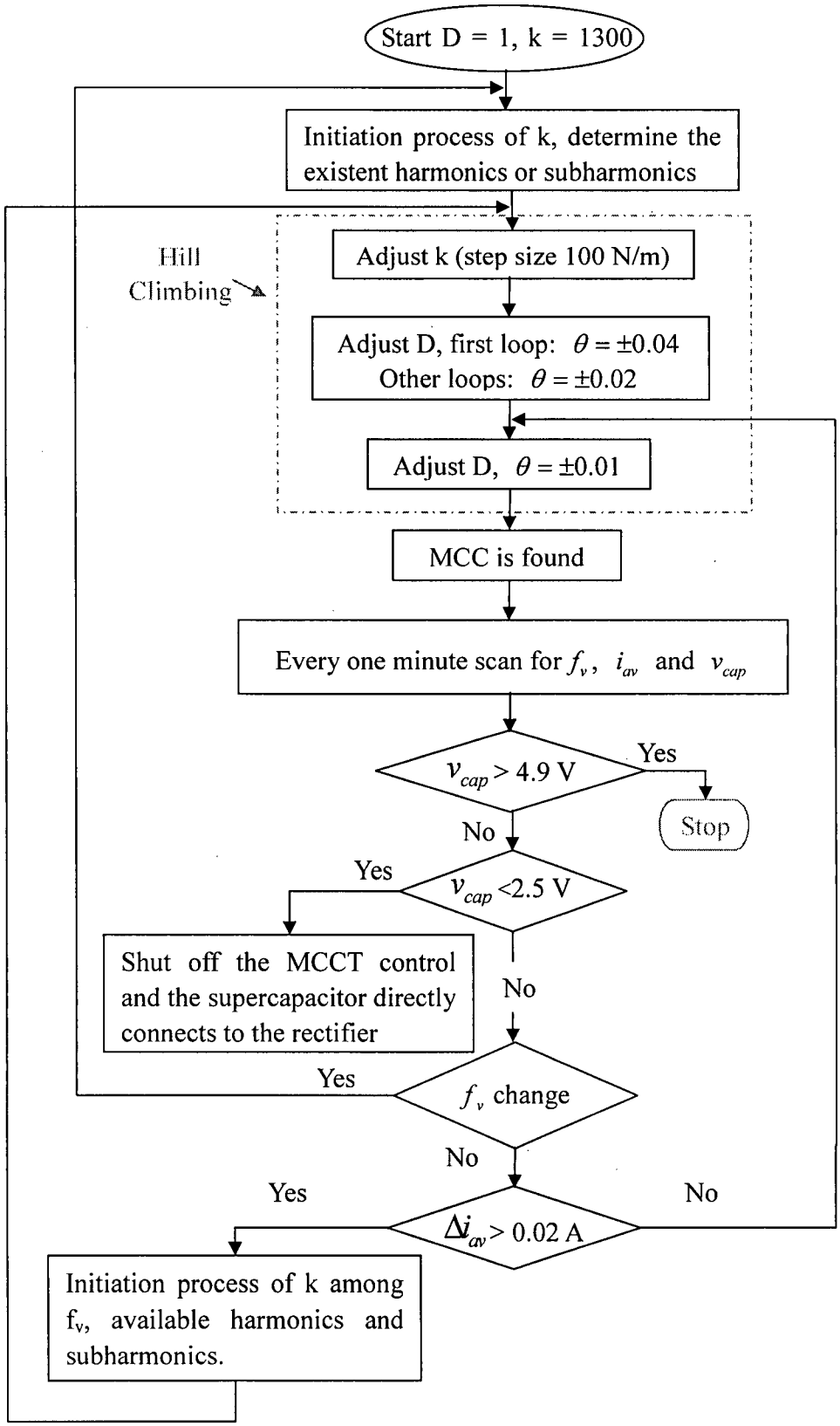

Figure 5.7 Flow chart for working process of the harvester

5.3.5 Adjustment in Parameters Variations

First, we analyze how the MCCT responds to variations in f_v. Table 3 in Appendix B shows a higher vibration frequency results in higher optimal induced voltage of the linear generator. This means D should be decreased as v_{cap} cannot increase instantaneously. The adjustment direction of D according to frequency change is shown below:

$$\begin{cases} \theta = -0.02, \text{ for } \Delta f_v > 0 \\ \theta = 0.02, \text{ for } \Delta f_v < 0 \end{cases}$$

The reason to choose 0.02 as step size instead of 0.04 is because the variations in optimal D caused by the environmental changes may be less than 0.04. For example, the optimal value of D varies from 0.29 to 0.28 when frequency changes from 15 to 16 Hz. The heuristic search will carry on until no larger charging current can be found with this step size. Then, the step size is revised to 0.01 as shown in Figure 2 of Appendix C and the hill climbing restarts. The adjustment of k is the same as shown in Figure 1 in Appendix C.

Then, we analyze how the MCCT responds to sudden change in i_{av}. One particular case is the variation in rp. If rp suddenly increases to a certain value such as $Y_2 = 0.5Y_1$, the measured f_v remains the same while the optimal value of k changes to resonant at the 2nd harmonic in stead of the fundamental frequency (see Figure 5.14 b)). Thus, as stated previously, the initiation process of k has to be executed again among f_v, existent harmonics and subhamonics to escape from the possible local maxima. Since the variation in rp cannot be observed directly, the initiation process of k is required whenever a sudden change appears in i_{av}.

If k gained from the initiation process is still resonant at f_v, the default adjustment direction of k in the hill climbing is set to the direction required under the variation in ζ_m.

Furthermore, it can be noticed from Table 5.2 that a sudden increase in i_{av} requires D to reduce for the sake of a new MCCT. Likewise, a sudden decrease in i_{av} requires D to increase. The adjustment directions of k and D in the hill climbing regarding the variation in i_{av} are:

$$\begin{cases} \theta = -0.02, \ k = k + 100 \ \text{ for } \ \Delta i_{av} \geq 0.02 \\ \theta = 0.02, \ k = k - 100 \ \text{ for } \ \Delta i_{av} \leq -0.02 \end{cases}$$

Parameter increase	Effect on i_{av}	Direction of D (Based on equation 3.14)	Direction of k (Based on equation 3.10)	Result
rp	increase	negative	Determined by the initiation process of k	Figure 5.14
Y_1	increase	negative	Remain	Figure 5.20
ζ_m	decrease	positive	Negative	Figure 5.21

Table 5.2 Effects of parameters increase on i_{av} and resulting direction of k, D

5.3.6 Modification of MCCT in the Real System

In the real system, considering the difficulty and power consumption to alter the spring constant, the scan interval for f_v will be longer, for example 10 minutes. Since a progressive spring only has several different spring constants, the total adjustment of k is simplified to the initiation process of k without 100 N/m step size adjustment in the hill climbing process. The charging current is averaged and recorded every one second no matter a MCC is found or not. When the variation in the two nearby i_{av} is above a

threshold, the adjustment direction of D in the hill climbing is set as stated in the previous section. Even if no frequency variation or obvious i_{av} change is observed, D still needs adjusting by step size of 0.01 when v_{cap} changes more than certain value, say 0.1 V.

5.4 Simulation Results

In this section, simulation results obtained from the proposed MCCT algorithm are presented and compared to the simulation results obtained from global search. The two performance parameters evaluated here are the maximum charging current and the adjusting time. Section 5.4.1 tests how the energy harvester works under the vibration on the bow and the system response to the disturbance in rp. Section 5.4.2 evaluates the MCCT performance under constant conditions. In section 5.4.3, three disturbance scenarios were applied in the charging process separately and the system responses to the disturbances are evaluated. In order to save simulation time, the vibration signals in section 5.4.2 and section 5.4.3 are assumed to single frequency sinusoidal waves and the initial value of D is set to 0.5 (50 %). Due to different initial voltage/current of the filter capacitor/inductor, we expect the MCC obtained from MCCT to be slightly different from which obtained from global search with the same optimal duty cycle and spring constant. All simulations are run under standard conditions: $Y_1 = 5$ mm, $\zeta_m = 0.11$, $v_{cap} = 3$ V unless specify.

5.4.1 MCCT for Vibration on the Bow

The first problem the MCCT algorithm facing is that it needs to work properly under the ship vibration. As is seen from Figure 5.8 [33], there is no longer only one peak in acceleration magnitude at a specific frequency. The acceleration is distributed over a band of frequencies with several frequency spikes which may not be the harmonics of the

dominant frequency. It should also be noted that the dominant frequency and its acceleration magnitude are dependent both on the speed of the ship machines and the nature of the machines (i.e. smoothness of the blade and shaft), as are the other frequency spikes. These all add complexity in the implementation of MCCT.

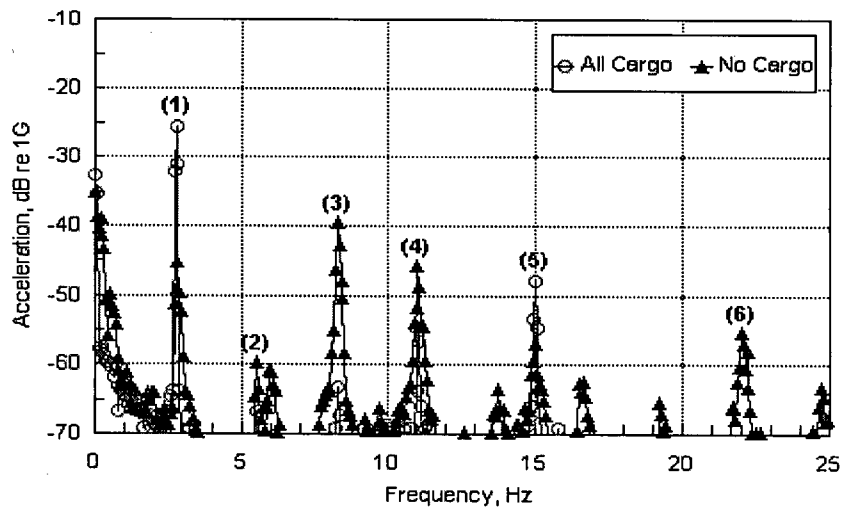

Figure 5.8 Vertical vibration of a bow above the main deck

ID	Frequency (Hz)	Description
1	2.75	Propeller Shaft Rotation Rate (RR)
2	5.5	2nd Harmonic of Propeller Shaft RR
3	8.25	3rd Harmonic of Propeller Shaft RR
4	11.0	Propeller Blade Rate (4 Blades)
5	15.0	Propulsion Diesel RR (900 rpm)
6	22.0	2nd Harmonic of Propeller Blade Rate

Table 5.3 Propulsion System Forcing Frequencies

Figure 5.8 shows a vibration spectrum measured in a ship of which peaks values are shown in Table 5.3. The resultant input force to the harvester from these vibrations is

shown in Figure 5.9.

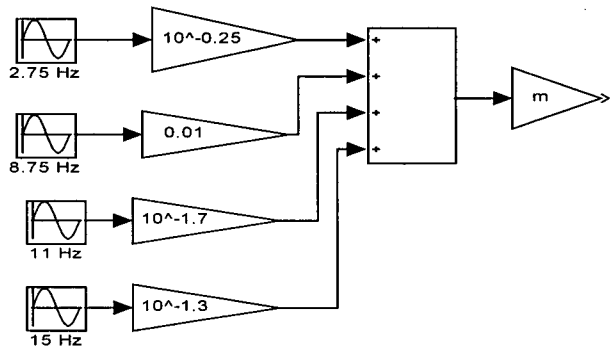

Figure 5.9 Resultant input force to the harvester from the vibration on the bow

Suppose ζ_m = 0.015 which is realizable since Shadrach Roundy [7] already built a vibration-based electromechanical power generator with damping factor of 0.013, the generated charging current and induced voltage (V_{in}) at initial condition $k = 1300$ N/m, $D = 1$ are shown in Figure 5.10 a). The measured f_v in this figure is 7 Hz. So k is adjusted to resonant at 7 Hz (700 N/m) and since the resulting measured f_v is 3 Hz, k is then adjusted to resonant at 3 Hz (100 N/m). The resulting i_{charge} and V_{in} at $k = 700$ and 100 N/m are shown in Figure 5.10 b) and c) respectively. We can see from Figure 5.10 that only resonant at 3 Hz, V_{in} is above 3 V and energy is stored in the supercapacitor. As stated previously, the fact that the measured f_v is 3 Hz when k resonant at 7 Hz indicates the harmonics magnitude at 6 Hz carries less power than 3 Hz. Thus, 3 Hz is the frequency carrying the largest power which matches the fundamental frequency (2.75 Hz) of the vibration spectrum. Then, the hill climbing starts at the point $k = 100$ N/m and $D = 1$ with charging current of 10 mA. Firstly, k is adjusted to 200 N/m and the resulting i_{charge} drops to zero which means the charging current can only appears when $k = 100$ N/m. Then k is changed back to 100 N/m and D drops to 0.96. The resulting charging current is 9 mA. In order to make sure this slight current change is not a misreading error, D is further

decreased to 0.92 and the resulting charging current is still 9 mA. Thus, the hill climbing restarts with θ resizing to -0.01. Finally, the hill climbing stops at $D = 0.97$ with the MCC of 10 mA. We can see from Figure 5.11, the charging currents in the range $D \in [0.97, 1]$ are all equal to 10mA since the actual current difference is less than 1mA. The relationship of i_{charge}-D gained by global search at $k = 100$ N/m is shown in Figure 5.12. In this figure, the largest charging current is achieved at $D = 1$ since the optimal value of the induced voltage for the tiny vibration signals is less than 3 V.

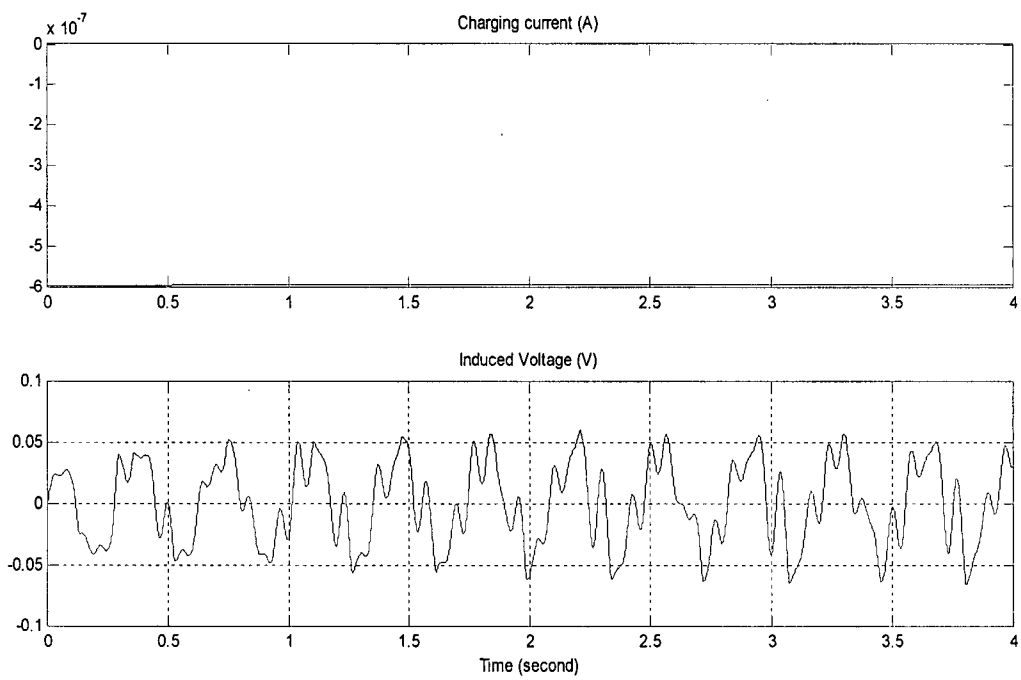

Figure 5.10 a) i_{charge} and V_{in} generated by the vibration on the bow at

$$k = 1300 \text{ N/m}, D = 1, \zeta_m = 0.015$$

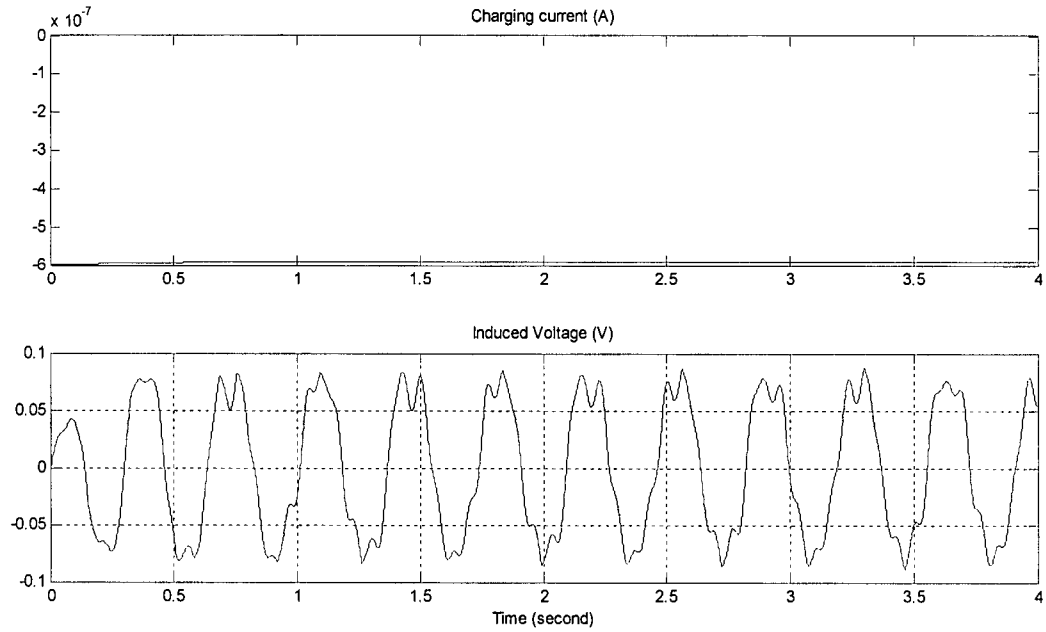

Figure 5.10 b) i_{charge} and V_{in} generated by the vibration on the bow at $k = 700$ N/m,

$$D = 1, \zeta_m = 0.015$$

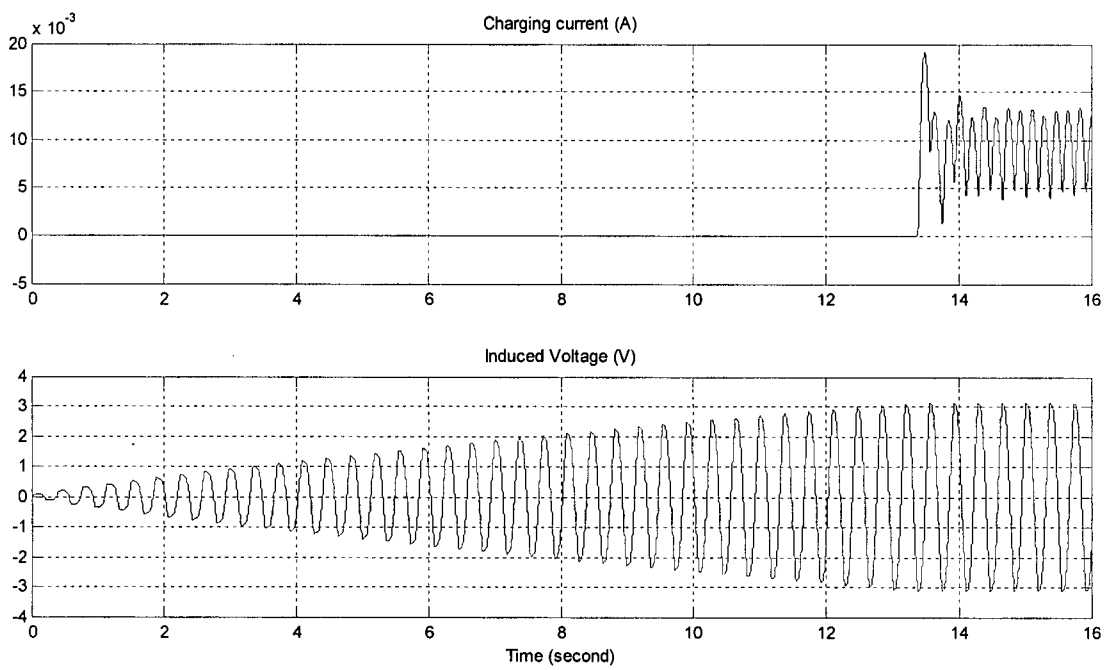

Figure 5.10 c) i_{charge} and V_{in} generated by the vibration on the bow at $k = 100$ N/m,

$$D = 1, \zeta_m = 0.015$$

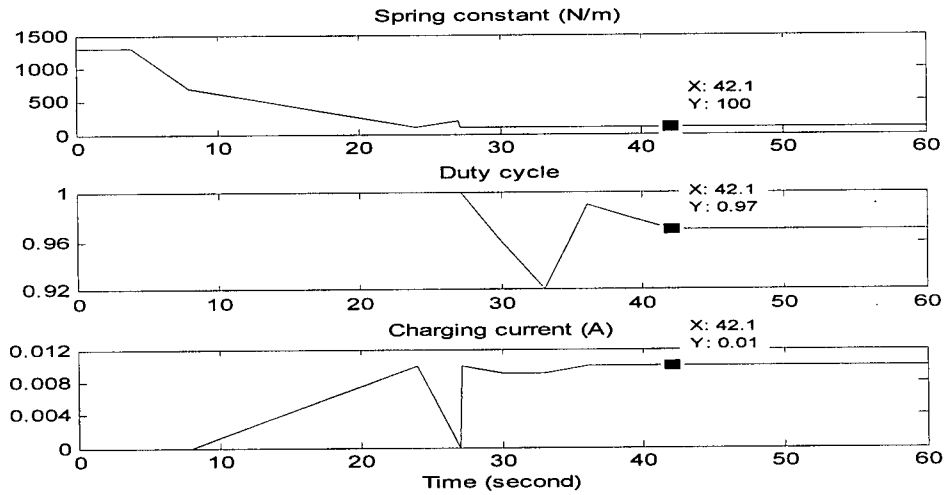

Figure 5.11 MCCT under the vibration on the bow at $\zeta_m = 0.015$

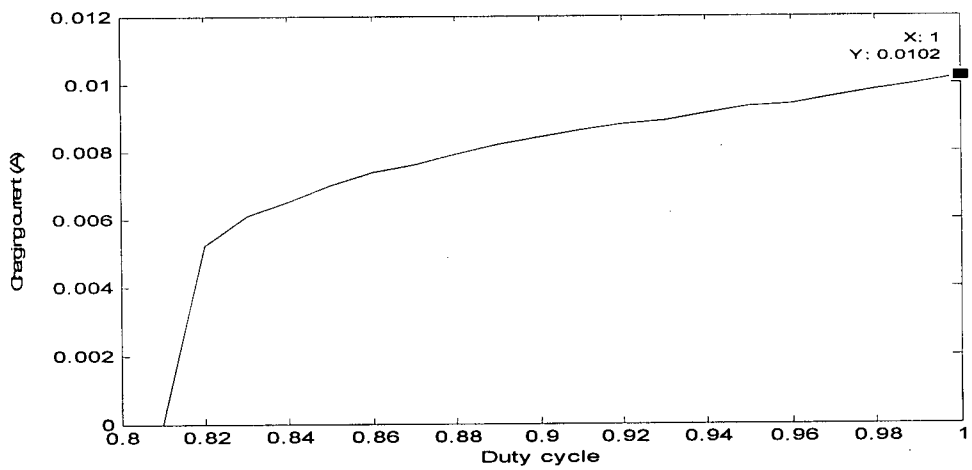

Figure 5.12 i_{charge} vs D under the vibration on the bow at $k = 100\,\text{N/m}$, $\zeta_m = 0.015$

At this value of MCC, the power flow to the supercapacitor is $0.01*3 = 30\,\text{mW}$, which is only 10 % of the power requirement. There are three effective ways to increase the power output: increasing the mass, decreasing the turns of coils or replacing the buck converter with a buck-boost converter. Decreasing the turns of coils can reduce ζ_e and the closer ζ_e to ζ_m (0.015), the larger the power output. A buck-boost converter is used to adjust the induced voltage toward the optimal value which turns out to be lower than 3V. When $m = 1.2\,\text{kg}$, $N = 100, k = 200\,\text{N/m}$ and using a buck-boost converter of 99% duty cycle, the

charging current enlarges to 0.1 A and the power flow to the supercapacitor is 0.3 W (see Figure 5.13). Also, if the load is a data-logging device for making occasional measurements or a wireless sensor only turning on for a short period of time, a "power-switching" circuit can be used to power the load occasionally with a low duty cycle or only when sufficient energy is stored in the supercapacitor. In this circuit, the supercapacitor needs to be large enough to supply enough charge to the load during "on" cycles without its voltage dropping too far.

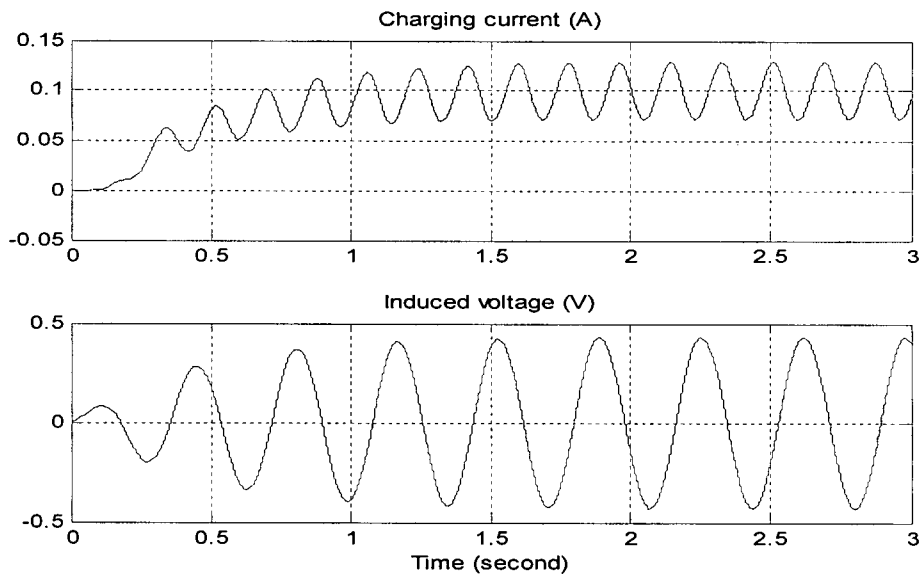

Figure 5.13 i_{charge} and V_{in} generated by the bow vibration at $m = 1.2\,\text{kg}$, $N = 100$, $k = 200\,\text{N/m}, \zeta_m = 0.015$, $D = 0.99$ with a buck-boost converter

Figure 5.14 shows the system's response to sudden changes in harmonic magnitude ratio (rp) when $f_1 = 7\,\text{Hz}$. At first $Y_2 = 0.1Y_1$, $k = 1300\,\text{N/m}$, $D = 1$, the measured frequency of induced voltage is $f_v = 7\,\text{Hz}$ and $i_{charge} = 2\,\text{mA}$. Following the initial process of k, k is adjusted to 700 N/m (resonant at 7 Hz) and the resulting i_{charge} is 165 mA while f_v is still 7 Hz. Then, the values of i_{charge} at $k = 200\,\text{N/m}$ (resonant at 4 Hz) and 2600 N/m (resonant at 14 Hz) are compared. The corresponding charging currents are 3 mA and zero respectively. Also, at $k = 2600\,\text{N/m}$, the measured f_v is identical to 14 Hz, which means

the 2nd harmonic exits in the vibration signals. Then, the MCCT starts from $k = 700\,\text{N/m}$, $D = 1$ and reaches a MCC of 0.178 A at $k = 700\,\text{N/m}$, $D = 0.68$. At the moment of 60 s, Y_2 suddenly increases to $0.3Y_1$. f_v is still 7 Hz and i_{charge} raise to 0.203 A. When k is adjusted to 2600 N/m (existent 2nd harmonic), i_{charge} is 0.161 A. So the hill climbing starts again at $k = 700\,\text{N/m}$, $D = 0.68$ and stops at a new MCC of 0.205A at $k = 700\,\text{N/m}$, $D = 0.58$. We can see from Figure 5.14 a), in the second hill climbing process, the charging current curve is rather constant with only 2mA variation from $D = 0.68$ to $D = 0.58$, and the optimal value of k is the same as before. This validates that the 2nd harmonic does not affect the MCC point much if its magnitude is less than $0.5Y_1$. When Y_2 suddenly increases to $0.5Y_1$, the measured f_v is still 7 Hz and i_{charge} raises to 0.29 A. However, i_{charge} at $k = 2600\,\text{N/m}$ is 0.412 A which is higher than i_{charge} at $k = 700\,\text{N/m}$. Thus, the hill climbing restarts at $k = 2600\,\text{N/m}$, $D = 0.68$ and stops at a new MCC of 0.432 A at $k = 2600\,\text{N/m}$, $D = 0.5$. The fact that different variations in rp result in different MCC points proves the necessity of the initiation process of k even no frequency change is observed.

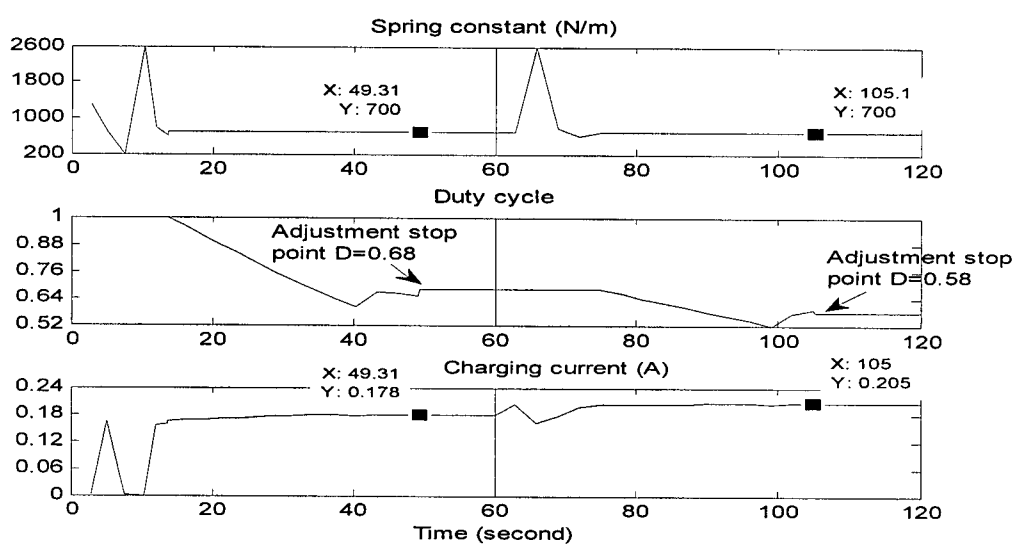

Figure 5.14 a) System response to a sudden change in $rp: 1:0.1 \rightarrow 1:0.3$ at $f_1 = 7\,\text{Hz}$

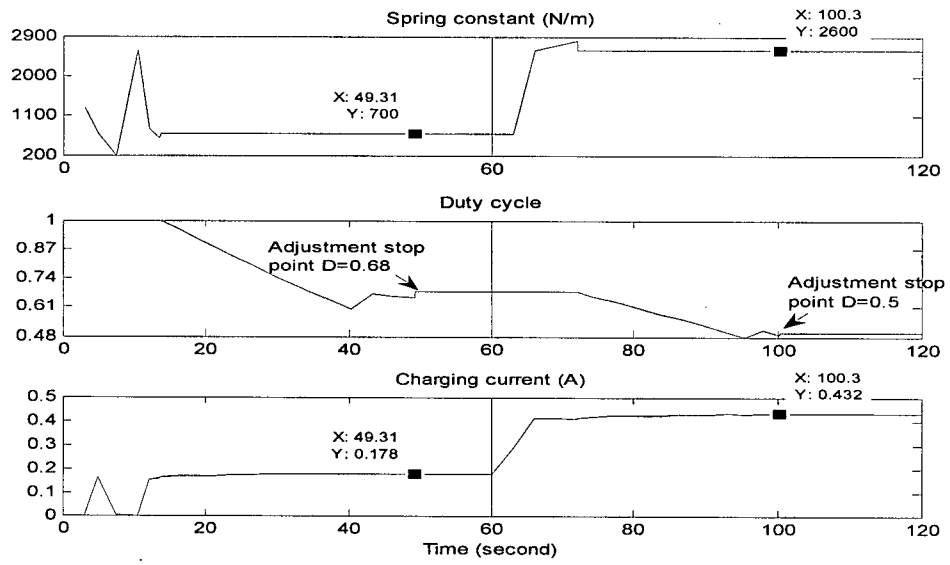

Figure 5.14 b) System response to a sudden change in $rp:1:0.1 \rightarrow 1:0.5$ at $f_1 = 7\,\text{Hz}$

5.4.2 Stability under Standard Conditions

If the conditions surrounding the harvester, i.e. f_v, Y_1 and rp, are kept constant as well as internal parameters ζ_m and v_{cap}, the duty cycle and the spring constant should be fixed at D_{opt} and k_{opt} to let the supercapacitor absorb maximum power. In Figure 5.15, MCCT using variable step size "θ" is compared with MCCT using fixed step size. f_v and i_{charge} are checked every 60 s. It shows clearly that both MCCT using variable step size and fixed small step size ($\theta = \pm 0.01$) can keep stable around the actual D_{opt}, which is 0.32 (point A) in Figure 5.16 (b), without diverge. However, adjusting time of the latter is much longer than the former. The MCCT using fixed large step size ($\theta = \pm 0.04$) demonstrates fast response, but it stops at $D = 0.3$ which corresponds to a smaller value of MCC. Also, its fluctuation in steady state is 8 mA, which is larger than 3 mA fluctuation in the other two cases. Table 5.4 illustrates better performance is achieved by means of variable step size both in dynamic response and steady state.

MCCT Algorithm	Variable "θ"	$\theta = \pm 0.04$	$\theta = \pm 0.01$
Tracking time	31.34 s	24.43 s	56.11 s
D_{opt}	0.32	0.3	0.32
MCC at 1st point	1.008 A	1.002 A	1.011 A
Tracking time	8.11 s	8.52 s	8.16 s
D_{opt}	0.32	0.3	0.32
MCC at 2nd point	1.006 A	1.001 A	1.009 A
Tracking time	8.1 s	8.1 s	8 s
D_{opt}	0.33	0.3	0.33
MCC at 3rd point	1.009 A	1 A	1.009 A
Steady-state fluctuation	3 mA	8 mA	3 mA

Table 5.4 Comparison on dynamic response and steady-state fluctuation

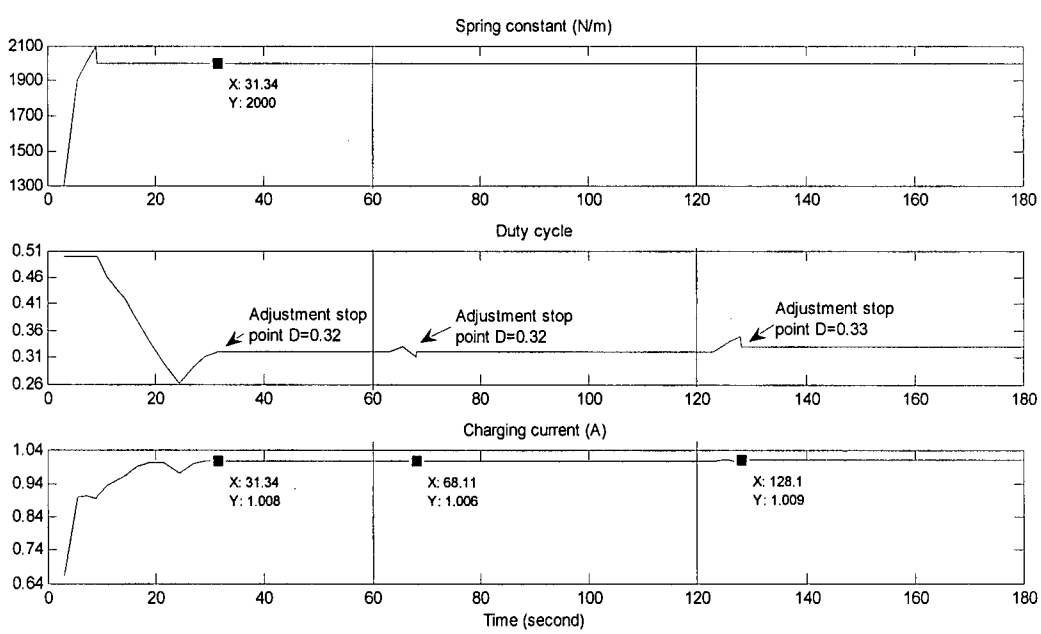

Figure 5.15 a) MCCT under standard conditions at 12 Hz, $\theta = \pm 0.04 \rightarrow \pm 0.01$

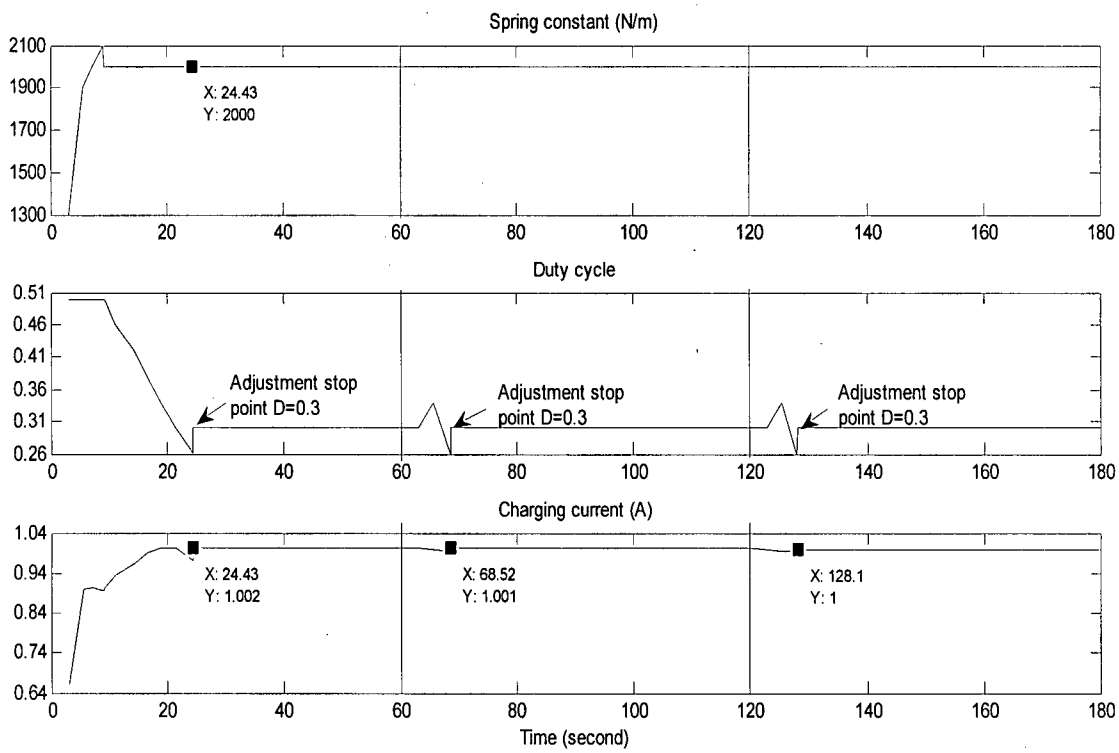

Figure 5.15 b) MCCT under standard conditions at 12 Hz, $\theta = \pm 0.04$

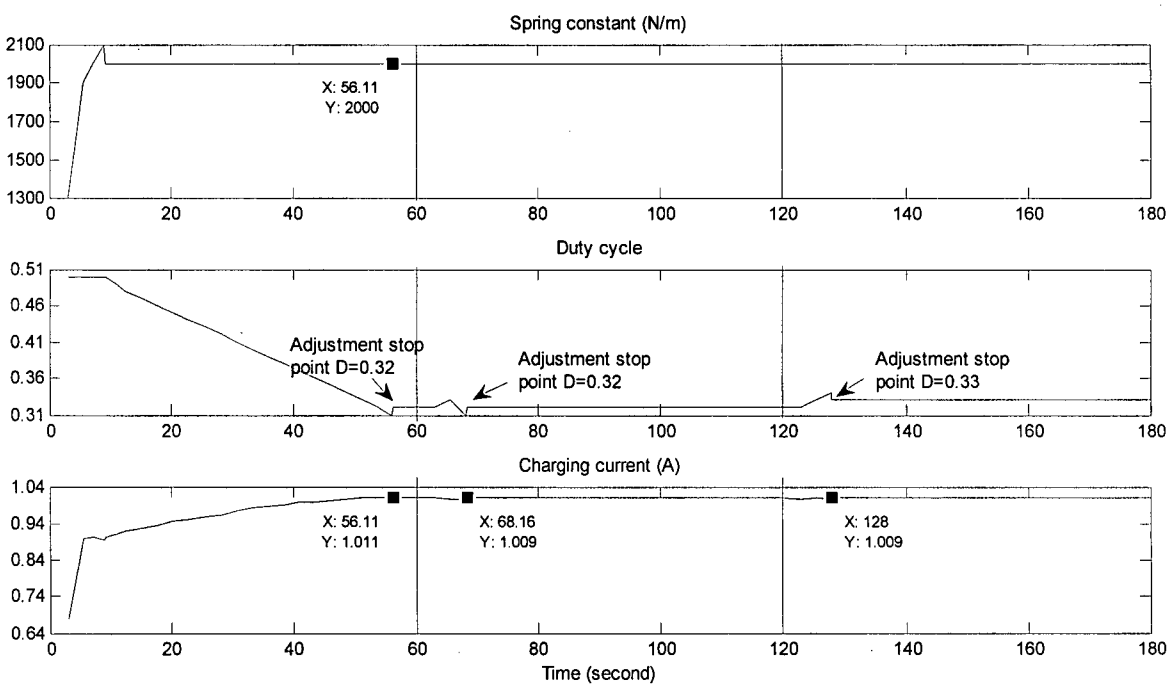

Figure 5.15 c) MCCT under standard conditions at 12 Hz, $\theta = \pm 0.01$

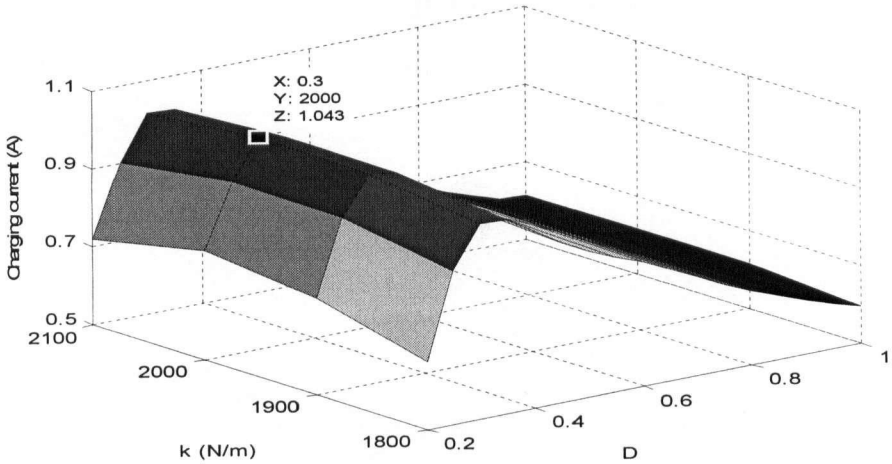

Figure 5.16 a) Global search of MCC at 12 Hz, D = 0.2:0.05:1

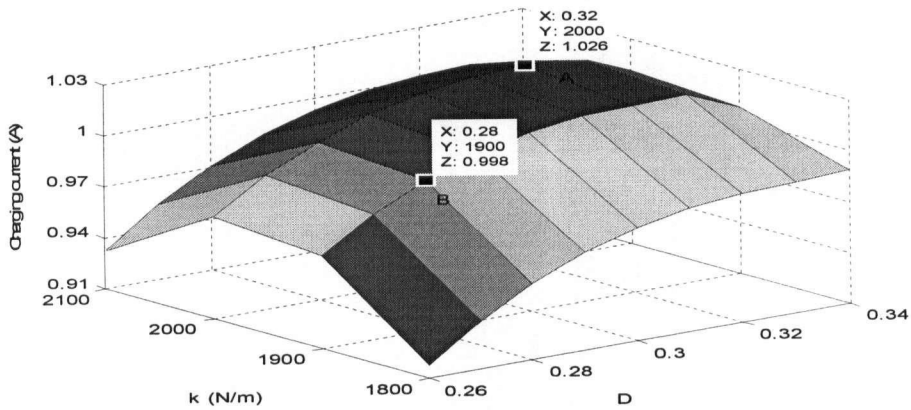

Figure 5.16 b) Global search of MCC at 12 Hz, D = 0.26:0.01:0.34

From Table 3 in Appendix B, we can see the simulated $P_{out\_\max}$ of the resistive load at 12 Hz is 3.9 W achieved at the point $V_{in\_opt2} = 13.45$ V. When $v_{cap} = 3$ V, $D_{opt} = 0.32$ results in $v_{in} = 13.43$ V and $MCC = 1.008$ A. The power supplied to the supercapacitor is $3 \times 1.008 = 3.024$ W. When $v_{cap} = 4$ V (see Figure 5.17), $D_{opt} = 0.41$ results in $v_{in} = 13.22$ V and $MCC = 0.802$ A. Power supplying to the supercapacitor is $4 \times 0.802 = 3.208$ W. It is interesting to notice that the power conversion ratio at $v_{cap} = 3$ V is smaller than $v_{cap} = 4$ V. This is because the smaller charging current tends to decrease the

power consumed in internal resistor of the filter inductor. In both cases, the values of V_{in} corresponding to optimal D are very close to the value of V_{in_opt2}. This proves no matter what v_{cap} is, we can adjust D to let the induced voltage stay at the constant optimal value.

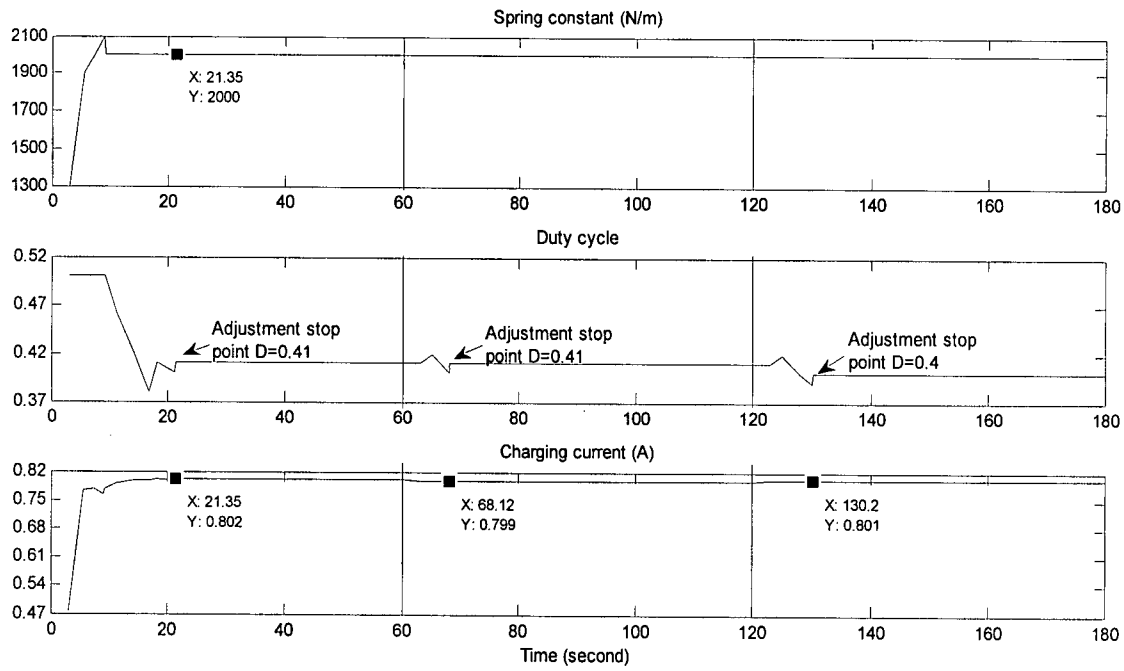

Figure 5.17 MCCT under standard conditions at $f = 12\,\text{Hz}$, $V_{cap} = 4\,\text{V}$

5.4.3 MCCT under Variable Operating Conditions

An important feature for the MCCT controller is how it reacts to disturbances in conditions such as vibration frequency, vibration displacement magnitude and mechanical damping factor. Figure 5.19-21 shows the system's response to sudden changes at the moment of 60 s and 120 s in f, Y_1 and ζ_m respectively.

Figure 5.19 illustrates the system's response following a sudden increase in vibration frequency from 12 to 16 Hz at 60 s and back to 12 Hz at 120 s. At the beginning, the MCCT controller manages to reach a MCC point by adjusting k and D to point A in Figure 5.16 (b). When the vibration frequency increases from 12 to 16 Hz, the charging current drops from 1.008 A to 0.928 A in 3 s. Then the MCCT restarts at 16 Hz and the charging

current gradually increases back to 2.047 A in 18.8 s. When the vibration frequency changes back to 12 Hz, the charging current drops dramatically to 4 mA in 3 s since $D = 0.28$ is too small to let the output voltage of converter higher than 3 V. Then the MCCT control restarts from point B in Figure 5.16 (b) and stops at point A again. Comparing Figure 5.18 and Figure 5.19, we can see the optimal values of k, D at 16 Hz obtained by the MCCT are also the same as the ones obtained by global search.

Figure 5.20 illustrates the system's response following sudden increase in Y_1: $5 \rightarrow 6 \rightarrow 7$ mm at 8 Hz. At the beginning, the charging current keeps stable after it reaches a MCC point at $k = 900$ N/m, $D = 0.46$. When Y_1 increases from 5 to 6 mm, the charging current raises from 0.337 to 0.46 A in 3 s. Based on this instant current increase, the MCCT restarts on the positive direction of k and negative direction of D. The charging current gradually increases to 0.48 A in 20.916 s. The optimal values of k, D corresponding to new MCC are $k = 900$ N/m and $D = 0.38$. When Y_1 further increases to 7 mm, the MCCT restarts and lets the charging current increase to 0.64 A at $k = 900$ N/m and $D = 0.33$.

Figure 5.21 illustrates the system's response following sudden increase in ζ_m: $0.11 \rightarrow 0.16 \rightarrow 0.21$ at 15 Hz. At the beginning, the charging current keeps stable after it reaches a MCC point at $k = 3100$ N/m, $D = 0.28$. When ζ_m increases from 0.11 to 0.16, the charging current drops from 1.754 to 1.091 A in 3 s. The MCCT restarts based on this instant current reduction and the charging current gradually increases to 1.216 A in 21.7 s. The optimal values of k, D corresponding to the new MCC are $k = 2900$ N/m and $D = 0.4$. When ζ_m further increases to 0.21, the MCCT starts again and lets the charging current stable at another MCC of 0.926 A when $k = 2800$ N/m and $D = 0.49$.

Compared with Table 5.5, the optimal values of k, D obtained from the MCCT with sudden changes in Y_1 or ζ_m are at most 1 percent different from which obtained from global search. All of these results demonstrate that the MCCT algorithm can follow closely

the dynamically varying environmental conditions and track accurately the MCC point.

f	Y_1 (mm)	MCC (A)	k_{opt} (N/m)	D_{opt}	D_{opt} by MCCT
8	5	0.339	900	0.45	0.46
	6	0.478	900	0.39	0.38
	7	0.639	900	0.32	0.33

f	ζ_m	MCC (A)	k_{opt} (N/m)	D_{opt}	D_{opt} by MCCT
15	0.11	1.736	3100	0.29	0.28
	0.16	1.214	2900	0.4	0.4
	0.21	0.925	2800	0.49	0.49

Table 5.5 Optimal value of k and D based on global search with sudden change in vibration displacement magnitude and mechanical damping factor

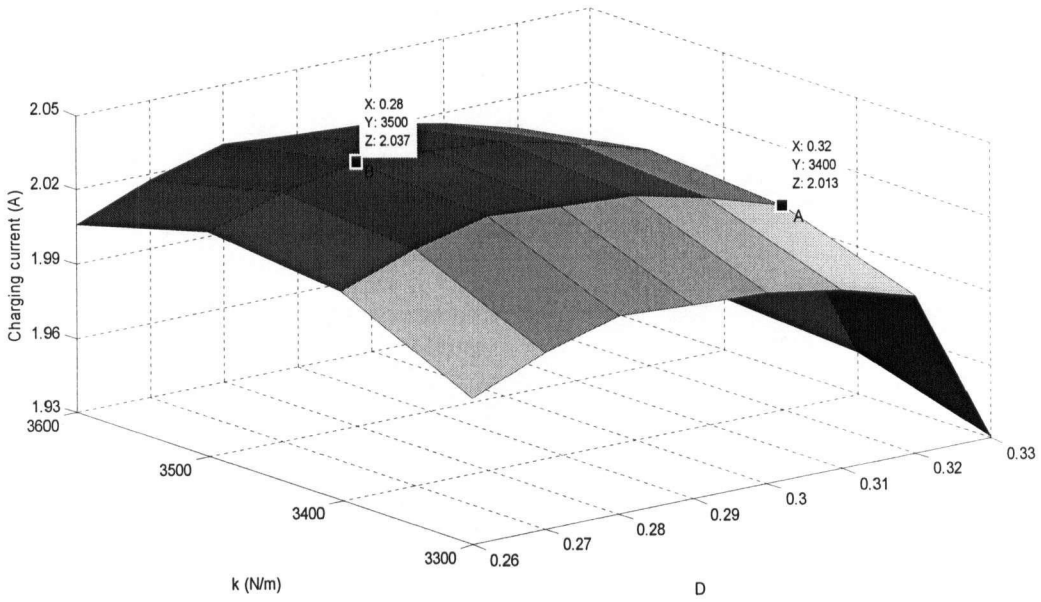

Figure 5.18 Global searching for MCC at 16 Hz

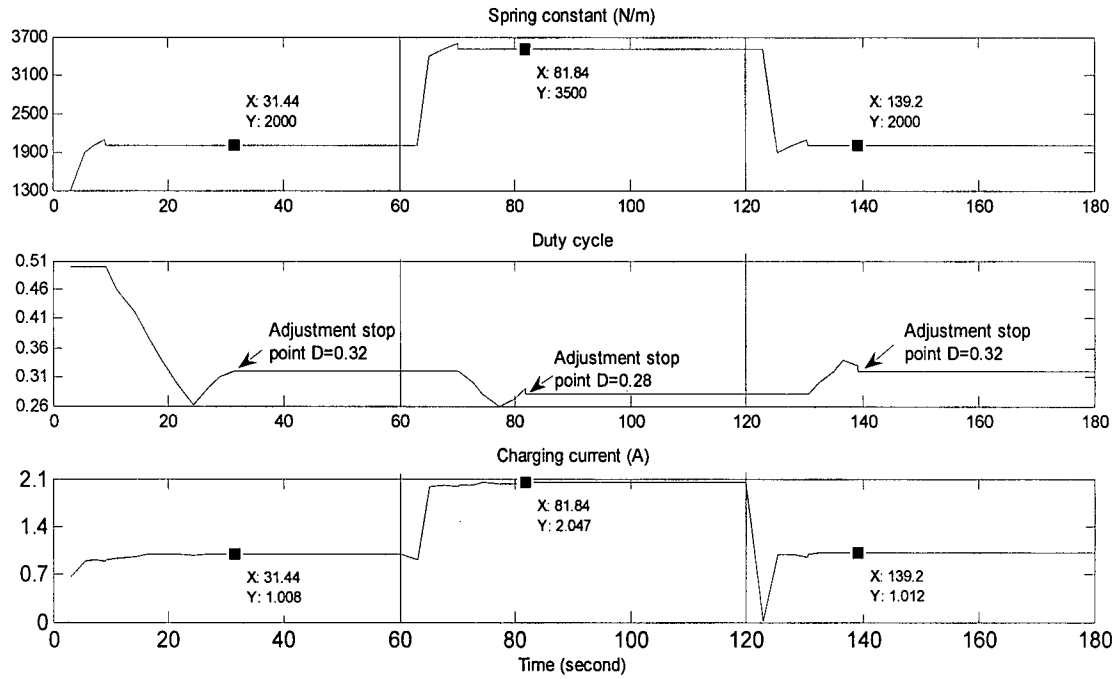

Figure 5.19 System response to sudden change in vibration frequency: $12 \rightarrow 16 \rightarrow 12$ Hz

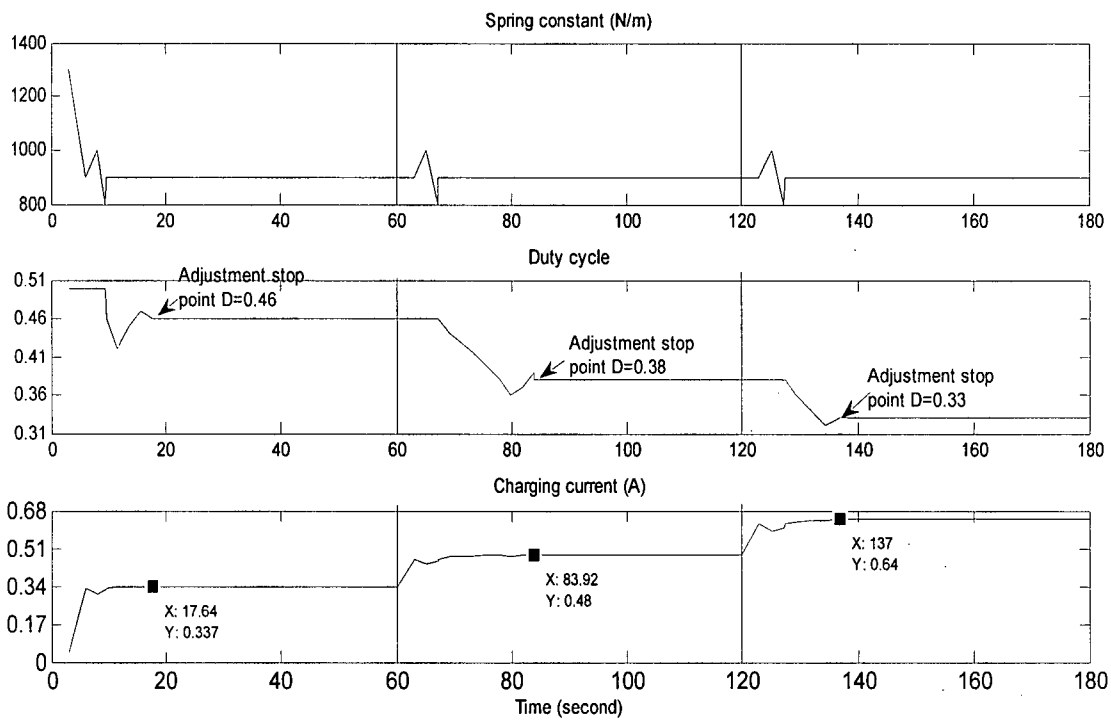

Figure 5.20 System response to sudden change in vibration displacement magnitude:

$5 \rightarrow 6 \rightarrow 7$ mm at 8 Hz

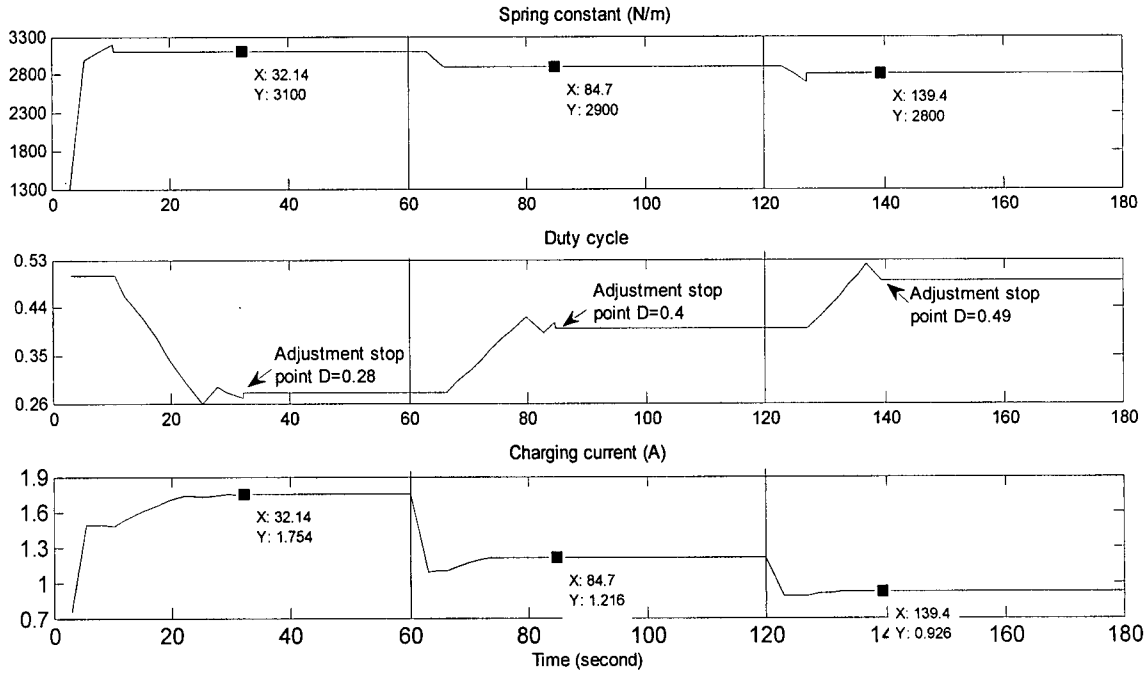

Figure 5.21 System response to sudden change in mechanical damping factor:

$$0.11 \rightarrow 0.16 \rightarrow 0.21 \quad \text{at 15 Hz}$$

5.5 Summary

In this chapter, a model to demonstrate the operation of energy harvester is developed by combining the mathematical model of linear generator in chapter 2 and the power management circuit in chapter 4 with simulation tool Simulink and Psim. An algorithm called MCCT is programmed in Matlab to track the maximum charging current flowing to the supercapacitor. The algorithm provides good performance on both tracking stages and steady-state stages, since a variable step size in adjusting D is applied rather than a constant value. In the execution of MCCT, firstly an initiation process of k is used to determine which frequency in the vibration spectrum contains the largest power. k is set to resonant at that frequency and D is set to 1. Then the hill climbing process begins from this point and varies one variable at a time. After a MCC is found, the values of k and D are remained until the next execution of MCCT. This one minute scan helps to escape from local maxima

during the hill climbing process as well as other two factors: initiation process of k and stabilized current measurement. If any obvious variation in the measured frequency or charging current appears, the MCCT will change k and D to reach a new MCC.

The vibration signals of the bow are used to test the performance of energy harvester. The optimal values of k and D gained by the MCCT match those gained by global search. A 1.2 kg mass can generate 0.3 W power flow to the supercapacitor by means of a buck-boost converter at a mechanical damping factor of 0.015. This verifies the feasibility of the energy harvester in a ship environment. Furthermore, the system responses of the energy harvester to variation in environmental conditions demonstrate it can not only follow the changes but also successfully track the real maximum power.

Chapter 6 Conclusions

6.1 Conclusions

The use of ambient energy to self-sustain a low power device has been a trend in the development of wireless sensor and actuator. This method has been dubbed "energy harvesting" since it converts the unused ambient energy in the environment into electricity by the electronics. Numerous potential sources for power harvesting exist such as light, thermal gradient and vibration. In order to tailor both the application demands (0.3 W) and environment (ship), vibration is used as a power source in this thesis. Three types of vibration to electricity converters have been considered: electromagnetic, electrostatic, and piezoelectric. After a preliminary investigation and comparison, electromagnetic scheme was chosen to be applied in an energy harvester.

In the electromagnetic converter (linear generator), the relative motion between a coil and magnetic field causes a current to flow in the coil. An electromechanical force is generated by the induced current which opposes the relative motion of the coils. This force works as an electrical damper and converts vibration energy to electrical energy. A detailed model with restive load has been developed. Parametric relationships resulting from this model are discussed in chapter 3 and serve as guiding principles for design the energy harvester. In this project, a capacitive load is more realistic than resistive load in terms of storing energy. In order to maintain the power flow to a supercapacitor at its peak value, the induced voltage is rectified and stays at its optimal value by adjusting duty cycle of a DC-DC converter. A maximum charging current tracking (MCCT) algorithm is used to achieve maximum charging current by adjusting spring constant and duty cycle through hill climbing method. Three characteristics in the MCCT including initiation process of spring constant, stabilized current measurement and one-minute scan can prevent the hill climbing process fall into a local maximum. The one minute scan also catches the changes in the

driving frequency and charging current and varies the spring constant and duty cycle according to the direction of variation until a new maximum charging current point is reached. Simulation shows that a 1.2 kg mass can provide 0.3 W power flow to the supercapacitor based on the vibration signals on the bow using a buck-boost converter. The performance of the energy harvester is also evaluated by applying four disturbance scenarios in harmonics magnitudes, vibration frequency, vibration displacement magnitude and mechanical damping factor separately. The simulation results confirm high tracking efficiency for the maximum power output and feasibility of the energy harvester.

6.2 Recommendations for Future Work

The next key step for this research is to fabricate the power management circuit of the energy harvester and connect to the prototype of the linear generator. It is important to gain a ship vibration spectrum from onboard measurement. So the driven frequency of the energy harvester can be adjusted to the main frequency of the spectrum to estimate the power flow to the supercapacitor in reality. If the largest ship vibration signals are similar to the vibration signals of the bow, a buck-boost converter should be used in the power management circuit to maintain the rectified voltage at its optimal value no matter it is above the supercapacitor's voltage or not.

Also, there are two critical problems in the fabrication of the energy harvester that need to be solved in the future. The first is although it is possible to adjust the spring constant by pressing the progressive spring, it will cost some power. Thus we need to design an extremely low power consumed mechanism to let the net power output be greater after adjustment of the spring constant. The second is to get power electronics specifically optimized for vibration to electricity conversion. These power electronics can not only consume as little power as possible (say 1 mW), but also perform well near strong magnets.

Bibliography

[1] Nicolas Mokhoff, Sensors get their field of dreams, http://www.automotivedesignline.com/howto/chassisandsuspension/170700197

[2] Rajeevan Amirtharajah and Anantha P. Chandrakasan, Self-Powered Signal Processing Using Vibration-Based Power Generation, IEEE Journal of Solid-State Circuits, vol. 33, no. 5, May 1998

[3] Erick O. Torres and Gabriel A. Rincon-Mora, Harvesting ambient energy, http://users.ece.gatech.edu/rincon-mora/publicat/trade_jrnls/ee_times_0805_harvest.pdf

[4] Shad Roudy, Paul K.Wright and Kristofer Pister, Micro-electrostatic vibration-to-electricity converters, Proceedings of IMECE2002,ASME International Mechanical Engineering Congress & Exposition, November 17-22, 2002

[5] Erick O. Torres and Gabriel A. Rincon-Mora, Harvesting ambient energy will make embedded devices autonomous, http://www.embedded.com/showArticle.jhtml?articleID=170102227

[6] Shad Roudy, Paul Wright and Jan Rabaey, A Study of Low Level Vibrations as a Power Source for Wireless Sensor Nodes, Computer Communications, vol. 26, no.11, pp.1131 – 1144, 2003

[7] Ferry Solutions Website, Millennial Net and Ferro Solutions Join Forces to Deliver Battery-Free Wireless Sensor Networks, http://www.ferrosi.com/pr1.htm

[8] Shad Roudy and Paul Wright, A Piezoelectric Vibration based Generator for Wireless Electronics, Smart Materials and Structures, Volume 13, pp.1131–1144, 2002

[9] Shad Roudy PhD thesis, Energy Scavenging for Wireless Sensor Nodes with a Focus on Vibration to Electricity Conversion, University of California at Berkeley, Berkeley CA, May 2003

[10] Williams C.B, and Yates R.B, Analysis of a micro-electric generator for Microsystems, Transducers 95/Eurosensors IX, pp.369 – 372, 1995

[11] Robert Stewart, Introduction to Physical Oceanography, http://oceanworld.tamu.edu/resources/ocng_textbook/

[12] Performance Foams Website, Seven design steps, http://www.dow.com/perffoam/info/design/step6.htm

[13] Answers.com, Definition of diesel engine, http://www.answers.com/topic/diesel-engine

[14] M.L.James, G.M.Smith, J.C.Wolford and P.W.Whaley, Vibration of Mechanical and Structural Systems, Harper Collins College Publishers, New York, NY 1994

[15] A.A.Shabana, Theory of Vibration an Introduction, second Edition, Springer-Verlag, New York 1995

[16] Engineers Edge Website, Extension Spring "k" Constant Calculator and Formula, http://www.engineersedge.com/spring_tension_calc_k.htm

[17] Hyperpro Racing Suspension Website, Spring review, http://www.hyperpro.com/cgi-bin/hpp.com/page.pl?page=products&dpage=pr_springs&ddpage=sp_overview

[18] Car turning, styling & performance site, Suspension Springs in General, http://www.tuninglinx.com/html/suspensionsprings.html

[19] C. B. Williams, S. Shearwood, M. A. Harradine, P. H. Mellor, T. S. Birch, and R. B. Yates, Development of an electromagnetic micro-generator, IEE Proc. Circuits, Devices and Syst.,, vol. 148, no. 6, pp. 337-342, Dec. 2001.

[20] Play-Hookey Website, Basic Rectifier Circuits, http://www.play-hookey.com/ac_theory/ps_rectifiers.html

[21] Switching Regulators, http://www.national.com/appinfo/power/files/f5.pdf

[22] Robert W. Erickson, DC-DC Power Converters, Article in Wiley Encyclopedia of Electrical and Electronics Engineering, http://ece-www.colorado.edu/~rwe/papers/Encyc.pdf

[23] Robert W Erickson and Dragan Maksimovic, Fundamentals of Power Electronics, 2nd edition, Kluwer Academic Publishers, 2001

[24] Isidor Buchmann, What's the role of the Supercapacitor, http://www.batteryuniversity.com/partone-8.htm

[25] Daniel W. O'Brien, Introduction to Electrochemical Capacitors in Pulse Power Applications,http://www.techonline.com/community/ed_resource/feature_article/14659

[26] CopQuest Website, Rechargeable Battery Information and Care, http://www.copquest.com/battery_care.htm

[27] POWERSIM Website, PSIM User Guide and Reference Manual, http://www.powersimtech.com/new-features-psim.html

[28] Mathworks Website, What is Simulink, http://www.mathworks.com/access/helpdesk_r13/help/toolbox/simulink/ug/ug.html

[29] POWERSIM Website, Simcoupler Module, http://www.powersimtech.com/simcoupler-module.html

[30] Wikipedia, the free encyclopedia website, hill climbing, http://en.wikipedia.org/wiki/Hill_climbing

[31] The Heuristic Wiki Website, Hill climbing, http://greenlightwiki.com/heuristic/Hill-Climbing

[32] Stuart Slade, Shake, Rattle and Roll (Vibration in ships), http://www.navweaps.com/index_tech/tech-005.htm

[33] Michael Bahtiarian, Diagnosing and Curing Global Ship Resonances, IEST PROCEEDINGS 2000, http://www.noise-control.com/shipvib.htm

Appendix A

A.1 Derivation of Equation 3.11:

The input average electrical power is:

$$P_{in} = \frac{2m^2B^2N^2l^2Y_0^2\omega^6R}{R^2(k-m\omega^2)^2+(c_mR+4B^2N^2l^2)^2\omega^2}$$

Equation 3.10 : $\frac{\partial P_{in}}{\partial k}=0$ can be solved as follow:

$$\Rightarrow 2R^2(k-m\omega^2)+2w^2R\zeta_m\sqrt{\frac{m}{k}}(c_mR+4B^2N^2l^2)=0$$

$$\Rightarrow R(k-m\omega^2+2m\omega^2\zeta_m^2)+4B^2N^2l^2\omega^2\zeta_m\sqrt{\frac{m}{k}}=0$$

which yields:

$$R=\frac{4B^2N^2l^2\omega^2\zeta_m\sqrt{\frac{m}{k}}}{m\omega^2(1-2\zeta_m^2)-k}$$

Substitute the above equation into equation 3.9: $R_{opt}=\frac{4B^2N^2l^2\omega}{\sqrt{c_m^2\omega^2+(k-m\omega^2)^2}}$, we get

$$\Rightarrow m\omega^2(1-2\zeta_m^2)-k=\omega\zeta_m\sqrt{\frac{m}{k}}\sqrt{4mk\omega^2\zeta_m^2+(k-m\omega^2)^2}$$

$$\Rightarrow m^2\omega^4(1-2\zeta_m^2)^2+k^2-2km\omega^2(1-2\zeta_m^2)=w^2\zeta_m^2[2m^2\omega^2(2\zeta_m^2-1)+mk+\frac{m^3\omega^4}{k}]$$

$$\Rightarrow m^2\omega^4-2\zeta_m^2m^2\omega^4+k^2-2km\omega^2+3km\omega^2\zeta_m^2=\frac{m^3\omega^6\zeta_m^2}{k}$$

which results in equation 3.11

$$k^3+k^2m\omega^2(3\zeta_m^2-2)+km^2\omega^4(1-2\zeta_m^2)-m^3\omega^6\zeta_m^2=0$$

while $\quad k<m\omega^2(1-2\zeta_m^2)$

A.2 Derivation of Equation 3.16:

The average input power can be represented by V_{in}

$$P_{in} = \frac{V_{in}^{\ 2}}{2R} = \frac{V_0\sqrt{4Y_0^{\ 2}m^2\omega^6B^2N^2l^2 - V_0^{\ 2}(k-m\omega^2)^2} - V_0^{\ 2}c_m\omega}{8B^2N^2l^2\omega}$$

Equation 3.15 : $\frac{\partial P_{in}}{\partial k} = 0$ can be solved as follow:

$$\Rightarrow \sqrt{4Y_0^{\ 2}m^2\omega^6B^2N^2l^2 - V_0^{\ 2}(k-m\omega^2)^2} - \frac{V_0^{\ 2}(k-m\omega^2)^2}{\sqrt{4Y_0^{\ 2}m^2\omega^6B^2N^2l^2 - V_0^{\ 2}(k-m\omega^2)^2}} - 2V_0c\omega = 0$$

$$\Rightarrow 4E^2 - 2V_0^{\ 2}G^2 - 2V_0c\omega\sqrt{4E^2 - V_0^{\ 2}G^2} = 0$$

$$\Rightarrow 4G^2V_0^{\ 4}(G^2 + c^2\omega^2) - 16V_0^{\ 2}E^2(G^2 + c^2\omega^2) + 16E^4 = 0$$

which yield

$$V_{in\_opt}^2 = \frac{4E^2(G^2 + c_m^2\omega^2) \pm 4E^2c_m\omega\sqrt{G^2 + c_m^2\omega^2}}{2G^2(G^2 + c_m^2\omega^2)}$$

since $\quad V_{in\_opt} < \frac{2E}{G} = \frac{2Y_0m\omega^3BNl}{|m\omega^2 - k|}$

$$V_{in\_opt}^2 = \frac{2E^2}{G^2}\left(1 - \frac{c_m\omega}{\sqrt{G^2 + c_m^2\omega^2}}\right)$$

which results in equation 3.16:

$$V_{in\_opt} = \frac{\sqrt{2}E}{G}\sqrt{1 - \frac{c_m\omega}{\sqrt{G^2 + c_m^2\omega^2}}}$$

$$= \frac{\sqrt{2}mY_0\omega^3BNl}{|m\omega^2 - k|}\sqrt{1 - \frac{c_m\omega}{\sqrt{(k-m\omega^2)^2 + c_m^2\omega^2}}}$$

where

$$E = Y_0m\omega^3BNl$$

$$G = |k - m\omega^2|$$

Appendix B

Simulation Parameter (constant)	Symbol	Value
Displacement Amplitude of Ship Vibration	Y_0	5 mm
Average Magnetic Flux Density	B	0.7 T
Number of Turns of A Coil	N	400
Length of a magnet	l	25 mm
Mechanical damping factor	ζ_m	0.11
Coils Inductance	L	1 mH
Coil Resistance	r	2 Ω

Simulation Parameter (Variable)	Symbol	Value
Ship vibration frequency	f	Input variable
Angular frequency of ship vibration	ω	$w = 2\pi f$
Spring constant	k	Adjustable (N/m)
Load resistance	R_l	Adjustable (Ω)
Nature angular frequency	ω_n	$\omega_n = \sqrt{k/m}$ (rad/s)
Mechanical Damping coefficient	c_m	$c_m = 2m\omega_n\zeta_m$

Table 1. Parameters in the simulation model of the linear generator

f (Hz)	V_{in_opt} (V)	$P_{in\_\max}$ (W)	f (Hz)	V_{in_opt} (V)	$P_{in\_\max}$ (W)
3	2.48	0.062	12	12.04	4.369
4	3.79	0.159	13	12.96	5.545
5	4.64	0.304	14	14.07	6.94
6	6.02	0.542	15	15.09	8.536
7	6.90	0.847	16	16.08	10.359
8	7.98	1.276	17	17.03	12.418
9	9.07	1.84	18	18.09	14.749
10	9.96	2.523	19	19.10	17.346
11	11.04	3.366	20	20.09	20.231

Table 2. Calculated $P_{in\_\max}$ and V_{in_opt} at various input frequencies

f (Hz)	k_{in_opt} (N/m)	R_{lin_opt} (Ω)	V_{in_opt1} (V)	p_{in_max} (W)	k_{out_opt} (N/m)	R_{lout_opt} (Ω)	V_{in_opt2} (V)	p_{out_max} (W)
3	100	50	2.54	0.0619	100	54	2.63	0.0596
4	200	45	3.87	0.159	200	49	4.03	0.153
5	300	33	4.61	0.304	300	37	4.86	0.288
6	500	31	5.98	0.542	500	35	6.32	0.511
7	700	26	6.88	0.846	700	30	7.34	0.79
8	900	23	7.99	1.276	900	27	8.58	1.181
9	1100	20	9	1.84	1100	24	9.76	1.689
10	1300	18	10.05	2.524	1300	22	10.95	2.29
11	1600	16	11.01	3.367	1600	20	12.11	3.032
12	1900	15	12.19	4.371	1900	19	13.45	3.899
13	2200	13	12.9	5.549	2300	17	14.44	4.909
14	2600	12	13.94	6.944	2600	16	15.7	6.088
15	3000	11	14.9	8.541	3000	15	16.92	7.425
16	3400	10	15.77	10.365	3400	14	18.07	8.93
17	3800	10	17.27	12.431	3900	14	19.71	10.621
18	4300	9	18.03	14.767	4300	13	20.8	12.502
19	4800	8	18.63	17.36	4800	12	21.82	14.579
20	5300	8	20.13	20.263	5400	12	23.47	16.866

Table 3 Simulation result of two sets of optimal k, R_l and V_{in} for maximum output and input power respectively at various input frequencies

Appendix C

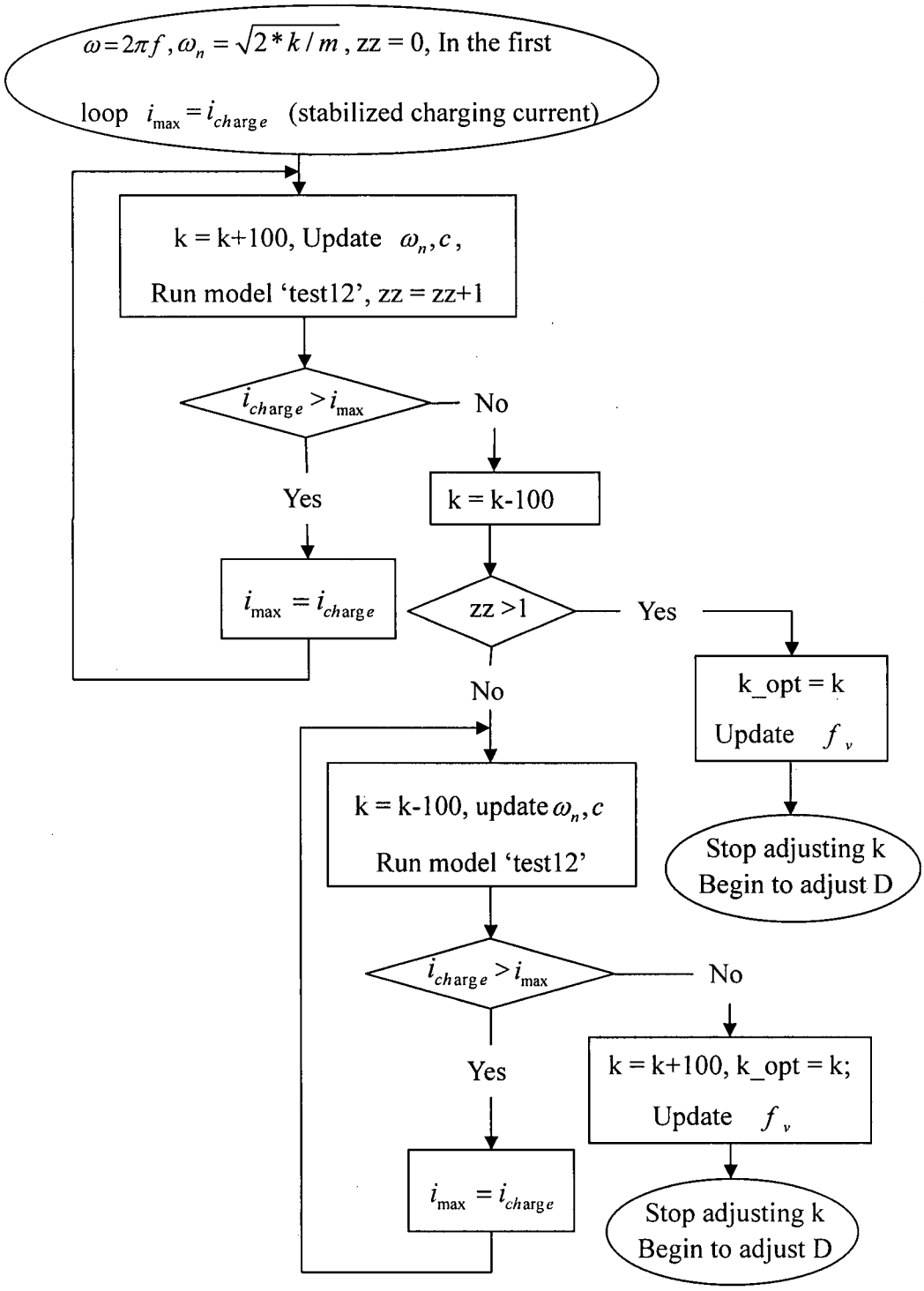

Figure 1. Flow chart of adjusting process of k

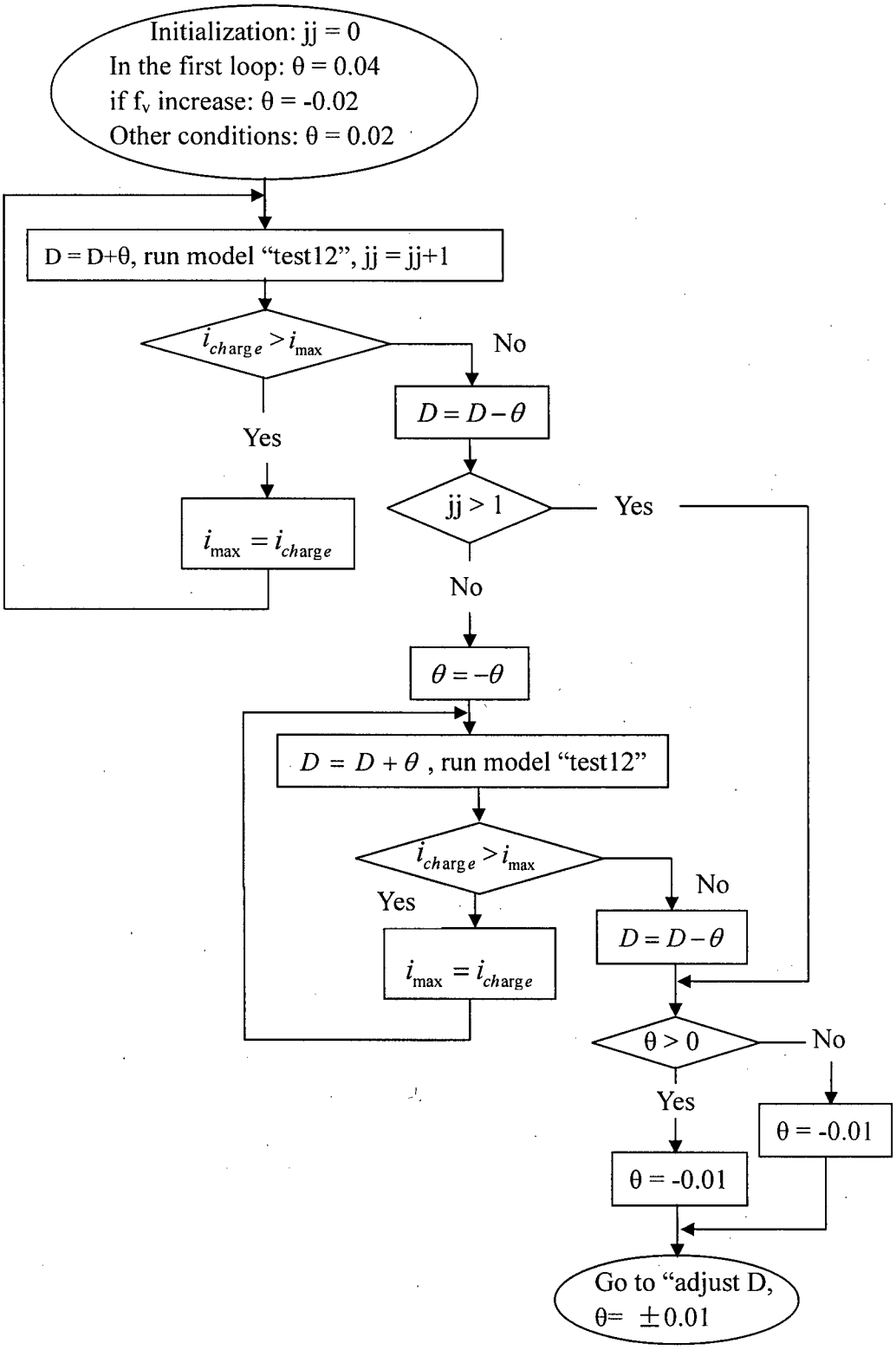

Figure 2. Flow chart of adjusting D with $\theta = \pm 0.04 / 0.02$

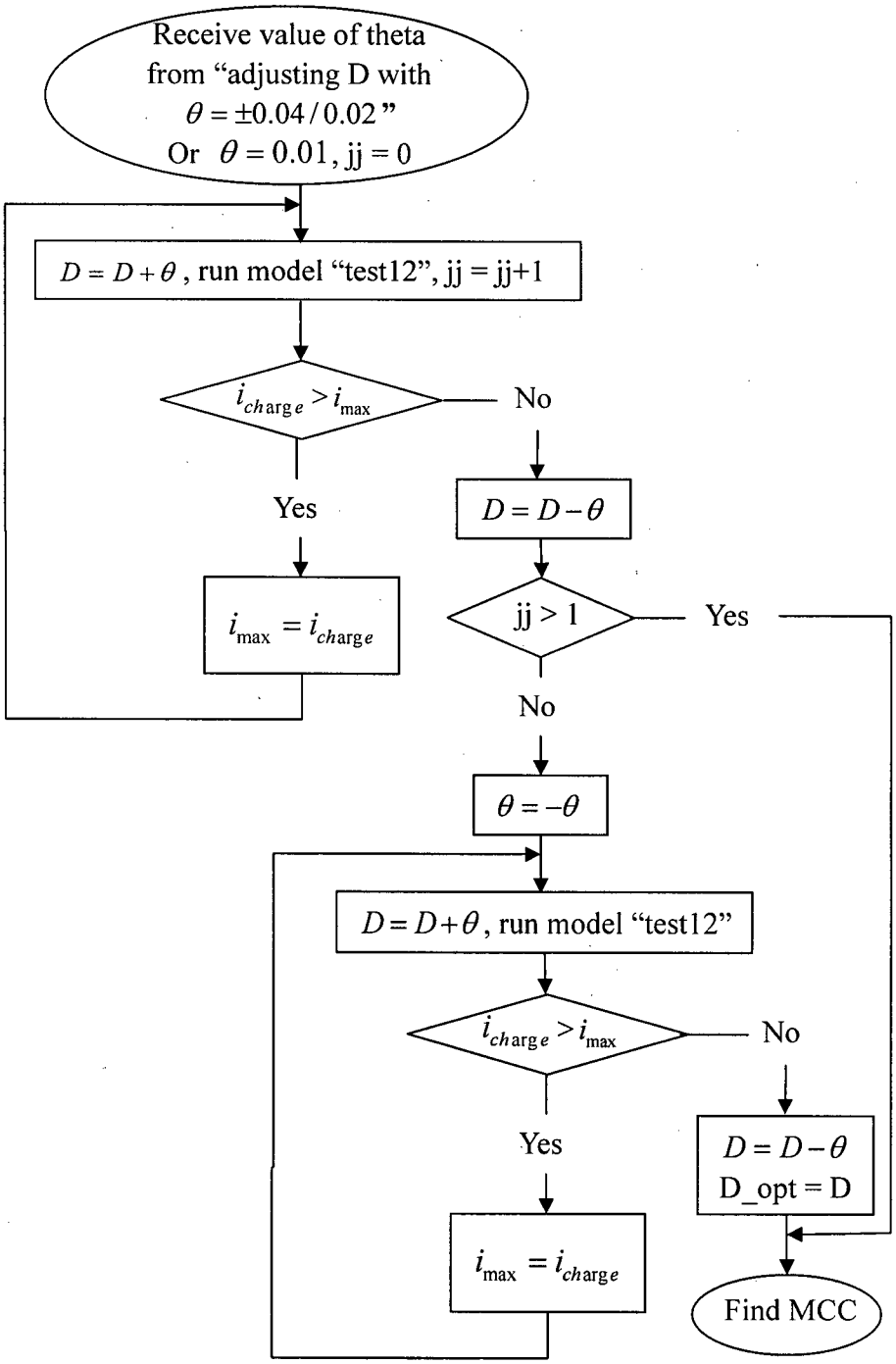

Figure3. Flow chart of adjusting D with $\theta = \pm 0.01$